INVESTIGATION OF THE LATTICE DYNAMICS OF α-Fe AND Fe_3Al BY NEUTRON INELASTIC SCATTERING

C. VAN DIJK

STELLINGEN

I

De werkzame doorsnede voor één-fononverstrooiing van neutronen in kristalroosters met meer dan één atoom per primitieve eenheidscel wordt op juiste wijze gegeven door Waller en Fröman. In de uitdrukking gegeven door Lomer en Low dient men de polarisatievectoren van de atomen door hun complex toegevoegde te vervangen om het juiste resultaat te verkrijgen.

I. Waller en P.O. Fröman, Ark. Fys. 4 (1952), 183.
W.M. Lomer en G.G. Low, in Thermal Neutron Scattering, ed. by P.A. Egelstaff, Academic Press, London, 1965, 28.

II

De inelastische structuurfactor voor neutronenverstrooiing zoals ingevoerd door Elliott en Thorpe bevat de debye-wallerfactor en heeft derhalve niet de door hen geponeerde periodiciteit.

R.J. Elliott en M.F. Thorpe, Proc. Phys. Soc. 91 (1967), 903.

III

Het gebruik van de inverse beryllium-filtermethode voor de bepaling van fonondispersierelaties in éénkristallen kan van groot nut zijn, mits met variaties in inelastische structuurfactoren terdege rekening wordt gehouden.

J. Bergsma, proefschrift Leiden, 1970, hoofdstuk V, stelling III.
Dit proefschrift, hoofdstuk VI.

IV

De door Schweiss, Furrer en Bührer berekende frequentieverdeling van spingolven in α-Fe is kwalitatief onjuist.

P. Schweiss, A. Furrer en W. Bührer, Helv. Phys. Acta 40 (1967), 378.

V

In tegenstelling tot hetgeen Warren beweert zijn voor de classificatie van de fonondispersierelaties in CsCl behalve groepentheoretische ook fysische argumenten gebruikt.

J.L. Warren, Revs. Modern Phys. 40 (1968), 38.
C. Kittel, Introduction to Solid State Physics, third edition, John Wiley & Sons, Inc., New York, 1967, 393.

VI

De veronderstelling, die Romanov en Shapiro maken omtrent de stralingsbreedte, Γ_γ, van de -400 eV resonantie in de $^{45}Sc(n,\gamma)$-reactie, is niet gefundeerd en leidt tot het fysisch onbevredigende resultaat van een negatieve verstrooiingslengte voor potentiaalverstrooiing in Sc. Door voor Γ_γ een weinig afwijkende, doch alleszins aanvaardbare keuze te doen, wordt wèl een realistische verstrooiingslengte verkregen.

S.A. Romanov en F.L. Shapiro, Sov. J. Nucl. Phys. 1 (1965), 159.
J.E. Lynn, The Theory of Neutron Resonance Reactions, Clarendon Press, Oxford, 1968, 273.
Neutron Cross Sections, BNL 325, 1964-1966.
H. Weigmann en H. Schmid, Nucl. Phys. A104 (1967), 513.

VII

Het door Summerfield en Kleinberg gelegde verband tussen incoherente neutronenverstrooiing en kernspinresonantiemetingen is zeer aanvechtbaar.

G.C. Summerfield en R. Kleinberg, J. Phys. Soc. Japan 28 (1970), 644.

VIII

De waarde van de magnetische wisselwerkingsenergie tussen naaste ijzerburen in geordend Fe_3Al, gevonden uit recente metingen met behulp van neutronen, wijkt aanzienlijk af van die, welke door Mary B. Stearns met behulp van moleculaire veldentheorie werd berekend uit resultaten van mössbauerexperimenten. Hiermee komt haar conclusie ten aanzien van het aantal niet-gelokaliseerde d-elektronen te vervallen.

Mary B. Stearns, Phys. Rev. 168 (1968), 588.
B. Antonini, F. Menzinger en A. Paoletti, International Conference on Magnetism 1970, Grenoble, 14-19 September, 1970, VeG 14.

IX

Voor de berekeningen van het dopplereffect in snelle reactoren, waarbij gebruik wordt gemaakt van ladders van resonanties met statistisch gegenereerde parameters, dient men, voor het verkrijgen van een juist inzicht in de nauwkeurigheid van de methode, na te gaan wat de invloed is van correlaties tussen de afstanden van de gegenereerde opeenvolgende resonantieniveaus.

C.N. Kelber en P.H. Kier, Nucl. Sci. Eng. 24 (1966), 389.
M.W. Dyos, Nucl. Sci. Eng. 34 (1968), 181.
C.R. Adkins, T.E. Murley en M.W. Dyos, Nucl. Sci. Eng. 36 (1969), 336.

X

Bij de implementatie van de gangbare programmeertalen wordt veelal grote nadruk gelegd op de leesbaarheid van de rekenmachineprogramma's. Dit leidt tot een te ruim gebruik van overtollige symbolen, hetgeen de kans op fouten bij de programmavoorbereiding aanzienlijk vergroot.

XI

Er bestaat in West-Europa behoefte aan een gepulseerde superhogefluxreactor voor fundamenteel wetenschappelijk onderzoek.

XII

Het is van sociaal-economisch belang dat aan de gehuwde, in haar gezin werkende vrouw een fictief salaris wordt toegekend, dat op basis van een standaard werktijd wordt berekend. Inkomsten door haar verkregen uit een andere werkkring dienen, afhankelijk van de aan deze werkkring besteedde tijd, fiscaal geheel of gedeeltelijk met deze standaard beloning verminderd te worden.

C. van Dijk

25 november 1970.

INVESTIGATION OF THE LATTICE DYNAMICS OF α-Fe AND Fe_3Al BY NEUTRON INELASTIC SCATTERING

PROEFSCHRIFT

TER VERKRIJGING VAN DE GRAAD VAN DOCTOR IN
DE WISKUNDE EN NATUURWETENSCHAPPEN AAN
DE RIJKSUNIVERSITEIT TE LEIDEN, OP GEZAG VAN
DE RECTOR MAGNIFICUS DR. C. SOETEMAN,
HOOGLERAAR IN DE FACULTEIT DER LETTEREN,
TEN OVERSTAAN VAN EEN COMMISSIE UIT DE SENAAT
TE VERDEDIGEN OP WOENSDAG 25 NOVEMBER 1970
TE KLOKKE 14.15 UUR

DOOR

CORNELIS VAN DIJK

GEBOREN TE WOUDENBERG IN 1934

PROMOTOR: Prof.Dr. J.A. Goedkoop

Aan Riet, Martine en Karel

Aan mijn ouders

VOORWOORD

Allen, die hebben bijgedragen aan het tot stand komen van dit proefschrift, wil ik hiervoor gaarne mijn dank en erkentelijkheid betuigen.

Dr. B.O. Loopstra heeft door zijn grote belangstelling en opbouwende kritiek mij sterk in mijn werk gestimuleerd. Ik ben hem zeer dankbaar voor de grondige wijze waarop hij het manuscript heeft gelezen en van commentaar heeft voorzien.

De vriendschappelijke en collegiale samenwerking met Dr. J. Bergsma is voor mij van grote betekenis geweest. De vele discussies met hem tijdens alle fasen van het onderzoek hebben belangrijk bijgedragen tot het uiteindelijke resultaat.

Dr. H.M. Rietveld dank ik voor de discussies over bepaalde rekenmachineprogramma's.

Dr. D. Tocchetti is gratefully acknowledged for his participation in the measurements on α-iron.

Met waardering vermeld ik hier de technische assistentie en de medewerking bij computerberekeningen van de heer G.C.J. van den Boogaard. Ook de figuren in dit proefschrift werden voornamelijk door hem, op accurate wijze, vervaardigd. Het onderhoud van de elektronische apparatuur werd op uitnemende wijze verzorgd door de heer Th. H. Terwisscha van Scheltinga.

Voor de uitvoering van de experimenten is de medewerking van de reactorbedrijfsgroep onder leiding van Ir. R.J. Swanenburg de Veye van groot belang geweest.

De directie van het Reactor Centrum Nederland ben ik erkentelijk voor de geboden mogelijkheid de tekst tegelijkertijd als proefschrift en als officieel RCN-rapport te laten verschijnen.

Ik heb grote waardering voor de wijze waarop mevrouw E.A.M. Endel-Kramer en mejuffrouw G.E. Möls het typewerk hebben verzorgd. De reprografische dienst onder leiding van de heer E. van Rooy komt dank toe voor de druktechnische uitvoering.

Mijn vrouw ben ik zeer dankbaar voor de steun en daadwerkelijke hulp, die zij mij verleend heeft.

C O N T E N T S

Chapter I

INTRODUCTION

The scattering of thermal neutrons by crystals has been recognized as an extremely powerful means for the study of lattice structures [1]) and lattice dynamics [2,3]). For the investigation of crystal structures neutron scattering can be considered to be complementary to X-ray scattering in samples containing both heavy and light elements, or elements with neighbouring atomic number. In addition, because the neutrons have a spin, they also allow the determination of magnetic structures.

For the study of lattice vibrations the use of neutrons is almost indispensable. Unlike other types of radiation, thermal neutrons have both a wavelength which is of the same order as interatomic distances in crystals, and an energy of the same order as that of the quantized lattice vibrations, the phonons. Thus both exchange of momentum and energy with the lattice vibrations can easily be detected by analysing direction and energy of the scattered neutrons. The scattering process in which the neutrons exchange energy with the lattice vibrations is usually referred to as neutron inelastic scattering by phonons.

For the analysis of the neutron energies two methods are used. In the first method, the diffraction technique, one determines the wavelength of the neutrons from the angles at which they are Bragg reflected from a single crystal. In the second method, the time-of-flight technique, the velocities of the neutrons are determined from the time they need to traverse a certain distance. For the study of phonon dispersion relations in single crystals the diffraction technique is in general to be preferred over the time-of-flight technique.

In this study the diffraction technique has been used for the determination of the phonon dispersion relations in α-Fe and its alloy Fe_3Al.

For the case of simple metals such as sodium, magnesium and aluminium, the experimental determined dispersion relations are easily interpreted in terms of physical quantities. This is the case to a lesser extent for more complicated metals, such as the transition

metals. The lattice dynamics of these metals is usually described in the more phenomenological Born-von Kármán theory. The experimental phonon dispersion relations yield the parameters, the interatomic force constants, for this model. It is then expected that systematic comparison of the results from properly chosen metals and alloys indicates how the theory for the simple metals should be extended or revised for more complicated systems.

The present study of the lattice dynamics of α-Fe and Fe_3Al fits also in this frame-work. There is a close relationship between the two structures and comparison of the lattice dynamics of both substances might yield some of the fundamental quantities necessary for arriving at the proper theory. In addition Fe_3Al is very interesting to investigate since it undergoes a phase transition under heat treatment from the ordered DO_3 structure to the 50% disordered B2 structure.

In the chapters II and III of this report some of the elements of the theory of lattice dynamics and neutron scattering by lattices are reviewed. After that a short description is given of the diffraction set-up, the triple-axis crystal spectrometer, together with the experimental methods which were applied. In chapter V the study of the lattice dynamics of α-Fe is presented and in chapter VI the investigation of Fe_3Al is described. The Born-von Kármán theory is used in the description of the lattice dynamics of both specimens. The description of Fe_3Al includes a group-theoretical analysis of the normal modes.

references I

References

1. G.E. Bacon, Neutron Diffraction, second edition, Clarendon press, Oxford, 1962.
2. G. Dolling and A.D.B. Woods, Thermal Neutron Scattering, edited by P.A. Egelstaff, Academic press, London, 1965.
3. B.N. Brockhouse, Phonons in Perfect Lattices and in Lattices with Point Imperfections, edited by R.W.H. Stevenson, B.A., Ph.D., Oliver and Boyd, Edinburgh, 1966.
4. W.A. Harrison, Phonons in Perfect Lattices and in Lattices with Point Imperfections, edited by R.W.H. Stevenson, B.A., Ph.D., Oliver and Boyd, Edinburgh, 1966.
5. T. Schneider and E. Stoll, Neutron Inelastic Scattering, Proc. Symp. Copenhagen, 1968, Vol.I, Vienna, IAEA (1968), 101.

Chapter II

BORN-VON KARMAN THEORY OF LATTICE VIBRATIONS

2.1. Introduction

The theoretical treatment of the lattice vibrations as used here is originally due to Born and von Kármán [1]). It has been described extensively a.o. by Born and Huang [2]) and by Maradudin *et al.* [3]). The following assumptions and approximations form the basis for this theory.

a. The adiabatic approximation.
   The electrons are always able to adapt themselves to the instantaneous nuclear positions. Thus the potential energy may be written as a general Taylor series in terms of the displacements of the atoms from their equilibrium positions.

b. The harmonic approximation.
   The atomic displacements are considered to be so small, that the above series expansion may be broken off after the quadratic term.

c. The requirement of periodic or cyclic boundary conditions.
   This is equivalent to replacing the finite specimen by an infinite medium without boundary effects.

In the present work the fundamental theory is treated classically, while it is indicated how to proceed to obtain the quantum mechanical results. The latter are used in the description of the thermodynamic quantities. In the last part of this chapter the relation between the long wavelength vibrations and the elastic constants is discussed.

2.2. Classical theory

Let us consider a general lattice structure with n atoms per primitive unit cell, the different atoms in the same cell being distinguished by an index λ and the different cells being labelled by an index ℓ.

We can represent the potential energy Φ of an arbitrary lattice as a function of the displacements of the atoms from their equilibrium positions by expanding Φ in a Taylor series with respect to the atomic displacements [1,2,3,4]). For small vibrations it suffices to trunkate

section 2.2.

after the second derivative of the potential energy, which leads to the harmonic approximation. Therefore we write for the lattice potential

$$\Phi = \Phi_o + \sum_{\ell} \sum_{\lambda} \sum_{\alpha} \Phi_\alpha(\ell\lambda)\, u_\alpha(\ell\lambda) + \\ + \tfrac{1}{2} \sum_{\ell\ell'} \sum_{\lambda\lambda'} \sum_{\alpha\beta} \Phi_{\alpha\beta}(\ell\lambda;\ell'\lambda')\, u_\alpha(\ell\lambda)\, u_\beta(\ell'\lambda') \,, \qquad (2.1)$$

where Φ_o is the potential energy of the static lattice, $u_\alpha(\ell\lambda)$ and $u_\beta(\ell'\lambda')$ are the α- and β-component of the displacements of the atoms $(\ell\lambda)$ and $(\ell'\lambda')$, respectively. Furthermore,

$\Phi_\alpha(\ell\lambda) = \left.\frac{\partial\Phi}{\partial u_\alpha(\ell\lambda)}\right|_o$ and $\Phi_{\alpha\beta}(\ell\lambda;\ell'\lambda') = \left.\frac{\partial^2\Phi}{\partial u_\alpha(\ell\lambda)\partial u_\beta(\ell'\lambda')}\right|_o$, where the subscript o indicates that the derivatives are taken in the equilibrium state.

It is obvious that a displacement of the lattice as a whole does not change the potential energy. This means in first order in the displacement

$$\sum_{\ell} \sum_{\lambda} \sum_{\alpha} \Phi_\alpha(\ell\lambda) u_\alpha(\ell\lambda) = N \sum_{\lambda} \sum_{\alpha} \Phi_\alpha(\lambda)\varepsilon_\alpha = 0 \,, \qquad (2.2)$$

where N is the total number of cells and ε_α the α-component of the displacement vector $\underline{\varepsilon}$ of the lattice. Since (2.2) must hold for an arbitrary vector $\underline{\varepsilon}$ it follows that

$$\sum_{\lambda} \Phi_\alpha(\lambda) = 0. \qquad (2.3)$$

Likewise the value of $\frac{\partial\Phi}{\partial u_\alpha(\ell\lambda)}$ can not be affected by a translation of the lattice over a vector $\underline{u}(\ell\lambda) = \underline{\varepsilon}$. Expansion of $\frac{\partial\Phi}{\partial u_\alpha(\ell\lambda)}$ in a power series and substituting $u_\beta(\ell'\lambda') = \varepsilon_\beta$ yields

$$\frac{\partial\Phi}{\partial u_\alpha(\ell\lambda)} = \Phi_\alpha(\ell\lambda) + \sum_{\ell'\lambda'\beta} \Phi_{\alpha\beta}(\ell\lambda;\ell'\lambda')\varepsilon_\beta + \ldots \qquad (2.4)$$

Since (2.4) must hold independently of ε_β, we obtain also

$$\sum_{\ell'\lambda'} \Phi_{\alpha\beta}(\ell\lambda;\ell'\lambda') = 0. \tag{2.5}$$

The $-\Phi_{\alpha\beta}(\ell\lambda;\ell'\lambda')$ are usually called the interatomic force constants. $-\Phi_{\alpha\beta}(\ell\lambda;\ell'\lambda')$ is the α-component of the force on atom $(\ell\lambda)$ due to a unit displacement of atom $(\ell'\lambda')$ in the β-direction. From the formal definition of the force constants it follows that they are symmetric in the indices $(\ell\ \lambda\ \alpha)$ and $(\ell'\lambda'\beta)$

$$\Phi_{\alpha\beta}(\ell\lambda;\ell'\lambda') = \Phi_{\beta\alpha}(\ell'\lambda';\ell\lambda)\ . \tag{2.6}$$

In view of (2.1), (2.3) and (2.6) the equations of motion for the atoms of the crystal become

$$\begin{aligned} M(\lambda)\ \ddot{u}_\alpha(\ell\lambda) &= -\frac{\partial\Phi}{\partial u_\alpha(\ell\lambda)} \\ &= -\sum_{\ell'\lambda'\beta} \Phi_{\alpha\beta}(\ell\lambda;\ell'\lambda')u_\beta(\ell'\lambda')\ , \end{aligned} \tag{2.7}$$

where $M(\lambda)$ is the mass of the atom of type λ. Because of the periodicity of the lattice $\Phi_{\alpha\beta}(\ell\lambda;\ell'\lambda')$ does not depend on the absolute positions of the cells (ℓ) and (ℓ'), but only on the distance between them. Hence

$$\Phi_{\alpha\beta}(\ell\lambda;\ell'\lambda') = \Phi_{\alpha\beta}(\ell-\ell';\lambda\lambda')\ , \tag{2.8}$$

and consequently we may write (2.7) as

$$M(\lambda)\ddot{u}_\alpha(\ell\lambda) = -\sum_{\ell'\lambda'\beta} \Phi_{\alpha\beta}(\ell-\ell';\lambda\lambda')u_\beta(\ell'\lambda')\ . \tag{2.9}$$

The infinite number of equations given by (2.9) can be simplified to a set of 3n equations by inserting the plane wave

$$u_\alpha(\ell\lambda) = \left[u_\alpha(\lambda)/M(\lambda)^{\frac{1}{2}}\right] \exp\left[i\underline{q}\cdot\underline{r}(\ell) - i\omega t\right]\ . \tag{2.10}$$

section 2.2.

The amplitude $\left[u_\alpha(\lambda)/M(\lambda)^{\frac{1}{2}}\right]$ is independent both of ℓ and the time t. Further $\underline{r}(\ell)$ is the position vector of the origin of the ℓ-th unit cell, ω is the angular frequency and $\underline{q}$, the wave vector, is an arbitrary vector in phase space, which has base vectors 2π times the base vectors of the reciprocal lattice. The reciprocal lattice is related to the crystal lattice in the following manner: let a lattice point be given by

$$\underline{r}(\ell) = \sum_{i=1}^{3} \ell_i \, \underline{a}_i \ , \tag{2.11}$$

where the $\underline{a}_i$ are the three base vectors of the normal lattice, while the ℓ_i are integers, then a reciprocal lattice point is determined by a reciprocal lattice vector $\underline{\tau}(h)$

$$\underline{\tau}(h) = \sum_{j=1}^{3} h_j \, \underline{b}_j \quad (h_j = \text{integer}) \ , \tag{2.12}$$

with $\underline{b}_j$ the base vectors of the reciprocal lattice defined by

$$\underline{a}_i \cdot \underline{b}_j = \delta_{ij} \ . \tag{2.13}$$

Substitution of (2.10) in (2.9) yields the following result for the 3n equations of the reduced amplitudes $u_\alpha(\lambda)$

$$\omega^2 u_\alpha(\lambda) = \sum_{\lambda'\beta} D_{\alpha\beta}(\lambda\lambda';\underline{q}) u_\beta(\lambda') \ , \tag{2.14}$$

where $D_{\alpha\beta}(\lambda\lambda';\underline{q})$ are the elements of the so-called Fourier-transformed dynamical matrix $D(\underline{q})$, hereafter referred to as dynamical matrix. These are given by

$$D_{\alpha\beta}(\lambda\lambda';\underline{q}) = \left(M(\lambda)M(\lambda')\right)^{-\frac{1}{2}} \sum_{\ell'} \Phi_{\alpha\beta}(\ell-\ell';\lambda\lambda') \exp\left[-i\underline{q}\cdot\left(\underline{r}(\ell)-\underline{r}(\ell')\right)\right] \ . \tag{2.15}$$

For (2.14) to yield non-trivial solutions the following determinantal equation should be fulfilled

$$| \omega^2 \delta_{\lambda\lambda'} \delta_{\alpha\beta} - D_{\alpha\beta}(\lambda\lambda';\underline{q}) | = 0. \qquad (2.16)$$

Equation (2.16) is called the secular equation. For every wave vector $\underline{q}$ there are 3n solutions for ω^2, every solution $\omega_j^2(\underline{q})$ corresponding to one vibrational mode. The relations between the angular frequency ω and the wave vector of the lattice vibrations $\underline{q}$ are called the dispersion relations of the vibrational modes or normal modes. They consist of 3 acoustical and 3n-3 optical dispersion relations usually referred to as branches. The acoustical branches are characterized by frequencies which vanish with vanishing wave vector $\underline{q}$, while the optical branches always have frequencies different from zero. For small values of $\underline{q}$ the frequencies of the acoustical branches are linearly proportional to $|\underline{q}|$ and all atoms in the same cell move in phase. Thus in the limit of long wavelengths the acoustical branches are in fact identical to the ordinary elastic vibrations. For the long wavelength optical vibrations, the atoms within the same cell move in such a way that their centre of mass is at rest. Such vibrations may be excited by light waves with frequencies within the infrared region.

The solution of (2.16) is in fact the solution of an eigenvalue problem; the $\omega_j^2(\underline{q})$ are the eigenvalues of the matrix $D(\underline{q})$, and the $u_\alpha(\lambda)$ the components of the corresponding eigenvectors. To show the fact that $u_\alpha(\lambda)$ is unambiguously connected to $\omega_j^2(\underline{q})$, we change our notation and replace the former by $e_{\alpha j}(\lambda;\underline{q})$. This brings us to the following expressions for (2.10) and (2.14)

$$u_{\alpha j}(\ell\lambda) = \left[e_{\alpha j}(\lambda;\underline{q})/M(\lambda)^{\frac{1}{2}}\right] \exp\left[i\underline{q}\cdot\underline{r}(\ell) - i\omega_j(\underline{q})t\right] \qquad (2.17)$$

and

$$\omega_j^2(\underline{q}) e_{\alpha j}(\lambda;\underline{q}) = \sum_{\lambda'\beta} D_{\alpha\beta}(\lambda\lambda';\underline{q})\, e_{\beta j}(\lambda';\underline{q}) \,. \qquad (2.18)$$

The eigenvector $\underline{e}_j(\lambda;\underline{q})$ is composed of the n three-dimensional polarisation vectors of the n different atoms in the unit cell.

It is now possible to derive some general properties of the dynamical matrix which are of relevance for the further treatment of the dynamical theory. From the definition of the reciprocal lattice as given in (2.11), (2.12) and (2.13) it follows that the dynamical matrix

section 2.2.

D($\underline{q}$) defined by (2.15) is a periodic function of $\underline{q}$ with the period of the reciprocal lattice

$$D_{\alpha\beta}(\lambda\lambda';\underline{q} + 2\pi\underline{\tau}) = D_{\alpha\beta}(\lambda\lambda';\underline{q}) \ . \tag{2.19}$$

Further (2.15) leads immediately to

$$D_{\alpha\beta}(\lambda\lambda';\underline{q}) = D^{*}_{\alpha\beta}(\lambda\lambda';-\underline{q}) \ . \tag{2.20}$$

Combination of (2.6) and (2.15) yields the result

$$D_{\alpha\beta}(\lambda'\lambda;\underline{q}) = D^{*}_{\alpha\beta}(\lambda\lambda';\underline{q}) \ , \tag{2.21}$$

which means that D($\underline{q}$) is a Hermitian matrix.
As a consequence of (2.19) it follows from (2.16) that the normal mode frequency has the reciprocal lattice periodicity, hence

$$\omega_j(\underline{q} + 2\pi\underline{\tau}) = \omega_j(\underline{q}) \ . \tag{2.22a}$$

Moreover, we may choose

$$\underline{e}_j(\lambda;\underline{q} + 2\pi\underline{\tau}) = \underline{e}_j(\lambda;\underline{q}) \ , \tag{2.22b}$$

where the arbitrary phase factor of unit modulus, which, strictly speaking, relates the lefthand side of (2.22b) to its righthand side, has been put equal to unity.

For a Hermitian matrix the eigenvalues are real, and the eigenvectors can be chosen to obey the following relations

$$\sum_{\alpha\lambda} e^{*}_{\alpha j}(\lambda;\underline{q})\, e_{\alpha j'}(\lambda;\underline{q}) = \delta_{jj'} \tag{2.23a}$$

and

$$\sum e^{*}_{\alpha j}(\lambda;\underline{q})\, e_{\beta j}(\lambda';\underline{q}) = \delta_{\alpha\beta}\, \delta_{\lambda\lambda'} \ . \tag{2.23b}$$

Furthermore we may demand

$$e_{\alpha j}(\lambda;\underline{q}) = e^{*}_{\alpha j}(\lambda;-\underline{q}) \ , \tag{2.24a}$$

while from (2.20) we obtain

$$\omega_j(\underline{q}) = \omega_j(-\underline{q}) \ . \tag{2.24b}$$

The above relations give some of the fundamental properties of ω and $\underline{e}$ of importance for the treatment in the forthcoming sections.

2.3. Quantum mechanical approach

The classical treatment sofar of the lattice dynamics explains many physical aspects in a very elegant way. However, for a proper description of some thermodynamic quantities, and also to understand many of the neutron scattering properties a quantum mechanical description is needed. We will now sketch the quantum mechanical treatment.

It can be shown [5]) using (2.17), (2.23) and (2.24) that the displacement of atom $(\ell\lambda)$ from its equilibrium position can be written in the general form

$$\underline{u}(\ell\lambda,t) = \sum_{\underline{q}} \sum_{j=1}^{3n} \underline{e}_j(\lambda;\underline{q})\{\alpha_j(\lambda;\underline{q})\exp\left[i\underline{q}\cdot\underline{r}(\ell)-i\omega_j(\underline{q})t\right] +$$

$$+ \alpha^{*}_j(\lambda;-\underline{q})\exp\left[i\underline{q}\cdot\underline{r}(\ell)+i\omega_j(\underline{q})t\right]\} \ . \tag{2.25}$$

N is the total number of unit cells. The summation of $\underline{q}$ is over N points of the first Brillouin zone, which is the cell containing all points in reciprocal space lying nearer to the origin than to any other point of the reciprocal lattice. This restriction on $\underline{q}$, which simplifies many of the lattice dynamical calculations, is obtained by adopting the cyclic boundary conditions. The latter postulate that $\underline{u}(\ell\lambda,t)$ repeats when going, say L cells in the direction of any of the base vectors of the crystal lattice as defined by (2.11). This together with the lattice periodicity, reflected by (2.10), enables us to confine ourselves to the $L^3 = N$ values of $\underline{q}$ in the first Brillouin zone of reciprocal space. The variables $\alpha_j(\lambda;\underline{q})$ are complex numbers, containing the arbitrary

section 2.3.

amplitudes and phases of the 3nN uncoupled harmonic oscillators into which the movement is broken down. In (2.25) $\underline{u}(\ell\lambda,t)$ is always real. Expression (2.25) is particularly suited for proceeding to the quantum mechanical approach, in which $\underline{u}(\ell\lambda,t)$ as well as the variables $\alpha_j(\lambda;\underline{q})$ are considered as operators. The former then must obey the commutation relations

$$\begin{aligned}\left[u_\alpha(\ell\lambda,t),u_\beta(\ell'\lambda',t)\right] &= \left[\dot{u}_\alpha(\ell\lambda,t),\dot{u}_\beta(\ell\lambda,t)\right] = 0,\\ \left[\dot{u}_\alpha(\ell\lambda,t),u_\beta(\ell'\lambda',t)\right] &= -\frac{i\hbar}{M(\lambda)}\cdot\delta_{\ell\ell'}\delta_{\lambda\lambda'}\delta_{\alpha\beta}\,.\end{aligned} \tag{2.26}$$

By introducing the operators

$$a_j(\underline{q}) = \left(2nNM(\lambda)\omega_j(\underline{q})/\hbar\right)^{\frac{1}{2}}\alpha_j(\lambda;\underline{q})\,,$$

one obtains

$$\begin{aligned}\underline{u}(\ell\lambda,t) = \sum_{\underline{q}}\sum_{j=1}^{3n}&\left(2nNM(\lambda)\omega_j(\underline{q})/\hbar\right)^{-\frac{1}{2}}\underline{e}_j(\lambda;\underline{q})\cdot\\ \cdot\{a_j(\underline{q})&\exp\left[i\underline{q}\cdot\underline{r}(\ell) - i\omega_j(\underline{q})t\right] + a_j^*(-\underline{q})\exp\left[i\underline{q}\cdot\underline{r}(\ell) + i\omega_j(\underline{q})t\right]\},\end{aligned} \tag{2.27}$$

in which the $a_j(\underline{q})$ satisfy the commutation relations

$$\begin{aligned}\left[a_j(\underline{q}).\ a_j^*,(\underline{q}')\right] &= \delta_{jj'}\delta_{\underline{q}\underline{q}'}\,,\\ \left[a_j(\underline{q}),\ a_{j'}(\underline{q}')\right] &= \left[a_j^*(\underline{q}),\ a_{j'}^*(\underline{q}')\right] = 0.\end{aligned} \tag{2.28}$$

The Hamiltonian of the crystal can be written in terms of these operators

$$H = \sum_{\underline{q}j}\hbar\omega_j(\underline{q})\left\{a_j^*(\underline{q})\ a_j(\underline{q}) + \tfrac{1}{2}\right\}\,, \tag{2.29}$$

with eigenvalues

$$E = \sum_{\underline{q}j}\hbar\omega_j(\underline{q})\left(n_j(\underline{q}) + \tfrac{1}{2}\right)\,, \tag{2.30}$$

where the quantum numbers $n_j(\underline{q})$ may have values 0, 1, 2, etc. At zero temperature the crystal is in the ground state: all quantum numbers $n_j(\underline{q})$ are zero. The operators $a_j(\underline{q})$ and $a_j^*(\underline{q})$ represent the usual annihilation and creation operators for the quanta of eigenvibrations, the phonons. The average energy of a particular phonon is

$$\langle E_j \rangle = \hbar\omega_j(\underline{q})\left(\langle n_j(\underline{q})\rangle + \tfrac{1}{2}\right) . \qquad (2.31)$$

$\langle n_j(\underline{q})\rangle$ is obtained by statistical mechanical considerations [2]) from the partition function for harmonic oscillators,

$$\langle n_j(\underline{q})\rangle = \frac{1}{\exp(\hbar\omega_j/kT)-1} = \frac{\coth(\hbar\omega_j/2kT)-1}{2} . \qquad (2.32)$$

k = Boltzmann's constant and T the absolute temperature.

For a macroscopic crystal the number of phonons is very large and to obtain the total energy of the crystal we may replace the summation of (2.30) by an integration over the frequency ν ($=\omega/2\pi$).

$$E = N\int_0^\infty \left[\tfrac{1}{2} + \frac{1}{\exp(h\nu/kT)-1}\right] h\nu f(\nu)d\nu . \qquad (2.33)$$

Here $f(\nu)$ represents the density of phonon states, the so-called frequency distribution function, which gives the total number of frequencies per unit range at a particular frequency. Its normalisation is obtained from the condition

$$\int f(\nu)\, d\nu = 3n , \qquad (2.34)$$

with n the number of atoms per primitive unit cell.

From (2.33) follows for the molar heat capacity at constant volume due to the lattice vibrations

$$C_V = \frac{\partial E}{\partial T} = N_A k \int_0^\infty \frac{\exp(h\nu/kT)}{\left(\exp(h\nu/kT)-1\right)^2}\left(\frac{h\nu}{kT}\right)^2 f(\nu)d\nu , \qquad (2.35)$$

section 2.4.

where N_A is Avogadro's number. For large T (2.35) approaches the classical result, the Dulong-Petit law for the specific heat

$$C_V \simeq 3\, knN_A \,. \tag{2.36}$$

The frequency distribution function plays also an important role in the Debye-Waller factor e^{-2W}. For the case of a cubic crystal with one atom per primitive unit cell 2W can be written [6,7] as

$$2W = \frac{\hbar Q^2}{3M} \int_0^\infty \left(\frac{1}{\exp(h\nu/kT)-1} + \tfrac{1}{2} \right) \frac{f(\nu)}{2\pi\nu}\, d\nu \,, \tag{2.37a}$$

or

$$2W = R.C(T) \,. \tag{2.37b}$$

$R = \hbar^2 Q^2/2M$ is the recoil energy of a free scattering atom and

$$C(T) = \frac{2}{3h} \int_0^\infty \left(\frac{1}{\exp(h\nu/kT)-1} + \tfrac{1}{2} \right) \frac{f(\nu)}{\nu}\, d\nu \,. \tag{2.38}$$

The Debye-Waller factor will be discussed in more detail in connexion with neutron scattering in the next chapter.

2.4. Long wavelength vibrations and the elastic stiffness constants

In the limit of infinitely long waves the atoms in a unit cell move in parallel with zero frequency in the case of the acoustical modes. For very small but finite values of the wave vector $\underline{q}$ this is still approximately true. Such low frequency vibrations correspond to sound waves in the crystal. Since the frequencies of sound waves in a solid are determined by the macroscopic elastic constants and the frequencies of the normal modes in a crystal by the atomic force constants, there must exist relations between the force constants $\Phi_{\alpha\beta}(\ell\lambda,\ell'\lambda')$ and the elastic (stiffness) constants $c_{\alpha\gamma,\beta\delta}$. These relations can be obtained by studying the equations of motion (2.18) in the long wavelength limit and comparing them with the corresponding equations from the theory of elasticity. For small values of $\underline{q}$ (2.18) can be solved by a perturbation method [2,3,8], originally due to Born [9], which here merely will be sketched.

Both sides of equation (2.18) are expanded in powers of $\underline{q}$, breaking off after the first three terms.
For $D_{\alpha\beta}(\lambda\lambda';\underline{q})$ we write using (2.15)

$$D_{\alpha\beta}(\lambda\lambda';\underline{q}) = D^{(0)}_{\alpha\beta}(\lambda\lambda';\underline{q}) + D^{(1)}_{\alpha\beta}(\lambda\lambda';\underline{q}) + D^{(2)}_{\alpha\beta}(\lambda\lambda';\underline{q}) + \ldots , \tag{2.39}$$

with

$$D^{(0)}_{\alpha\beta}(\lambda\lambda';\underline{q}) = \left(M(\lambda)M(\lambda')\right)^{-\frac{1}{2}} \sum_{\ell'} \Phi_{\alpha\beta}(\ell\lambda;\ell'\lambda') , \tag{2.40a}$$

$$D^{(1)}_{\alpha\beta}(\lambda\lambda';\underline{q}) = -i\left(M(\lambda)M(\lambda')\right)^{-\frac{1}{2}} \sum_{\ell'} \Phi_{\alpha\beta}(\ell\lambda;\ell'\lambda')\left[\underline{q}\cdot\left(\underline{r}(\ell)-\underline{r}(\ell')\right)\right], \tag{2.40b}$$

$$D^{(2)}_{\alpha\beta}(\lambda\lambda';\underline{q}) = -\tfrac{1}{2}\left(M(\lambda)M(\lambda')\right)^{-\frac{1}{2}} \sum_{\ell'} \Phi_{\alpha\beta}(\ell\lambda;\ell'\lambda')\left[\underline{q}\cdot\left(\underline{r}(\ell)-\underline{r}(\ell')\right)\right]^2. \tag{2.40c}$$

The expansions for $\omega_j(\underline{q})$ and $e_{\alpha j}(\lambda;\underline{q})$ are

$$\omega_j(\underline{q}) = \omega^{(0)}_j(\underline{q}) + \omega^{(1)}_j(\underline{q}) + \omega^{(2)}_j(\underline{q}) + \ldots , \tag{2.41}$$

$$e_{\alpha j}(\lambda;\underline{q}) = e^{(0)}_{\alpha j}(\lambda;\underline{q}) + e^{(1)}_{\alpha j}(\lambda;\underline{q}) + e^{(2)}_{\alpha j}(\lambda;\underline{q}) + \ldots , \tag{2.42}$$

For acoustic vibrations the zeroth order term $\omega^{(0)}(\underline{q}) = 0$. As a consequence of the fact that terms of the same order on both sides of (2.18) have to be equal, it follows that the zeroth and first order terms are zero. Hence

$$\sum_{\lambda'\beta} D^{(0)}_{\alpha\beta}(\lambda\lambda';\underline{q})\, e^{(0)}_{\beta j}(\lambda';\underline{q}) = 0 \tag{2.43a}$$

$$\sum_{\lambda'\beta} \{D^{(0)}_{\alpha\beta}(\lambda\lambda';\underline{q})\, e^{(1)}_{\beta j}(\lambda';\underline{q}) + D^{(1)}_{\alpha\beta}(\lambda\lambda';\underline{q})\, e^{(0)}_{\beta j}(\lambda';\underline{q})\} = 0. \tag{2.43b}$$

For the second order terms the following relation holds

$$\sum_{\lambda'\beta} \Big[D^{(0)}_{\alpha\beta}(\lambda\lambda';\underline{q})\, e^{(2)}_{\beta j}(\lambda';\underline{q}) + D^{(1)}_{\alpha\beta}(\lambda\lambda';\underline{q})\, e^{(1)}_{\beta j}(\lambda';\underline{q}) + D^{(2)}_{\alpha\beta}(\lambda\lambda';\underline{q})\, e^{(0)}_{\beta j}(\lambda';\underline{q})\Big] = \omega^{(1)2}_j(\underline{q})\, e^{(0)}_{\alpha j}(\lambda;\underline{q}). \tag{2.43c}$$

section 2.4.

From (2.5) and (2.40) it is clear that (2.43a) has solutions $e^{(0)}_{\beta j}(\lambda';\underline{q}) \equiv M(\lambda')^{\frac{1}{2}} \cdot e_{\beta j}(\underline{q})$, with $e_{\beta j}(\underline{q})$ independent of λ'. The $\underline{q}$-dependence will be determined below from a simplified version of (2.43c). (2.43b) represents a system of 3n inhomogeneous linear equations for the vectors $\underline{e}^{(1)}_j(\lambda';\underline{q})$, when the $\underline{e}^{(0)}_j(\lambda';\underline{q})$ are known. (2.43c) can be simplified by multiplying by $M(\lambda)^{\frac{1}{2}}$ and then summing over λ. The first term then vanishes because of (2.5), (2.8) and (2.40a). Hence (2.43c) transforms into

$$\sum_{\lambda\lambda'\beta} M(\lambda)^{\frac{1}{2}}\left[D^{(1)}_{\alpha\beta}(\lambda\lambda';\underline{q})e^{(1)}_{\beta j}(\lambda';\underline{q}) + M(\lambda')^{\frac{1}{2}}D^{(2)}_{\alpha\beta}(\lambda\lambda';\underline{q})e_{\beta j}(\underline{q})\right] =$$

$$= \sum_{\lambda} M(\lambda)\omega^{(1)2}_j(\underline{q})e_{\alpha j}(\underline{q}). \qquad (2.43d)$$

Inserting the solution for the $\underline{e}^{(1)}_j(\lambda';\underline{q})$ in (2.43d) provides the final set of inhomogeneous equations for the $\underline{e}_j(\underline{q})$. If we further devide by V_o, the volume of the unit cell, (2.43d) transforms into the general form

$$K(\underline{q}) \cdot \underline{e}_j(\underline{q}) = \rho\omega^2_j(\underline{q}) \cdot \underline{e}_j(\underline{q}) \ . \qquad (2.44)$$

$\rho = \sum_{\lambda} M(\lambda)/V_o$, the macroscopic density.

Equation (2.44) is directly comparable with the macroscopic equation describing elastic waves

$$K'(\underline{q}) \cdot \underline{e} = \rho\omega^2\underline{e} \ , \qquad (2.45)$$

where

$$K'_{\alpha\beta} = \sum_{\gamma\delta} c_{\alpha\gamma,\beta\delta}\, \underline{q}_\gamma\, \underline{q}_\delta \ . \qquad (2.46)$$

$c_{\alpha\gamma,\beta\delta}$, the elastic constants, are the coefficients occurring in the generalised Hooke's law, which gives the linear relationship between the elastic stress and the elastic strain components. Written in tensor notation

$$S_{\alpha\gamma} = \sum_{\beta\delta} c_{\alpha\gamma,\beta\delta}\, s_{\beta\delta} \ . \qquad (2.47)$$

The elastic constants in the more familiar Voigt notation with single indices are obtained from those in tensor notation by a simple transcription of the indices, $(\alpha\gamma) \rightarrow \mu$, according the following scheme

Pair of indices:	$\alpha\gamma$	11	22	33	23(32)	31(13)	12(21)
Single index :	μ	1	2	3	4	5	6

By equating the coefficients of same orders of $\underline{q}$ in (2.44) and (2.45) one readily obtains the relations between the elastic constants and the interatomic force constants.

references II

References

1. M. Born and T. von Kármán, Physik. Z., 13 (1912), 297.
2. Max Born and Kun Huang, Dynamical Theory of Crystal Lattices, First edition, Clarendon Press, Oxford, 1956.
3. A.A. Maradudin, E.W. Montroll and G.H. Weiss, "Theory of lattice dynamics in the harmonic approximation" in Solid State Physics ed. by F. Seitz and D. Turnbell, Academic Press, New York, 1963.
4. A.A. Maradudin and S.H. Vosko, Revs. Mod. Phys., 40 (1968), 1.
5. B.R.A. Nijboer and J.J.J. Kokkedee, Ned. T. Natuurk., 29 (1963), 61.
6. R.E. DeWames, T. Wolfram, and G.W. Lehman, Phys. Rev., 131 (1963), 528.
7. R.W. James, The Optical Principles of the Diffraction of X-Rays, G. Bell and Sons, London, 1953.
8. L. Merten, Z. Naturforschg., 13a (1958), 662.
9. M. Born, Atomtheory des Festen Zustandes, second edition, Teubner, 1923.

Chapter III

THEORY OF NEUTRON SCATTERING BY LATTICES

3.1. Introduction

The interaction involved in scattering of thermal neutrons by bound atoms results mainly from two effects: a) the interaction of the neutron with nuclei via nuclear forces, b) the interaction of the neutron with unpaired electrons in atoms via magnetic forces due to the neutron magnetic moment. In this work only the nuclear scattering will be encountered.

Usually the theory of slow-neutron scattering by bound nuclei is discussed [1,2,3,4,5,6] in terms of the first Born approximation by introducing a special potential for the neutron-nucleus interaction. Although the nuclear interaction potential cannot be regarded as a small perturbation and the neutron wave function cannot be assumed to be a plane wave within the range of nuclear forces, it is, however, possible to calculate the scattering cross section by this approximation, because of the fact that the form of the cross section is determined by the behaviour of the wave function well away from the scattering centre. It is therefore possible to use the fact that the region within which the interaction works is very small, in fact in the calculation of the cross section it is put equal to zero. The form of the interaction potential is then chosen such that the correct answer is obtained for the experimentally determined scattering amplitude. In this approach the interaction between the neutron and the target nucleus can not be described by a true potential, but only by a delta-function of adjustable strength, the so-called Fermi pseudo-potential

$$V(\underline{r}) = \frac{2\pi\hbar^2 b}{m}\,\delta(\underline{r}). \tag{3.1}$$

b is the neutron scattering length (which may be complex) and m is the neutron mass. Such a "potential" leads to the required short range nature of the forces and thus to isotropy of the scattering. The asymptotic form of the neutron wave function at large distances is [5]

$$\psi_o + \psi_1 = e^{ik_o z} - \frac{b}{r}\,e^{ik'r}\quad, \tag{3.2}$$

section 3.1.

where Ψ_o represents the incident neutron wave function, and Ψ_1 the scattered one.

In case of scattering by a macroscopic system of nuclei, the total scattering may be evaluated by proper summation of independent but possibly coherent scattering from all nuclei present. Every nucleus ℓ is accounted for by a scattering Fermi pseudo-potential

$$V(\ell) = \frac{2\pi\hbar^2}{m} b(\ell)\delta\left(\underline{r}-\underline{r}'(\ell)\right) \quad , \tag{3.3}$$

where $\underline{r}'(\ell) = \underline{r}(\ell) + \underline{u}(\ell)$.
Schiff [7] gives for the cross section in first Born approximation for a process in which the scattering system goes from a quantum state p to a state p', while the neutron is scattered from $\underline{k}_o$ to $\underline{k}'$ ($\underline{k}_o$ and $\underline{k}'$ are neutron wave vectors) with spin state s to s'

$$\frac{d\sigma}{d\Omega}(ps\rightarrow p's') = \frac{k'}{k_o}\left(\frac{m}{2\pi\hbar^2}\right)^2 \left| \left\langle p's' \left| \int d\underline{r}\, e^{i\underline{Q}\cdot\underline{r}}\, V(\underline{r}) \right| ps \right\rangle \right|^2 . \tag{3.4}$$

$V(\underline{r})$ is the interaction potential, and $\underline{Q} = \underline{k}_o - \underline{k}'$ is the neutron scattering vector. k' must satisfy the condition for energy conservation

$$\frac{\hbar^2 k'^2}{2m} + E_{p'} = \frac{\hbar^2 k_o^2}{2m} + E_p \quad , \tag{3.5}$$

where E_p and $E_{p'}$ are the total energies of the state before and after scattering, respectively.

To obtain the double differential cross section we must sum over all final states p',s' and average over the states p,s, weighted according to their probabilities P_p and P_s ,

$$\frac{d^2\sigma}{d\Omega dE} = \sum_{ps} P_p P_s \sum_{p's'} \frac{k'}{k_o}\left(\frac{m}{2\pi\hbar^2}\right)^2 \left| \left\langle p's' \left| \int d\underline{r} e^{i\underline{Q}\cdot\underline{r}}\, V(\underline{r}) \right| ps \right\rangle \right|^2 \cdot$$

$$\cdot\, \delta\left\{ \frac{\hbar^2 k'^2}{2m} + E_{p'} - \frac{\hbar^2 k_o^2}{2m} - E_p \right\} . \tag{3.6}$$

In the equilibrium state P_p is given by the Boltzmann distribution,

$$P_p = \frac{\exp\left(-E_p/(kT)\right)}{\sum_p \exp\left(-E_p/(kT)\right)} \quad . \tag{3.7}$$

For an unpolarised neutron beam

$$P_s = \tfrac{1}{2} \quad . \tag{3.8}$$

3.2. Elastic scattering

When we restrict ourselves to nuclear scattering we can evaluate the matrix elements of (3.6) by substitution for the potential $V(\underline{r})$ the one given by (3.3) summed over ℓ. Equation (3.6) then becomes

$$\frac{d^2\sigma}{d\Omega dE} = \sum_{ps} P_p P_s \sum_{p's'} \frac{k'}{k_o} \left| \left\langle p's' \left| \sum_\ell b(\ell) e^{i\underline{Q}\cdot\underline{r}'(\ell)} \right| ps \right\rangle \right|^2 \cdot$$

$$\cdot\, \delta\left\{ \frac{\hbar^2 k'^2}{2m} + E_{p'} - \frac{\hbar^2 k_o^{\,2}}{2m} - E_p \right\} \quad . \tag{3.9}$$

In the case of scattering by a rigid lattice, where $\underline{u}(\ell) = 0$, there is no energy transfer from the neutrons to the lattice or oppositely. Thus the scattering is elastic and $k' = k_o$. Writing $\underline{r}'(\ell) = \underline{r}(\ell)$ and summing over p',s', we obtain by closure

$$\frac{d\sigma}{d\Omega} = \sum_{ps} P_p P_s \sum_{p's'} \left\langle ps \left| \sum_{\ell'} b^*(\ell') e^{-i\underline{Q}\cdot\underline{r}(\ell')} \right| p's' \right\rangle \left\langle p's' \left| \sum_\ell b(\ell) e^{i\underline{Q}\cdot\underline{r}(\ell)} \right| ps \right\rangle$$

$$= \sum_{\ell\ell'} \exp\left[i\underline{Q}\cdot\left(\underline{r}(\ell) - \underline{r}(\ell')\right) \right] \left\langle b^*(\ell') b(\ell) \right\rangle \quad , \tag{3.10}$$

where $\langle b^*(\ell')\, b(\ell) \rangle$ means the average value of $b^*(\ell')\, b(\ell)$.

Let us consider that the lattice contains one atomic species only. Then in general $b(\ell)$ is dependent upon the actual isotope and nuclear spin orientation present at $\underline{r}(\ell)$. We assume further that there is no correlation between $b(\ell)$ and $b(\ell')$ if ℓ and ℓ' are different.

section 3.2.

In this case we have

$$\langle b(\ell)b^*(\ell')\rangle = \langle b(\ell)\rangle\langle b^*(\ell')\rangle = |\langle b\rangle|^2 \quad , \quad \text{if } \ell \neq \ell', \tag{3.11a}$$

$$= \langle|b(\ell)|^2\rangle = \langle|b^2|\rangle \quad , \quad \text{if } \ell = \ell'. \tag{3.11b}$$

This we can write as

$$\langle b(\ell)b^*(\ell')\rangle = |\langle b\rangle|^2 + \{\langle|b|^2\rangle - |\langle b\rangle|^2\}\,\delta_{\ell\ell'} \, . \tag{3.11c}$$

By substitution of (3.11) in (3.10) we may split the differential cross section $d\sigma/d\Omega$ in a coherent and an incoherent part

$$\frac{d\sigma}{d\Omega} = \left(\frac{d\sigma}{d\Omega}\right)_{coh} + \left(\frac{d\sigma}{d\Omega}\right)_{inc} \quad , \tag{3.12a}$$

where

$$\left(\frac{d\sigma}{d\Omega}\right)_{coh} = |\langle b\rangle|^2 \left|\sum_{\ell} e^{i\underline{Q}\cdot\underline{r}(\ell)}\right|^2 \quad , \tag{3.12b}$$

and

$$\left(\frac{d\sigma}{d\Omega}\right)_{inc} = N\{\langle|b|^2\rangle - |\langle b\rangle|^2\} \, . \tag{3.12c}$$

For scattering vectors $\underline{Q}$ equal to 2π times a reciprocal lattice vector $\underline{\tau}$, for which $\exp\left(2\pi i\underline{\tau}\cdot\underline{r}(\ell)\right)=1$ (see (2.11), (2.12) and (2.13)), the expression $\left|\sum_{\ell} \exp\left[i\underline{Q}\cdot\underline{r}(\ell)\right]\right|^2$ is equal to N^2. As $\underline{Q}$ moves away from a reciprocal lattice point this factor rapidly drops to zero. Consequently the $(d\sigma/d\Omega)$coh shows strong interference in certain directions, the maximum value being proportional to $|\langle b\rangle|^2$. The $(d\sigma/d\Omega)$coh represents the well-known Laue-Bragg scattering. It is interesting to note that it is only the mean scattering potential which gives rise to interference effects. The deviations from the mean potential, which are randomly distributed, can not lead to interference effects and hence cause the incoherent scattering.

3.3. Inelastic scattering

We will now evaluate the double differential cross section (3.9) including energy transfer. We consider a harmonic crystal in which $\underline{r}'(\ell)$ is time dependent

$$\underline{r}'(\ell,t) = \underline{r}(\ell) + \underline{u}(\ell,t) \ . \tag{3.13}$$

Furthermore we write the delta-function for the energy in (3.9) as an integral

$$\delta\left\{\frac{\hbar^2 k'^2}{2m} - \frac{\hbar^2 k_o^2}{2m} + E_{p'} - E_p\right\} = \frac{1}{2\pi\hbar}\int_{-\infty}^{\infty} \exp\left[-i\omega t + i\frac{E_{p'}-E_p}{\hbar}t\right] dt, \tag{3.14}$$

where

$$\omega = \frac{\hbar}{2m}(k_o^2 - k'^2). \tag{3.15}$$

We now introduce the time-dependent Heisenberg operators

$$T_{\underline{Q}}(t) = \exp\left(\frac{itH}{\hbar}\right) T_{\underline{Q}} \exp\left(-\frac{itH}{\hbar}\right) \ , \tag{3.16}$$

where

$$T_{\underline{Q}} = \sum_{\ell} b(\ell)\exp\left(i\underline{Q}\cdot\underline{r}'(\ell)\right) \tag{3.17}$$

and H is the hamiltonian for the lattice vibrations.

Then

$$\exp\left\{i(E_{p'}-E_p)t/\hbar\right\}\langle p's'|T_{\underline{Q}}|ps\rangle = \langle p's'|T_{\underline{Q}}(t)|ps\rangle \ . \tag{3.18}$$

With the help of (3.14) and (3.18) and making use of the closure procedure we find that (3.9) transforms into

$$\frac{d^2\sigma}{d\Omega dE} = \frac{k'}{2\pi\hbar k_o}\int_{-\infty}^{\infty} dt\ e^{-i\omega t}\langle T_{\underline{Q}}^*(0)\ T_{\underline{Q}}(t)\rangle_T \ , \tag{3.19}$$

where

$$\langle T_{\underline{Q}}^*(0)T_{\underline{Q}}(t)\rangle_T = \sum_{ps} P_p P_s \langle ps|T_{\underline{Q}}^*(0)T_{\underline{Q}}(t)|ps\rangle \tag{3.20}$$

section 3.3.

means the thermal average of $T^{*}_{\underline{Q}}(0)T_{\underline{Q}}(t)$.

Let us now assume for simplicity that we have a random distribution of the isotopes and spin orientations over the lattice sites of a harmonic crystal, which has one atom per primitive cell only. Using (3.13) we find for (3.19)

$$\frac{d^2\sigma}{d\Omega dE} = (\langle b^2\rangle - \langle b\rangle^2)\frac{Nk'}{2\pi\hbar k_o}\int_{-\infty}^{\infty} dt\, e^{-i\omega t}\langle \exp\{-i\underline{Q}\cdot\underline{u}(0,0)\}\exp\{i\underline{Q}\cdot\underline{u}(0,t)\}\rangle_T$$

$$+ \langle b\rangle^2 \frac{Nk'}{2\pi\hbar k_o}\int_{-\infty}^{\infty} dt\, e^{-i\omega t}\sum_{\ell}\langle \exp\{-i\underline{Q}\cdot\underline{u}(0,0)\}\exp\{i\underline{Q}\cdot\underline{u}(\ell,t)\}\rangle_T e^{i\underline{Q}\cdot\underline{r}(\ell)}\ , \tag{3.21}$$

where the cross section again has been split up in an incoherent and a coherent part (cf. (3.12) for elastic scattering). The thermal averages in (3.21) can be calculated by means of Bloch's theorem [8]. This theorem states for a harmonic crystal

$$\langle \exp\left\{i\underline{Q}\cdot\left(\underline{u}(\ell)-\underline{u}(\ell')\right)\right\}\rangle_T = \exp\left\{-\tfrac{1}{2}Q^2\langle u^2(\ell\ell'\underline{Q})\rangle_T\right\}\ , \tag{3.22}$$

where $u(\ell\ell'\underline{Q})$ is the component of the vector $\underline{u}(\ell) - \underline{u}(\ell')$ along the vector $\underline{Q}$.

In the quantum mechanical treatment of the lattice vibrations (cf. section 2.3) the $\underline{u}(\ell,t)$ are operators and we may write

$$\langle \exp\{-i\underline{Q}\cdot\underline{u}(0,0)\}\exp\{i\underline{Q}\cdot\underline{u}(\ell,t)\}\rangle_T =$$

$$= \exp\left\{\tfrac{1}{2}\left[\underline{Q}\cdot\underline{u}(0,0),\underline{Q}\cdot\underline{u}(\ell,t)\right]\right\}\langle \exp\left\{i\underline{Q}\cdot\left(\underline{u}(\ell,t)-\underline{u}(0,0)\right)\right\}\rangle_T\ . \tag{3.23}$$

Here the term between square brackets is the commutator of the two operators. Equation (3.23) actually states Hausdorff's theorem [9], which is valid when the commutator is a number. Combining (3.22) and (3.23) we readily arrive at

$$< \exp\left\{-i\underline{Q}\cdot\underline{u}(0,0)\right\}\exp\left\{i\underline{Q}\cdot\underline{u}(\ell,t)\right\} >_T =$$

$$= \exp\left\{-<(\underline{Q}\cdot\underline{u}(0,0))^2>_T + <(\underline{Q}\cdot\underline{u}(0,0))(\underline{Q}\cdot\underline{u}(\ell,t))>_T\right\}$$

$$\equiv \exp\left\{-\sum_{\alpha\beta}(M_{\alpha\beta}(0,0) - M_{\alpha\beta}(\ell,t))Q_\alpha Q_\beta\right\} , \qquad (3.24)$$

where α,β stands for x,y,z.
We note that

$$-\sum_{\alpha\beta} M_{\alpha\beta}(0,0)Q_\alpha Q_\beta \equiv -2W(\underline{Q}) , \qquad (3.25)$$

is the exponent in the so-called Debye-Waller factor $\exp(-2W(\underline{Q}))$.

Combination of (3.21), (3.24) and (3.25) results in

$$\left(\frac{d^2\sigma}{d\Omega dE}\right)_{coh} = <b>^2 \frac{Nk'}{2\pi\hbar k_o} e^{-2W(\underline{Q})} \sum_\ell e^{i\underline{Q}\cdot\underline{r}(\ell)} \int_{-\infty}^{\infty} dt\, e^{-i\omega t} \cdot$$

$$\cdot \exp\left(\sum_{\alpha\beta} M_{\alpha\beta}(\ell,t)Q_\alpha Q_\beta\right) . \qquad (3.26)$$

and

$$\left(\frac{d^2\sigma}{d\Omega dE}\right)_{inc} = (<b^2>-<b>^2) \frac{Nk'}{2\pi\hbar k_o} e^{-2W(\underline{Q})} \int_{-\infty}^{\infty} dt\, e^{-i\omega t} \exp\left(\sum_{\alpha\beta} M_{\alpha\beta}(0,t)Q_\alpha Q_\beta\right) . \qquad (3.27)$$

3.4. Phonon expansion

In order to perform the integration over t in (3.26) and (3.27) we expand $\exp\left(\sum_{\alpha\beta} M_{\alpha\beta}Q_\alpha Q_\beta\right)$ in a power series. This leads to the so-called phonon expansion, the first term of which describes the elastic scattering processes, and the second term the inelastic processes, in which a single phonon is created or annihilated. The higher-order terms represent the multi-phonon processes. Before doing this we first rewrite $M_{\alpha\beta}(\ell,t)$ in a more explicit form. With the help of (2.27), (2.28), (2.31), (2.32) and (3.24) one readily obtains

section 3.4.

$$M_{\alpha\beta}(\ell,t) = \frac{\hbar}{2NM} \sum_{\underline{q}} \sum_{j=1}^{3} e^{*}_{\alpha j}(\underline{q}) e_{\beta j}(\underline{q}) e^{i\underline{q}\cdot\underline{r}(\ell)} \cdot$$

$$\cdot \left\{ \coth\left(\omega_j(\underline{q})/(2kT)\right) \frac{\cos\left(\omega_j(\underline{q})t\right)}{\omega_j(\underline{q})} + \frac{i \sin\omega_j(\underline{q})t}{\omega_j(\underline{q})} \right\} , \qquad (3.28)$$

where λ has been omitted in $\underline{e}_j(\lambda;\underline{q})$ because the crystal has only one atom per primitive unit cell. For macroscopic crystals the summation over $\underline{q}$ may be replaced by an integration over the first Brillouin zone [10]) according to the rule

$$\sum_{\underline{q}} f(\underline{q}) \simeq \frac{NV_o}{8\pi^3} \int d\underline{q} f(\underline{q}) , \qquad (3.29)$$

where V_o is the volume of the unit cell. Furthermore

$$(2\pi\hbar)^{-1} \int_{-\infty}^{\infty} e^{-i\omega t} dt = \delta(\hbar\omega) \qquad (3.30)$$

and

$$\sum_{\ell} e^{i\underline{Q}\cdot\underline{r}(\ell)} = \frac{8\pi^3}{V_o} \sum_{h} \delta\left(\underline{Q}-2\pi\underline{\tau}(h)\right) , \qquad (3.31)$$

where $\underline{\tau}(h)$ is a reciprocal lattice vector as defined in (2.12). Combining (3.28), (3.29), (3.30) and (3.31) with (3.26) and (3.27) we obtain

$$\left(\frac{d^2\sigma}{d\Omega dE}\right)_{coh} = N\langle b\rangle^2 \frac{k'}{k_o} e^{-2W(\underline{Q})} \left[\frac{8\pi^3}{V_o} \sum_{h} \delta\left(\underline{Q}-2\pi\underline{\tau}(h)\right) \delta(\hbar\omega) + \right.$$

$$+ \frac{\hbar}{4M} \sum_{j,\varepsilon} \int d\underline{q} |\underline{Q}\cdot\underline{e}_j(\underline{q})|^2 \omega_j^{-1}(\underline{q}) \left\{ \coth\left(\tfrac{1}{2}\hbar\beta\omega_j(\underline{q})\right) + \varepsilon \right\} \cdot$$

$$\cdot \sum_{h} \delta\left(\underline{Q}-2\pi\underline{\tau}(h)-\varepsilon\underline{q}\right) \delta\left(\hbar\omega-\varepsilon\hbar\omega_j(\underline{q})\right) +$$

$$\left. + \text{coherent multi-phonon processes} \right] , \qquad (3.32)$$

and

$$\left(\frac{d^2\sigma}{d\Omega dE}\right)_{inc} = N\left(\langle b^2\rangle - \langle b\rangle^2\right) \frac{k'}{k_o} e^{-2W(\underline{Q})} \Big[\delta(\hbar\omega) +$$

$$+ \frac{\hbar V_o}{32\pi^3 M} \sum_{j,\varepsilon} \int d\underline{q} \left|\underline{Q}\cdot\underline{e}_j(\underline{q})\right|^2 \omega_j^{-1}(\underline{q}) \left\{\coth\left(\tfrac{1}{2}\hbar\beta\omega_j(\underline{q})\right) + \varepsilon\right\} \cdot$$

$$\cdot\, \delta\left(\hbar\omega - \varepsilon\hbar\omega_j(\underline{q})\right) + \text{incoherent multi-phonon processes}\Big]. \quad (3.33)$$

Here ε can only have the value +1 and -1, corresponding respectively to the creation and annihilation of a single phonon by the neutron, $\beta = 1/(kT)$.

The first terms of (3.32) and (3.33) are equivalent to the expressions (3.12b,c) for the elastic scattering, except for the factor $\exp\left[-2W(\underline{Q})\right]$. Thus we see that if one takes into account the lattice vibrations, but neglects energy transfer between neutron and lattice a reduction of the cross section results by a factor $\exp\left[-2W(\underline{Q})\right]$ compared to the scattering formula for the rigid lattice. The result obtained by cutting off the expansion after the first term is usually indicated as the static approximation.

3.5. One-phonon scattering

For the investigation of the lattice dynamics of crystals the single phonon or one-phonon processes are of extreme importance.

Placzek and van Hove [11]) have shown that in cases where the phonon frequencies $\omega_j(\underline{q})$ are independent of the polarisation suffix j it is possible to replace the integration over $\underline{q}$ in the second term of (3.33) by an integration over ω using the frequency distribution function defined in (2.33). The result is that the incoherent cross section for single phonon processes is directly proportional to $f(\nu)$. Actually, it can be shown [7,12]) that for cubic crystals with polarisation dependent frequencies this cross section has the same simple form. This provides, in principle, a direct method for measurement of the frequency distribution function, which thermodynamically is very important.

section 3.5.

In practice, however, the relation is much less simple because of multi-phonon processes and coherent scattering.

More reliable results may be obtained by means of one-phonon coherent scattering experiments. The coherent cross section for single phonon processes (3.32) is only non-zero if

$$\hbar\omega = \frac{\hbar^2}{2m}\,(k_o^{\,2}-k'^2) = \varepsilon\hbar\omega_j(\underline{q}) \tag{3.34a}$$

and

$$\underline{Q} = \underline{k}_o - \underline{k}' = \varepsilon\underline{q} + 2\pi\underline{\tau}(h) \tag{3.34b}$$

are satisfied simultaneously, thus providing a direct method for measurement of the dispersion relations $\omega_j(\underline{q})$. Expression (3.34a) represents the law of conservation of energy and (3.34b) is often interpreted as the law of conservation of quasi-momentum.
This direct method of determination of the dispersion laws for harmonic crystals has been applied in the experimental work described here, and therefore special attention will be paid to expressions (3.32) and (3.34). We split out from (3.32) the one-phonon part and write, using (2.32),

$$\left(\frac{d^2\sigma^{(1)}}{d\Omega dE}\right)_{coh} = N\,\langle b\rangle^2 \sum_{j,\varepsilon} \frac{\hbar k'}{4Mk_o\omega_j(\underline{q})}\, e^{-2W(\underline{Q})} \left|\underline{Q}\cdot\underline{e}_j(\underline{q})\right|^2 \cdot$$

$$\cdot \left\{ 2\langle n_j(\underline{q})\rangle + 1 + \varepsilon \right\} \delta\left(\hbar\omega - \varepsilon\hbar\omega_j(\underline{q})\right) \tag{3.35}$$

under the restriction (3.34b).

The intensity in a single peak is obtained by integration over the energy $E = \hbar^2k'^2/(2m)$, which results in the total cross section for a single phonon process

$$\left(\frac{d\sigma^{(1)}}{d\Omega}\right)_{coh} = N\,\langle b\rangle^2\, \frac{\hbar k'\{2\langle n_j(\underline{q})\rangle + 1 + \varepsilon\}}{4Mk_o\omega_j(\underline{q})\,|J_j|}\, |\underline{Q}\cdot\underline{e}_j(\underline{q})|^2 e^{-2W(\underline{Q})}\,, \tag{3.36}$$

where

$$|J_j| = \left|\frac{d\left(\hbar\omega - \varepsilon\hbar\omega_j(\underline{q})\right)}{dE}\right|_{\hbar\omega=\varepsilon\hbar\omega_j(\underline{q})} = \left|1 + \frac{\varepsilon\hbar}{2E}\,\underline{k}'\cdot\underline{\nabla}_{\underline{q}}\,\omega_j(\underline{q})\right| \tag{3.37}$$

is the Jacobian involved in this integration.

At low temperatures $\langle n_j(\underline{q})\rangle$ approaches zero and consequently the cross section for phonon annihilation ($\varepsilon = -1$) vanishes. In this case only experiments with energy loss of the neutrons are possible. Further it can be seen that $(d\sigma^{(1)}/d\Omega)$coh is inversely proportional with the frequency of the observed phonon and proportional with the square of the scalar product of the scattering vector $\underline{Q}$ of the neutron and the polarisation vector $\underline{e}$ of the phonon. The latter factor is of great importance in the choice of the experimental conditions.

3.6. Inelastic structure factor

In our treatment of neutron scattering, sofar, we considered for simplicity only lattices with one atom per primitive unit cell. The result for the more general case of more atoms per primitive unit cell can be obtained in an analogous but much more complicated manner. An expression corresponding to (3.35) is then [2,5]

$$\left(\frac{d^2\sigma^{(1)}}{d\Omega dE}\right)_{coh} = \sum_{j,\varepsilon} \frac{N\hbar k'}{4k_o\omega_j(\underline{q})} \left\{2\langle n_j(\underline{q})\rangle + 1 + \varepsilon\right\} \delta\left(\hbar\omega - \varepsilon\hbar\omega_j(\underline{q})\right) \cdot$$

$$\cdot \left| \sum_{\lambda} \langle b(\lambda)\rangle M(\lambda)^{-\frac{1}{2}} e^{-W_\lambda(\underline{Q})} e^{i\underline{Q}\cdot\underline{r}(\lambda)} \underline{Q}\cdot\underline{e}_j^*(\lambda;\underline{q}) \right|^2 \qquad (3.38)$$

where $\underline{r}(\lambda)$, the position vector in the unit cell is defined by $\underline{r}(\ell,\lambda) = \underline{r}(\ell) + \underline{r}(\lambda)$. In (3.38) is implied that $\varepsilon\underline{q} = \underline{Q} - 2\pi\underline{\tau}(h)$ is satisfied. We define the structure factor for one-phonon scattering by

$$g_s(\underline{Q}) \equiv \sum_{\lambda} \langle b(\lambda)\rangle M(\lambda)^{-\frac{1}{2}} e^{-W_\lambda(\underline{Q})} e^{i\underline{Q}\cdot\underline{r}(\lambda)} \underline{Q}\cdot\underline{e}_j^*(\lambda;\underline{q}) \quad . \qquad (3.39)$$

This we will call the "inelastic structure factor". For simple structures, such as usually dealt with in inelastic neutron scattering, it is meaningful to introduce a reduced structure factor, which under certain circumstances is a periodic function of $\underline{Q}$. In the directions of higher symmetry the polarisation vectors $\underline{e}_j(\lambda;\underline{q})$ for a particular mode are often all parallel. Put in formula

section 3.6.

$$\underline{e}_j(\lambda;\underline{q}) = c(\lambda;\underline{q})\underline{e}_j \quad . \tag{3.40}$$

The reduced structure factor $g_{sr}(\underline{Q})$ is now defined by

$$|g_{sr}(\underline{Q})|^2 \equiv \frac{\left|\sum_\lambda \langle b(\lambda)\rangle\, M(\lambda)^{-\frac{1}{2}}\, e^{i\underline{Q}\cdot\underline{r}(\lambda)}\, \underline{Q}\cdot\underline{e}_j^*(\lambda;\underline{q})\right|^2}{\sum_\lambda \left|\langle b(\lambda)\rangle\, M(\lambda)^{-\frac{1}{2}}\, \underline{Q}\cdot\underline{e}_j^*(\lambda;\underline{q})\right|^2} \tag{3.41}$$

If (3.40) is satisfied and furthermore all fractional atom coordinates are rational we have that

$$\left|g_{sr}(\underline{Q})\right|^2 = \left|g_{sr}(\underline{Q} \pm 2\pi\, \underline{\tau})\right|^2 , \tag{3.42}$$

$2\pi\underline{\tau}$ being vectors of the "structure lattice", which is defined by $\underline{\tau}\cdot\underline{r}(\lambda)$ = integer.

It is obvious that knowledge of the inelastic structure factor is of great importance for the measurement of the dispersion relations $\omega_j(\underline{q})$. As the Debye-Waller factor $\exp(-2W_\lambda)$ usually can be estimated the eigenvectors $\underline{e}_j(\lambda;\underline{q})$ constitute the big uncertainty in the inelastic structure factor, because they are dependent upon the dynamical behaviour of the specimen under investigation. It will be shown in chapter VI that the eigenvectors are to a large extent determined by symmetry and that a crude guess at the dynamics of the crystal provides sufficient initial information about the inelastic structure factor.

References

1. R. Weinstock, Phys. Rev., 65 (1944), 1.
2. I. Waller and P.O. Fröman, Arkiv fysik, 4 (1952), 183.
3. A. Sjölander, Arkiv Fysik, 7 (1957), 375.
" , " " , 13 (1958), 199, 215.
" , " " , 14 (1958), 315.
4. L.S. Kothari and K.S. Singwi, In Solid State Physics, 8, edited by F. Seitz and D. Turnbell, Academic Press inc., New York, 1958.
5. W.M. Lomer and G.G. Low, In Thermal Neutron Scattering, edited by P.A. Egelstaff, Academic Press Inc., London, 1965.
6. L. van Hove, Phys. Rev., 95 (1954), 249.
7. L.I. Schiff, Quantum Mechanics, second edition, Mc Graw-Hill, New York, 1955.
8. F. Bloch, Z. Phys., 74 (1932), 295.
9. A. Messiah, Quantum Mechanics, Vol.I, North-Holland Publishing Company, Amsterdam, 1961, 442.
10. B.R.A. Nijboer and J.J.J. Kokkedee, Ned. T. Natuurk., 29 (1963), 61.
11. G. Placzek and L. van Hove, Phys. Rev., 93 (1954), 1207.

Chapter IV

EXPERIMENTAL TECHNIQUE

4.1. Description of the principle of the triple-axis crystal spectrometer

For the study of coherent one-phonon neutron scattering the triple-axis crystal spectrometer has proved to be the most powerful instrument. In the literature [1,2]) excellent review articles can be found about the theory of this method, and comparisons between its performance and that of other instruments used in neutron scattering. Bergsma [3]) has given a rather detailed description of the triple-axis crystal spectrometer at one of the beam holes of the Petten H.F.R., which has been used for the experiments presented in chapter V and VI. For this reason we will confine ourselves to an outline of the method, giving only those details about the experimental set-up which are of importance for the understanding of the measurements.

A schematic diagram of the triple-axis spectrometer is given in fig. 4.1. A neutron beam from the reactor impinges on a monochromating crystal, which by Bragg reflection selects neutrons of energy E_o and wave vector $\underline{k}_o$ in the direction of the specimen. Neutrons, which are scattered by the specimen through an angle ϕ are analysed with respect to their energy E' (wave vector $\underline{k}'$) by Bragg reflection at the analyser crystal, which scatters neutrons obeying the Bragg condition into the neutron detector. Collimators may be placed at different positions in the beam in order to reduce the spread in direction and energy of the neutrons. It is possible to set automatically all four angles $2\theta_M$, $2\theta_A$, ϕ and Ψ, which are the scattering angle at the monochromator crystal, the analyser crystal

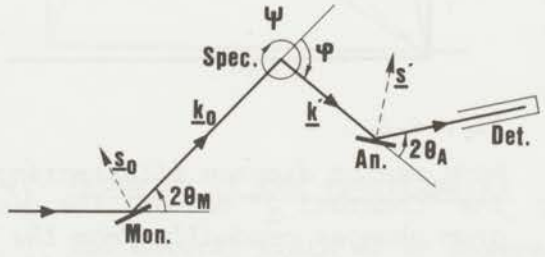

Fig. 4.1.

Schematic diagram of a triple-axis neutron crystal spectrometer. Mon.=monochromator crystal, An.=analyser crystal, Spec.=specimen and Det.=detector. $\underline{k}_o$ and $\underline{k}'$ are neutron wave vectors, $\underline{S}_o$ and $\underline{S}'$ are scattering vectors, $2\theta_M$, ϕ and $2\theta_A$ are scattering angles and Ψ is the orientation angle of the specimen.

and the specimen, and the orientation of the specimen in the horizontal plane, respectively.

For neutrons scattered as indicated in fig. 4.1 the wave vector diagram in reciprocal space is displayed in fig. 4.2. It is obvious from this diagram that by a proper choice of the different variables the experiment may be arranged to satisfy the conditions for conservation of energy and quasi-momentum, given in (3.34). For given $\underline{Q}$, for instance, it is possible by varying only two of the angles to obtain the situation that $\underline{k}_o - \underline{k}' = \underline{Q} = \underline{q} + 2\pi\underline{\tau}(h)$, *i.e.* the condition for conservation of quasi-momentum. After this has been realised one may vary the parameters

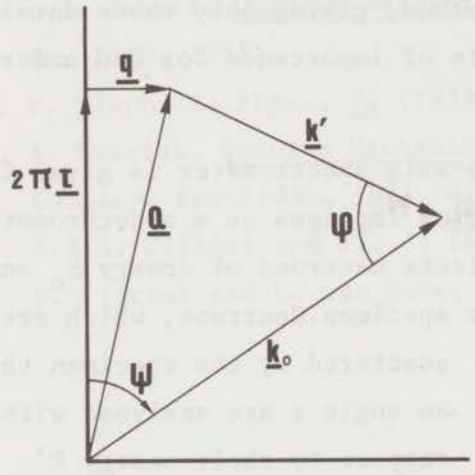

Fig. 4.2.

Wave vector diagram for a neutron scattering experiment corresponding to fig. 4.1. $\underline{\tau}$ is a reciprocal lattice vector, $\underline{q}$ the wave vector of a phonon.

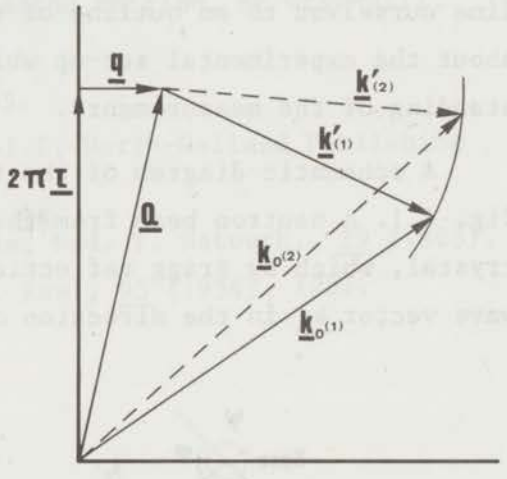

Fig. 4.3.

Wave vector diagram illustrating the "Constant $\underline{Q}$" method. The diagram changes gradually from the arrangement with $\underline{k}_o(1)$ and $\underline{k}'(1)$ to that of $\underline{k}_o(2)$ and $\underline{k}'(2)$. $\underline{Q}$ and $|\underline{k}'(1)| = |\underline{k}'(2)|$ remain fixed.

in the way as displayed in fig. 4.3. The length of $\underline{k}'$ is kept fixed, while its endpoint moves along a circle of radius k'. As soon as the energy conservation law $\hbar\omega \equiv \hbar^2/(2m)(k_o^2 - k'^2) = \pm\hbar\omega_j(\underline{q})$, is satisfied a peak in the scattered intensity may be observed. This mode of operation of the triple-axis spectrometer is called the "constant momentum transfer" or shortly "constant $\underline{Q}$" method [4]). The great virtue of this method is that the parameters, determining the energy transfer of the

section 4.2.

neutrons $\hbar\omega$, are varied without changing $(\underline{k}_o - \underline{k}')$. With this method it is therefore possible to observe phonons at any desired $\underline{q}$-value.

Other modes of operation are the "constant energy transfer"- and the "normal to the gradient" methods. In the first case k_o as well as k' are kept fixed, while $(\underline{k}_o - \underline{k})$ is changed in order to satisfy eqs. (3.34). In the latter method the path in reciprocal space is chosen in such a way that the scan in $(\omega - \underline{q})$-space is normal to the gradient of the observed dispersion relation. In the latter two methods it is to be understood that $\underline{q}$ is in the plane of $\underline{k}_o$ and $\underline{k}'$, the scattering plane. In fig. 4.4 the three scans in $(\omega - \underline{q})$-space are illustrated.

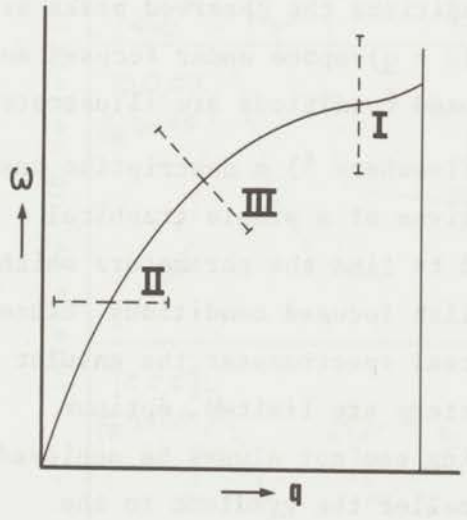

Fig. 4.4.

Paths in $(\omega - \underline{q})$-space of three different methods for observing the phonon dispersion relation with a triple-axis neutron crystal spectrometer. I: constant Q; II: constant energy; III: normal to the gradient.

4.2. Focusing of the spectrometer

The natural width of an observed phonon peak, which in the harmonic approximation would be a delta-function, is determined by the finite phonon lifetime. Additional broadening is caused by the experimental resolution and geometrical effects, the minimizing of which is usually referred to as focusing. The possibility of optimizing the experimental resolution by operating the spectrometer under focused conditions has been discussed by several authors [5,6,7,8]). The experimental resolution arises because of finite collimation and because of the mosaic spread of monochromating and analysing crystals. Hence for a particular scattering configuration, instead of one single

energy transfer, a certain range of energy transfers is possible for neutrons arriving at the detector. Because of the relation between the energy and direction of the neutrons at different positions of the scattering system, this range of energy transfer in (ω -$\underline{q}$)-space is an ellipsoid with a rather large ratio between the major and minor axes. The flexibility of a triple-axis crystal spectrometer often enables one to obtain a particular orientation of this ellipsoid at a given value of $\hbar\omega$ and ($\underline{k}_o$ - $\underline{k}'$) [6]. Operation under focused conditions means now that during a scan in (ω - $\underline{q}$)-space, the long axis is kept parallel to the gradient of the dispersion relation. Scattering is only observed when the ellipsoid coincides with the dispersion relation, and it is therefore obvious that under focused conditions the observed peaks are of minimum width. In fig. 4.5 scans in (ω - $\underline{q}$)-space under focused and defocused conditions are illustrated.

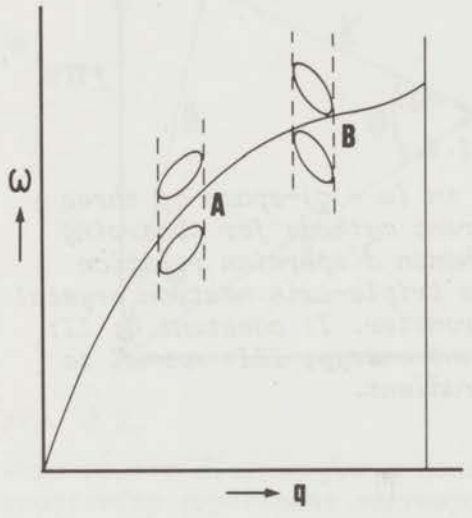

Fig. 4.5.

Illustration of the path in (ω-$\underline{q}$)-space for the observation of a phonon under focused (A) and under defocused (B) conditions of the spectrometer. Both paths correspond to a "constant Q" scan, but in case A the scattering ellipsoid is parallel to the gradient of the dispersion relation, while in case B it is perpendicular to it. This results in a sharp, high peak for case A and a low peak for case B.

Elsewhere [6] a description has been given of a simple graphical method to find the parameters which establish focused conditions. Since in a real spectrometer the angular parameters are limited, optimum focusing can not always be achieved. The smaller the gradient to the dispersion curve, the more difficult it is to obtain focused conditions. For zero gradient the scattering angles $2\Theta_M$ and $2\Theta_A$ have to be 180°, which is, of course, experimentally impossible.

In fig. 4.6 some selected phonon peaks in α-iron (see chapter V) are displayed. These phonons have been measured when the spectrometer setting in a varying degree was removed from complete focusing. The conditions for complete focusing [6] are

section 4.2.

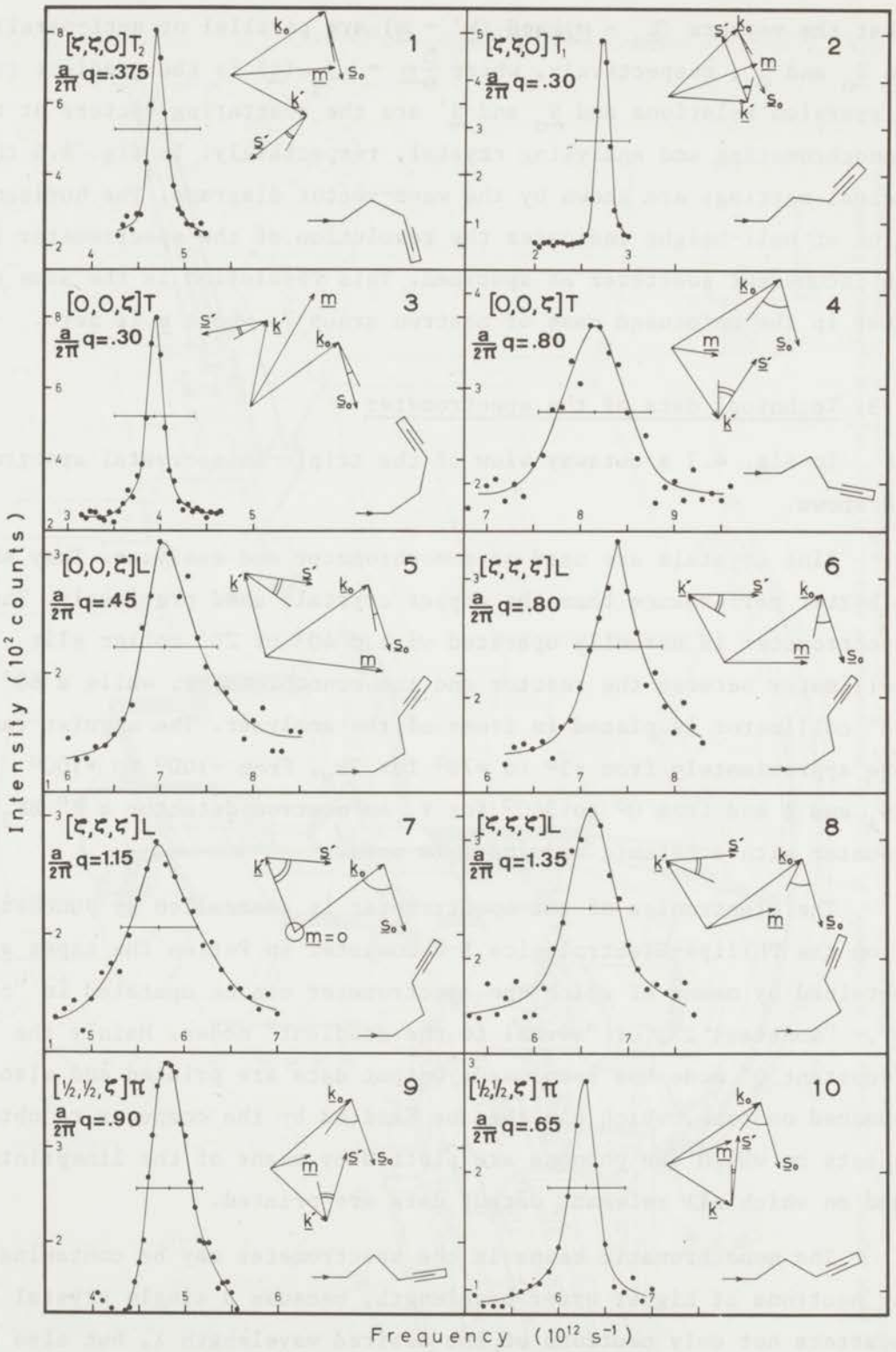

Fig. 4.6.

Some selected neutron groups due to scattering by phonons in α-Fe together with the corresponding wave vector diagrams and the scattering arrangements of the spectrometer. This picture illustrates qualitatively the dependence of the observed peak widths on the extent of focusing of the spectrometer: the smaller the angles between ($\underline{k}_o$-$\underline{m}$) and $\underline{S}_o$ and between ($\underline{k}'$-$\underline{m}$) and $\underline{S}'$, the smaller the peak width of the observed phonon. The horizontal line at half height of the peak indicates the line width for incoherent scattering.

that the vectors ($\underline{k}_o - \underline{m}$) and ($\underline{k}' - \underline{m}$) are parallel or anti-parallel to $\underline{S}_o$ and $\underline{S}'$, respectively, where $\frac{\hbar}{m}\underline{m} = \nabla_{\underline{q}}\omega(\underline{q})$ is the gradient to the dispersion relations and $\underline{S}_o$ and $\underline{S}'$ are the scattering vectors at the monochromating and analysing crystal, respectively. In fig. 4.6 the actual settings are shown by the wave-vector diagrams. The horizontal line at half-height indicates the resolution of the spectrometer for an incoherent scatterer as specimen. This resolution is the same as that in the unfocused case of neutron group 7, where $\underline{m}$ is zero.

4.3. Technical data of the spectrometer

In fig. 4.7 a cutaway view of the triple-axis crystal spectrometer is shown.

Zinc crystals are used as monochromator and analyser. They show a better performance than the copper crystals used previously. The spectrometer is normally operated with a 40' or 20' soller slit collimator between the reactor and the monochromator, while a 60' or 30' collimator is placed in front of the analyser. The angular ranges are approximately from -5° to +78° for $2\theta_M$, from -100° to +100° for $2\theta_A$ and ϕ and from 0° to 360° for Ψ. As neutron detector a 2" BF_3-counter with a ceramic endwindow is used.

The electronics of the spectrometer is controlled by punched tape. From the Philips-Electrologica X-8 computer in Petten the tapes are obtained by means of which the spectrometer can be operated in "constant $\underline{Q}$", "constant ω", or "normal to the gradient" modes. Mainly the "constant $\underline{Q}$" mode has been used. Output data are printed and also punched on tape, which can then be handled by the computer to obtain sheets on which the phonons are plotted by means of the lineprinter and on which all relevant output data are printed.

The monochromatic beams in the spectrometer may be contaminated by neutrons of higher order wavelength, because a single crystal scatters not only neutrons of the desired wavelength λ, but also those of wavelengths $\lambda/2$, $\lambda/3$, etc., if such neutrons are present. Since the spectrometer is always operated with energy loss of the scattered neutrons, especially the analyser crystal may suffer from second order

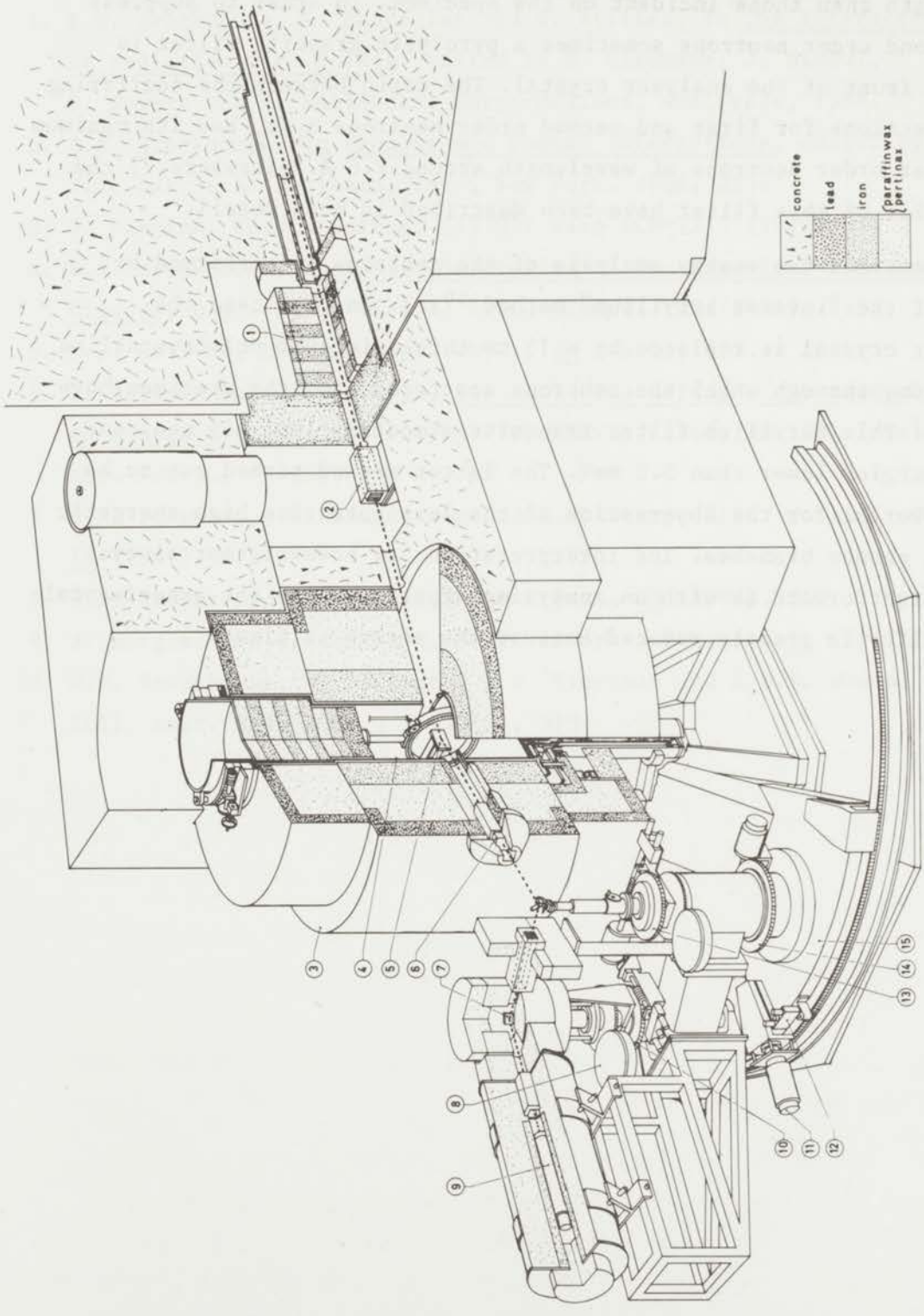

Fig. 4.7 A cutaway view of the triple-axis crystal spectrometer.

1: beam shutter, 2: Soller slit collimator, 3: rotating monochromator shield, 4: half-angling cylinder, 5: monochromator crystal, 6: monitor counter, 7: analyzer crystal, 8: analyzer half-angling gear box, 9: neutron counter, 10: gear for $2\theta_A$-motion, 11: driving motor $2\theta_M$, 12: digitizer, 13: gear for ψ-motion, 14: gear for ϕ-motion, 15: platform.

contamination, because it is adjusted to reflect neutrons of longer wavelength than those incident on the specimen. In order to suppress the second order neutrons sometimes a pyrolytic graphite filter is used in front of the analyser crystal. The ratio between the scattering cross sections for first and second order neutrons σ_1/σ_2 has its maximum for first order neutrons of wavelength around 2.6 Å. Elsewhere [9]) the properties of this filter have been described in more detail.

Sometimes the energy analysis of the neutrons is performed by means of the "inverse beryllium" method [10,3]). In that case the analyser crystal is replaced by a 15 cm thick piece of polycrystalline beryllium, through which the neutrons scattered from the specimen have to pass. This beryllium filter transmits almost exclusively neutrons with energies lower than 5.2 meV. The latter method turned out to be very powerful for the observation of the less intensive high energetic optical phonon branches. The interpretation is, however, not always as straightforward as with an analysing crystal, while the experimental flexibility is greatly reduced because the energy is fixed.

references IV

References

1. B.N. Brockhouse, S. Hautecler and H. Stiller, in The Interaction of Radiation with Solids, edited by R. Strumane, J. Nihoul, R. Gevers and S. Amelinckx, North-Holland, Amsterdam, 1964.
2. B.N. Brockhouse, in Phonons and Phonon Interactions, edited by T.A. Bak, W.A. Benjamin, Inc., New York, 1964, 221.
3. J. Bergsma, thesis Leiden, (1970); also RCN-121, (1970).
4. B.N. Brockhouse, Inelastic Scattering of Neutrons in Solids and Liquids, Proc. Symp. Vienna, 1960, Vienna, IAEA(1961), 113.
5. M.F. Collins, Brit.J. Appl. Phys., 14 (1963), 805.
6. J. Bergsma and C. van Dijk, Inelastic Scattering of Neutrons by Condensed Systems, Proc. Symp. Brookhaven, 1965, BNL940, (1966), 163; also RCN-34, (1965).
7. G.E. Peckham, D.H. Saunderson and R.I. Sharp, Brit. J. Appl. Phys., 18 (1967), 473.
8. M.J. Cooper and R. Nathans, Acta Cryst., 23 (1967), 357.
9. J. Bergsma and C. van Dijk, Nucl. Instr. and Meth., 51 (1967), 121.
10. B.N. Brockhouse, M. Sakamoto, R.N. Sinclair and A.D.B. Woods, Bull. Amer. Phys. Soc., 5 (1960), 373.

Chapter V

INVESTIGATION OF THE LATTICE DYNAMICS OF α-IRON

5.1. Introduction

Several authors have discussed the lattice dynamics of b.c.c. metals, and different attempts have been made to account for the effect of the conduction electrons [1]. For the case of α-iron, which has the b.c.c. structure, inclusion of this effect is rather difficult due to its complicated electronic structure. At the time that this investigation was started the experimental data about the phonon dispersion relations of α-iron consisted of the work by Curien [2], based on diffuse X-ray scattering, and the rather incomplete neutron scattering data by Iyengar *et al.* [3] and Low [4]. These data were rather inaccurate and could not be used for a detailed comparison with the different theoretical approaches. The reason for the lack of neutron data was the difficulty to obtain suitable samples, in spite of the excellent scattering properties for neutrons that result from the high coherent scattering cross section. The growing of single crystals of sufficient size and quality had been a major problem, stemming from the two phase transitions during cooling down from the melt, which can be seen in the phase diagram of iron [5]. Only recently a special technique has been developed to grow single crystals of sizes of the order of some cubic centimeters, needed in elastic neutron scattering experiments. As soon as such a crystal was at our disposal the measurements were started.

Since our first report [6] on the preliminary experimental results a large number of experimental neutron studies on α-iron were published [7,8,9,10], amongst which only those of Brockhouse *et al.*[7] and Minkiewicz *et al.*[8] are about as extensive as the one reported here. Therefore, in the discussion of our experimental results, attention will also be paid to their data.

5.2. Lattice dynamics of α-Fe in the Born-von Kármán model

Treatment of the lattice dynamics of α-Fe in the Born-von Kármán model following the line of chapter II is rather straightforward. The dynamical matrix is given by a simplified version of (2.15); because

section 5.2.

b.c.c. iron has only one atom per primitive unit cell there are no λ-indices. In the development of the dynamical matrix we shall include interactions out to fifth neighbours.

Symmetry considerations lead readily to the general form of the force constant matrices, which are the three times three matrices that contain the interatomic force constants $-\Phi_{\alpha\beta}$, defined in section 2.2. In table 5.1 these matrices are given for the interactions with the first five neighbours.

Table 5.1.

Force constant matrices for the first five neighbours in α-Fe.

s	atom position	r	n_s	force constant matrix
1	(111)a/2	$\frac{1}{2}a\sqrt{3}$	8	$\begin{pmatrix} \alpha_1 & \beta_1 & \beta_1 \\ \beta_1 & \alpha_1 & \beta_1 \\ \beta_1 & \beta_1 & \alpha_1 \end{pmatrix}$
2	(200)a/2	a	6	$\begin{pmatrix} \alpha_2 & 0 & 0 \\ 0 & \beta_2 & 0 \\ 0 & 0 & \beta_2 \end{pmatrix}$
3	(220)a/2	$a\sqrt{2}$	12	$\begin{pmatrix} \alpha_3 & \gamma_3 & 0 \\ \gamma_3 & \alpha_3 & 0 \\ 0 & 0 & \beta_3 \end{pmatrix}$
4	(311)a/2	$\frac{1}{2}a\sqrt{11}$	24	$\begin{pmatrix} \alpha_4 & \delta_4 & \delta_4 \\ \delta_4 & \beta_4 & \gamma_4 \\ \delta_4 & \gamma_4 & \beta_4 \end{pmatrix}$
5	(222)a/2	$a\sqrt{3}$	8	$\begin{pmatrix} \alpha_5 & \beta_5 & \beta_5 \\ \beta_5 & \alpha_5 & \beta_5 \\ \beta_5 & \beta_5 & \alpha_5 \end{pmatrix}$

The $-\Phi_{\alpha\beta}$ are replaced by α_s, β_s . . . *etc.*, according to the generally adopted convention [11]), where s indicates the neighbour concerned, n_s is the number of neighbours of a particular kind and r the distance to these neighbours. Since only symmetry considerations have been used, no assumptions have been made about the nature of the interatomic forces, *i.e.* we are dealing with general forces.

Inserting the data of table 5.1 in (2.15) leads to the expressions for the elements of the dynamical matrix given in table 5.2. Here the suffix i runs from 1 to 3, corresponding to x,y,z. The values i + n are to be counted modulo 3.

If the wave vector $\underline{q}$ of a phonon lies along one of the symmetry axes [100], [110] or [111], either the dynamical matrix is diagonal for all values of $\underline{q}$ or can be diagonalised by an appropriate rotation of axes [12]). Such phonons correspond to displacements in the lattice in which all atoms in a plane perpendicular to the symmetry axis move as a whole. Such a vibration can be considered as the motion of a one-dimensional lattice in which each point represents a plane of atoms in the three-dimensional lattice. It is straightforward to show that for the lattice vibrations in these directions the following relation holds [12,13])

$$M\omega_j^2 = \sum_n \phi_n{}^j \left[1 - \cos(n\pi q/q_{max})\right] \qquad (5.1)$$

where the $\phi_n{}^j$, which can be written as linear combinations of the interatomic force constants, must be interpreted as interplanar force constants for the j-th branch. q_{max} is a function of the direction.

In the symmetry directions exist purely longitudinal (polarisation vector along the direction of $\underline{q}$) and transverse (polarisation vectors perpendicular to $\underline{q}$) modes. For $\underline{q}$-vectors of the form [ζ00] and [$\zeta\zeta\zeta$] the transverse modes are degenerate.

For phonons with propagation vector of the form [$\zeta\zeta$1] and [$\frac{1}{2}\frac{1}{2}\zeta$] the dynamical matrix can also be diagonalised and similar relations, except for a constant term, as (5.1) hold, although this can not be associated with movements of planes of atoms as a whole.

section 5.2.

Table 5.2.

Coefficients of the dynamical matrix $D(\underline{q})$ for α-Fe with interactions out to fifth neighbours.

$$D_{ii}(\underline{q}) = 8\alpha_1(1 - C_iC_{i+1}C_{i+2})$$
$$+ 2\alpha_2(1 - C_{2,i}) + 2\beta_2(2 - C_{2,i+1} - C_{2,i+2})$$
$$+ 4\alpha_3\{2 - C_{2,i}(C_{2,i+1} + C_{2,i+2})\}$$
$$+ 4\beta_3(1 - C_{2,i+1}C_{2,i+2})$$
$$+ 8\alpha_4(1 - C_{3,i}C_{i+1}C_{i+2})$$
$$+ 8\beta_4\{2 - C_i(C_{3,i+1}C_{i+2} + C_{i+1}C_{3,i+2})\}$$
$$+ 8\alpha_5(1 - C_{2,i}C_{2,i+1}C_{2,i+2})$$

$$D_{i,i+1}(\underline{q}) = 8\beta_1 S_iS_{i+1}C_{i+2}$$
$$+ 4\gamma_3 S_{2,i}S_{2,i+1}$$
$$+ 8\gamma_4 S_iS_{i+1}C_{3,i+2}$$
$$+ 8\delta_4 C_{i+2}(S_{3,i}S_{i+1} + S_iS_{3,i+1})$$
$$+ 8\beta_5 S_{2,i}S_{2,i+1}C_{2,i+2}$$

where $C_i = \cos(\frac{aq_i}{2})$, $S_i = \sin(\frac{aq_i}{2})$

$$C_{m,i+n} = \cos(\frac{maq_{i+n}}{2}), \quad S_{m,i+n} = \sin(\frac{maq_{i+n}}{2}),$$

i = 1,2,3 means x,y,z. The suffix i+n is counted modulo 3.

The relations between the ϕ_n^j of these particular directions and the interatomic force constants are presented in table 5.3.

Table 5.3.

Relations between the interplanar force constants and the interatomic force constants including 5-th neighbours.

		α_1	β_1	α_2	β_2	α_3	β_3	γ_3	α_4	β_4	γ_4	δ_4	α_5	β_5
$[00\zeta]$ L	ϕ_1	+8	+0	+0	+0	+0	+0	+0	+0	+16	+0	+0	+0	+0
	ϕ_2	+0	+0	+2	+0	+8	+0	+0	+0	+0	+0	+0	+8	+0
	ϕ_3	+0	+0	+0	+0	+0	+0	+0	+8	+0	+0	+0	+0	+0
$[00\zeta]$ T	ϕ_1	+8	+0	+0	+0	+0	+0	+0	+8	+8	+0	+0	+0	+0
	ϕ_2	+0	+0	+0	+2	+4	+4	+0	+0	+0	+0	+0	+8	+0
	ϕ_3	+0	+0	+0	+0	+0	+0	+0	+0	+8	+0	+0	+0	+0
$[\zeta\zeta 0]$ L	ϕ_1	+4	+4	+2	+2	+4	+4	+0	+4	+8	+4	-8	+0	+0
	ϕ_2	+0	+0	+0	+0	+2	+0	+2	+4	+4	+0	+8	+4	+4
$[\zeta\zeta 0]$ T_1	ϕ_1	+4	-4	+2	+2	+4	+4	+0	+4	+8	-4	+8	+0	+0
	ϕ_2	+0	+0	+0	+0	+2	+0	-2	+4	+4	+0	-8	+4	-4
$[\zeta\zeta 0]$ T_2	ϕ_1	+4	+0	+0	+4	+8	+0	+0	+4	+8	+0	+0	+0	+0
	ϕ_2	+0	+0	+0	+0	+0	+2	+0	+0	+8	+0	+0	+4	+0
$[\zeta\zeta\zeta]$ L	ϕ_1	+6	-4	+0	+0	+0	+0	+0	+2	+4	+4	-8	+0	+0
	ϕ_2	+0	+0	+2	+4	+0	+0	+0	+0	+0	+0	+0	+6	-4
	ϕ_3	+2	+4	+0	+0	+0	+0	+0	+4	+8	-8	+0	+0	+0
	ϕ_4	+0	+0	+0	+0	+4	+2	+4	+0	+0	+0	+0	+0	+0
	ϕ_5	+0	+0	+0	+0	+0	+0	+0	+2	+4	+4	+8	+0	+0
	ϕ_6	+0	+0	+0	+0	+0	+0	+0	+0	+0	+0	+0	+2	+4
$[\zeta\zeta\zeta]$ T	ϕ_1	+6	+2	+0	+0	+0	+0	+0	+2	+4	-2	+4	+0	+0
	ϕ_2	+0	+0	+2	+4	+0	+0	+0	+0	+0	+0	+0	+6	+2
	ϕ_3	+2	-2	+0	+0	+0	+0	+0	+4	+8	+4	+0	+0	+0
	ϕ_4	+0	+0	+0	+0	+4	+2	-2	+0	+0	+0	+0	+0	+0
	ϕ_5	+0	+0	+0	+0	+0	+0	+0	+2	+4	-2	-4	+0	+0
	ϕ_6	+0	+0	+0	+0	+0	+0	+0	+0	+0	+0	+0	+2	-2
$[\frac{1}{2}\frac{1}{2}\zeta]$ Λ	ϕ_0	+8	+0	+0	+8	+16	+0	+0	+8	+16	+0	+0	+0	+0
	ϕ_2	+0	+0	+2	+0	-8	+0	+0	+0	+0	+0	+0	+8	+0
$[\frac{1}{2}\frac{1}{2}\zeta]$ Π	ϕ_0	+8	+8	+4	+4	+8	+8	+0	+8	+16	+8	-16	+0	+0
	ϕ_1	+0	-8	+0	+0	+0	+0	+0	+0	+0	+0	+16	+0	+0
	ϕ_2	+0	+0	+0	+2	-4	-4	+0	+0	+0	+0	+0	+8	+0
	ϕ_3	+0	+0	+0	+0	+0	+0	+0	+0	+0	-8	+0	+0	+0
$[\zeta\zeta 1]$ Λ	ϕ_0	+16	+0	+0	+0	+0	+0	+0	+16	+32	+0	+0	+0	+0
	ϕ_1	-4	-4	+2	+2	+4	+4	+0	-4	-8	-4	+8	+0	+0
	ϕ_2	+0	+0	+0	+0	+2	+0	+2	-4	-4	+0	-8	+4	+4
$[\zeta\zeta 1]$ Π_2	ϕ_0	+16	+0	+0	+0	+0	+0	+0	+16	+32	+0	+0	+0	+0
	ϕ_1	-4	+0	+0	+4	+8	+0	+0	-4	-8	+0	+0	+0	+0
	ϕ_2	+0	+0	+0	+0	+0	+2	+0	+0	-8	+0	+0	+4	+0
$[\zeta\zeta 1]$ Π_1	ϕ_0	+16	+0	+0	+0	+0	+0	+0	+16	+32	+0	+0	+0	+0
	ϕ_1	-4	+4	+2	+2	+4	+4	+0	-4	-8	+4	-8	+0	+0
	ϕ_2	+0	+0	+0	+0	+2	+0	-2	-4	-4	+0	+8	+4	-4

The maximum value of n in ϕ_n for the different directions is related to the type of neighbours included in the following manner:

$[00\zeta]$: $n_m^1 = \max(h_i)$; $|\zeta\zeta 0|$: $n_m^2 = \max\{(h_i+k_i)/2\}$;

$[\zeta\zeta\zeta]$: $n_m^3 = \max(h_i+k_i+\ell_i)$; $|\frac{1}{2}\frac{1}{2}\zeta|$: $n_m^4 = n_m^1 + 1$;

$[\zeta\zeta 1]$: $n_m^5 = n_m^2 + 1$.

h_i, k_i and ℓ_i are the atomic coordinates of the neighbours under the restriction $h_i \geq k_i \geq \ell_i$.

section 5.3.

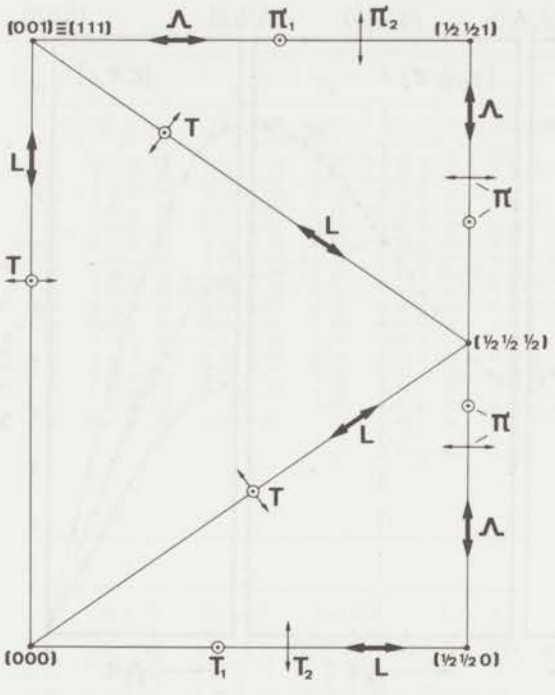

In fig. 5.1 the $(1\bar{1}0)$-plane is shown of the reduced zone of α-Fe, in which the polarisation vectors for the different branches in the above-mentioned directions are indicated.

Fig. 5.1.
The $(1\bar{1}0)$-plane of the reduced zone of the reciprocal lattice of α-Fe, in which the polarisation vectors for the different phonon branches in directions of high symmetry are indicated. A circle with dot denotes a polarisation vector perpendicular to this plane.

5.3. Measurements and experimental results

Using the previously described triple-axis crystal spectrometer, a large number of neutron groups, scattered by phonons belonging to branches in the three main symmetry directions and along $[\zeta\zeta 1]$ and $[\frac{1}{2}\frac{1}{2}\zeta]$ of α-Fe were collected. All measurements have been performed at room temperature. The experimentally determined dispersion relations for these directions are displayed in fig. 5.2. In table 5.4 the numerical values of the frequencies of the phonons are presented for the different branches.

The spectrometer was mainly operated in the "constant Q" mode with energy loss of the neutrons (phonon creation). Copper (111)-reflections were used both for the monochromator and for the analyser. Focusing was applied to the extent as was allowed by the gradient to the dispersion relations and the lattice spacings in the monochromator and analyser crystals. For the observation of high energetic phonons it is quite well possible that the scattered energy E' is close to one quarter of the incoming energy E_o. This may give rise to spurious neutron groups

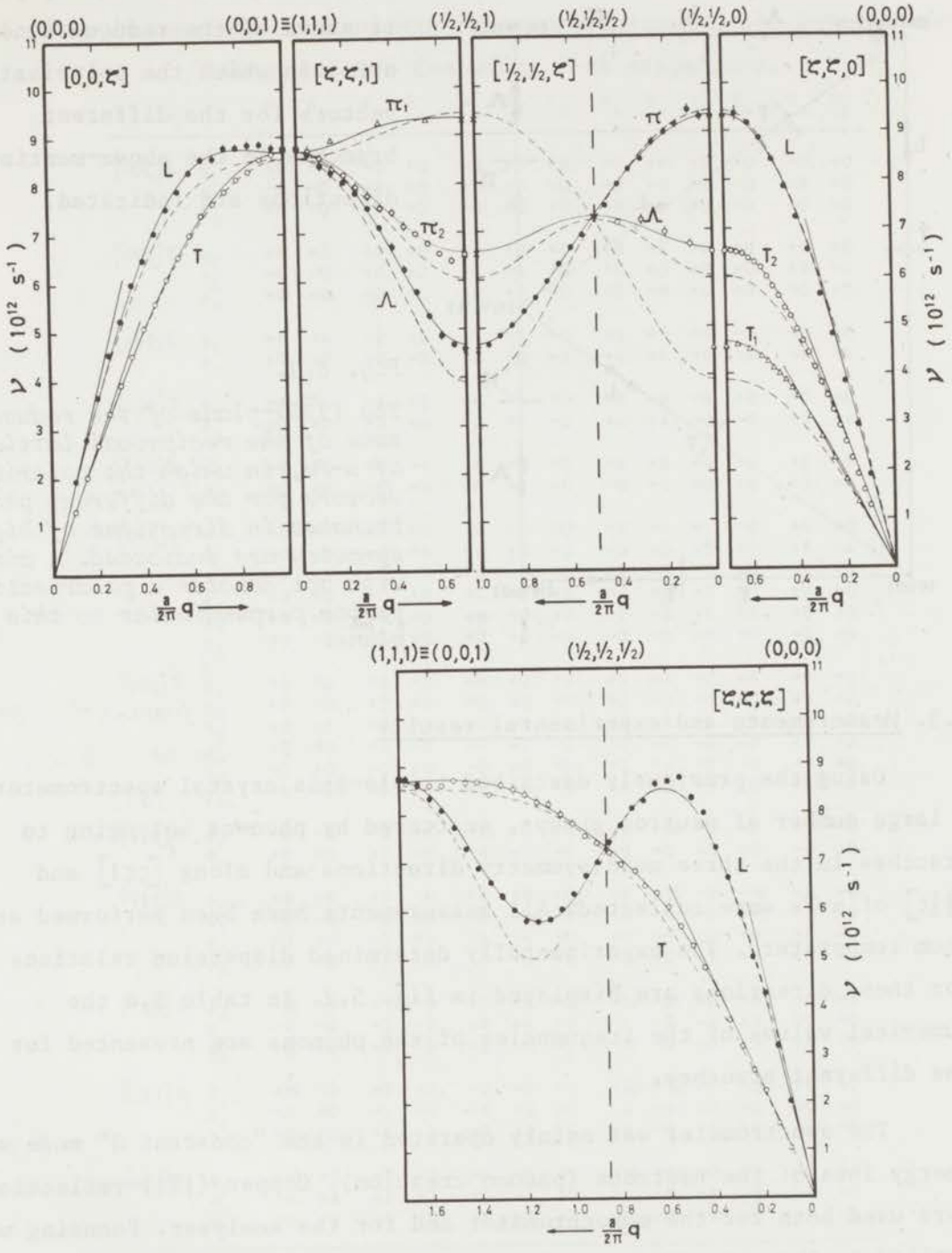

Fig. 5.2.

Phonon dispersion relations of α-Fe. The open and solid circles are experimental points. The solid curves correspond to a 5-th neighbour Born-von Kármán model, and the dashed curves to Krebs' model [22]. The labelling of the branches is according to fig. 5.1.

section 5.3.

ζ'	ν	ν	ζ'	ν	ν
	$[\xi,\xi,\xi]_L$	$[\xi,\xi,\xi]_T$		$[\xi,\xi,\xi]_L$	$[\xi,\xi,\xi]_T$
0.10	2.10 ± .05	1.05 ± .03	0.90	7.00 ± .05	7.40 ± .10
0.15	3.15 ± .07	1.55 ± .03	0.95	6.71 ± .04	7.55 ± .07
0.20	4.25 ± .05	2.23 ± .03	1.00	6.38 ± .05	7.80 ± .10
0.25	5.00 ± .05	2.65 ± .03	1.05	6.03 ± .04	8.00 ± .10
0.30	5.90 ± .07	3.15 ± .03	1.10	5.80 ± .05	8.20 ± .10
0.35	6.65 ± .05	3.70 ± .03	1.15	5.74 ± .03	8.25 ± .10
0.40	7.29 ± .03	4.25 ± .05	1.20	5.80 ± .07	8.40 ± .10
0.45	7.98 ± .05	4.80 ± .03	1.25	6.00 ± .03	8.50 ± .10
0.50	8.31 ± .05	5.25 ± .03	1.30	6.31 ± .03	8.60 ± .10
0.55	8.72 ± .07	5.65 ± .03	1.35	6.60 ± .03	8.40 ± .07
0.60	8.64 ± .06	6.05 ± .05	1.40	6.90 ± .07	8.67 ± .07
0.65	8.58 ± .10	6.35 ± .04	1.45	7.30 ± .05	8.67 ± .12
0.70	8.25 ± .07	6.54 ± .06	1.50	7.75 ± .07	8.70 ± .07
0.75	8.10 ± .04	6.80 ± .04	1.55	8.10 ± .05	8.60 ± .07
0.80	7.75 ± .05	7.00 ± .06	1.60	8.37 ± .10	8.60 ± .07
0.85	7.40 ± .03	7.20 ± .10	1.65	8.65 ± .07	8.62 ± .07
0.865	(7.27 ± .03)	(7.27 ± .03)	1.70	8.75 ± .10	8.65 ± .07
			1.71		8.72 ± .07
			1.73	8.75 ± .10	8.75 ± .10

ζ'	ν	ν	ν	ν
	$[0,0,\zeta]_L$	$[0,0,\zeta]_T$	$[\frac{1}{2},\frac{1}{2},\zeta]_\pi$	$[\frac{1}{2},\frac{1}{2},\zeta]_\Lambda$
0			(9.80 ± .07)	(6.52 ± .05)
0.10	1.97 ± .03	1.33 ± .03	9.50 ± .10	6.70 ± .10
0.15	2.82 ± .03	2.05 ± .03	9.15 ± .10	
0.20	3.68 ± .03	2.70 ± .03	9.00 ± .08	6.95 ± .10
0.25	4.55 ± .03	3.35 ± .03	8.80 ± .10	
0.30	5.25 ± .03	3.93 ± .03	8.45 ± .07	
0.35	6.00 ± .05	4.52 ± .03	8.25 ± .07	
0.40	6.50 ± .05	5.10 ± .03	7.95 ± .05	7.15 ± .07
0.45	7.05 ± .05	5.60 ± .03	7.50 ± .06	
0.50	7.55 ± .05	6.10 ± .03	(7.27 ± .03)	7.27 ± .03
0.55	7.90 ± .05	6.55 ± .03	6.90 ± .04	
0.60	8.30 ± .07	7.00 ± .03	6.65 ± .03	
0.65	8.56 ± .06	7.40 ± .05	6.30 ± .03	
0.70	8.58 ± .08	7.65 ± .05	5.95 ± .03	
0.75	8.80 ± .04	7.90 ± .05	5.62 ± .03	
0.80	8.80 ± .04	8.15 ± .05	5.35 ± .03	
0.85	8.85 ± .08	8.30 ± .07	5.05 ± .03	
0.90	8.85 ± .06	8.55 ± .10	4.85 ± .03	
0.95	8.78 ± .07	8.65 ± .10	4.65 ± .03	
1.00	8.75 ± .10	8.75 ± .10	(4.58 ± .04)	

ζ'	ν	ν	ν	ν	ν
	$[\xi,\xi,0]_{T_2}$	$[\xi,\xi,0]_{T_1}$	$[\xi,\xi,0]_L$	$[\xi,\xi,1]_\Lambda$	$[\xi,\xi,1]_{\pi_2}$
0*				8.75 ± .10	8.75 ± .10
0.05				8.65 ± .10	8.70 ± .12
0.100	1.28 ± .03		1.92 ± .03	8.40 ± .10	8.55 ± .08
0.125	1.60 ± .03				
0.150	1.93 ± .03	1.35 ± .03	2.95 ± .03	8.25 ± .10	8.30 ± .08
0.175	2.27 ± .03				
0.200	2.62 ± .03	1.82 ± .03	3.85 ± .03	8.05 ± .07	8.20 ± .05
0.225	2.93 ± .03				
0.250	3.25 ± .03	2.27 ± .03	4.82 ± .03	7.82 ± .05	7.95 ± .10
0.275	3.58 ± .03				
0.300	3.83 ± .03	2.72 ± .03	5.65 ± .05	7.50 ± .05	7.75 ± .10
0.325	4.15 ± .03				
0.350	4.45 ± .03	3.12 ± .03	6.57 ± .04	7.10 ± .05	7.50 ± .08
0.375	4.70 ± .03				
0.400	4.93 ± .03	3.55 ± .03	7.25 ± .03	6.70 ± .10	7.40 ± .08
0.425	5.20 ± .03	3.70 ± .03			
0.450	5.37 ± .03	3.88 ± .03	7.90 ± .04	6.22 ± .08	7.10 ± .10
0.475	5.62 ± .03	4.00 ± .03			
0.500	5.82 ± .03	4.13 ± .03	8.42 ± .03	5.75 ± .07	6.95 ± .07
0.525	6.02 ± .03	4.27 ± .05			
0.550	6.21 ± .03	4.37 ± .03	8.87 ± .03	5.25 ± .07	6.75 ± .07
0.575	6.32 ± .04				
0.600	6.40 ± .03	4.52 ± .07	9.38 ± .05	4.85 ± .08	6.55 ± .07
0.625	6.50 ± .08				
0.650	6.50 ± .03	4.62 ± .07	9.68 ± .08	4.65 ± .07	6.40 ± .07
0.675	6.55 ± .03				
0.707	6.52 ± .03	4.58 ± .04	9.80 ± .07	4.58 ± .07	6.52 ± .10

Table 5.4.
Phonon frequencies in α-Fe at room temperature (in units of $10^{12}s^{-1}$), $\zeta' = \frac{a}{2\pi} q$.

from second order reflections in the analyser crystal. For such cases the analyser crystal was set at 13 meV and pyrolytic graphite was used as second order filter. Almost all measurements were carried out on a single crystal of pure iron of cylindrical shape, 0.94 cm in diameter times 7.5 cm long. This sample, which had a mosaic spread of 7', was obtained from Research Crystals Incorporated, Richmond, Virginia, U.S.A. A few phonons, of high energy near the [110]-boundary are due to scattering by a larger crystal, 3 cm in diameter and 7 cm long, which contained 3.5% solicon. This crystal was kindly put at our disposal by C.E.N. - S.C.K., Mol, Belgium, through the courtesy of Dr Hautecler.

From (3.36) it is clear that the maximum intensity in the observed neutron peaks is obtained when the scattering vector $\underline{Q}$ is parallel to the polarisation vector of the phonon. Fig. 5.1 shows that this condition can be satisfied for the majority of the branches by scattering in the $(1\bar{1}0)$-plane. Only those phonons, which have their polarisation vectors perpendicular to this plane, were measured in the (100)-plane.

In fig. 5.3 the $(1\bar{1}0)$- and (100)-plane of the reciprocal lattice

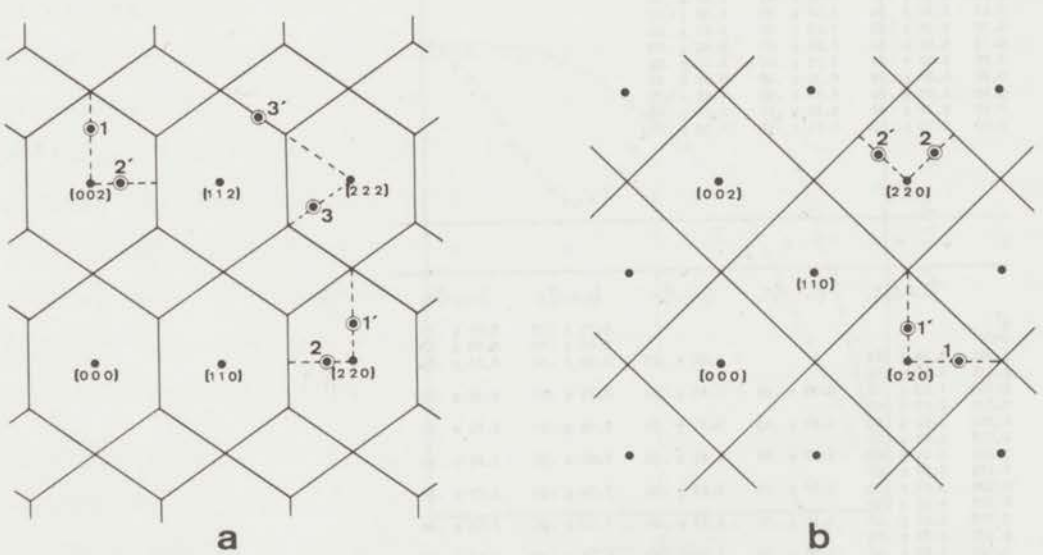

Fig. 5.3.

The $(1\bar{1}0)$- and (100)-planes of the reciprocal lattice of α-Fe with zone boundaries indicated. The numbered points indicate positions which are particularly suited for observation of longitudinal (1,2 and 3) and transverse (1',2' and 3') phonons.

section 5.4.

of α-Fe are shown. Positions 1,2 and 3 are typical for observation of longitudinal phonons, 1',2' and 3' for measurement of transverse phonons.

In addition to the data displayed in fig. 5.2 also phonons in off-symmetry directions in the $(1\bar{1}0)$-plane have been measured. These measurements, the results of which are shown in fig. 5.5, were carried out in order to check the accuracy of the model used in the analysis.

5.4. Analysis of the experimental results

The experimental data of fig. 5.2 have been analysed in terms of a general forces Born-von Kármán model. The range of the interactions was established by making a least squares fit of the individual dispersion relations to the cosine series given by (5.1) (*cf.* ref. [13]). After that a simultaneous least squares analysis was made for all measured branches using all data presented in table 5.4. In this analysis the ϕ_n^j are replaced by a linear combination of the interatomic force constants according to table 5.3. The elastic constants were also included in the analysis. We could have put constraints on the interatomic force constants by means of the relations (2.44) and (2.45), but for the sake of simplicity, only (2.45) was used; the frequencies obtained from this expression for very small values of the wave vector $\underline{q}$ in the different directions were inserted as experimental data with infinite weight. The polarisation vectors needed in (2.45) are shown in fig. 5.1. The elastic constants for α-Fe have been taken from Rayne and Chandrasekhar [14]). They report the room-temperature values $c_{44} = 11.78$, $c_{11} = 23.31$ and $c_{12} = 13.55$ in units of 10^{11}dyn/cm^2.

The analysis in which forces out to third neighbours had been taken into account gave already good qualitative agreement with the experimental data. But for reproducing the details of the dispersion relations also fourth- and fifth-neighbour forces had to be included. The 13 interatomic force constants resulting from this analysis are given in table 5.5 together with the results of Minkiewicz *et al.* [8]) and those of Brockhouse *et al.* [7]).

Dispersion relations calculated from these interatomic force

Table 5.5.

Interatomic force constants for α-Fe (10^2 dyn/cm).

	present results	Minkiewicz *et al.* [8])	Brockhouse *et al.* [7])
α_1 (1XX)	178.6 ± 1.0	168.8	162.8
β_1 (1XY)	149.1 ± 1.3	150.1	148.5
α_2 (2XX)	149.2 ± 2.5	146.3	155.2
β_2 (2XY)	3.6 ± 1.4	5.5	5.4
α_3 (3XX)	12.4 ± 0.8	9.2	11.8
β_3 (3ZZ)	-10.9 ± 1.3	- 5.7	- 8.8
γ_3 (3XY)	3.0 ± 1.2	6.9	12.7
α_4 (4XX)	- 6.0 ± 0.8	- 1.2	- 2.3
β_4 (4YY)	- 0.6 ± 0.4	0.3	2.4
γ_4 (4YZ)	2.8 ± 0.8	5.2	3.9
δ_4 (4XZ)	1.0 ± 0.5	0.07	0.7
α_5 (5XX)	- 2.3 ± 0.7	- 2.9	- 4.6
β_5 (5XY)	- 2.4 ± 1.0	3.2	- 3.0

constants are displayed in fig. 5.2 as solid lines.

Assuming that the interatomic force constants deduced from measurements in particular symmetry directions are also valid for all other directions we are now in a position to solve the dynamical matrix for all $\underline{q}$-values in the first Brillouin zone of the reciprocal lattice. Actually, to obtain all frequencies present it is only necessary to solve for those $\underline{q}$-values which lie within the irreducible unit which has a volume of 1/48-th of that of the first Brillouin zone. For b.c.c. iron the boundaries of this irreducible unit are determined by the planes $q_z = 0$, $q_x = q_y$, $q_x = q_z$ and $q_x + q_y = 1$. Fig. 5.4 shows the first Brillouin zone and its irreducible unit for the body-centred cubic structure. In figs. 5.5a,b lines of constant frequency are shown in the boundary planes of the irreducible unit, unfolded in the plane $q_z = 0$. Here also some experimental points are displayed which give some indication about the accuracy of the calculation.

section 5.4.

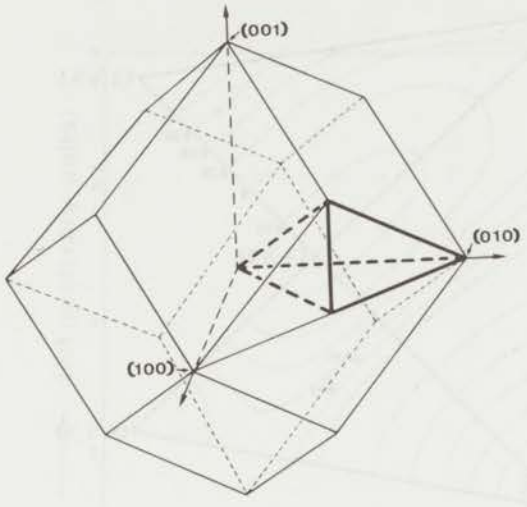

Fig. 5.4.
First Brillouin zone of b.c.c. iron, with its irreducible unit indicated by the heavy lines.

The phonon frequency distribution function f(ν) (*cf.* section 2.3) has been calculated following the method given by Gilat and Raubenheimer [15]) and is shown in fig. 5.6. This is an extrapolation method based on the exact calculation of the frequencies for a number of $\underline{q}$-values at regular intervals in the irreducible unit. By determining simultaneously the gradient in the x-, y-, and z-direction for those $\underline{q}$-values one obtains by extrapolation all frequencies belonging to a continuous set of $\underline{q}$-values in the region around each of the selected points. The total number of diagonalisations (exact calculations) which have been performed in the computation was 3287, the frequency channel width used was 3.10^9 cps.

The resulting frequency distribution function was applied in the calculation of the contribution from the lattice vibrations to the molar heat capacity at constant volume according to (2.35). Also the temperature dependent part C(T) of the Debye-Waller factor, which, apart from a factor $\hbar^2/2M$, represents the mean square displacements of the atoms (expression (2.36)), has been calculated. The results are shown in fig. 5.7a,b.

Inserting Debye's frequency distribution function defined by

$$\begin{aligned} f_D(\nu) &= \text{const}\cdot\nu^2 \quad \text{for} \quad \nu \leq \nu_{max} \\ f_D(\nu) &= 0 \qquad\quad\ \ \text{for} \quad \nu > \nu_{max} \end{aligned} \tag{5.2}$$

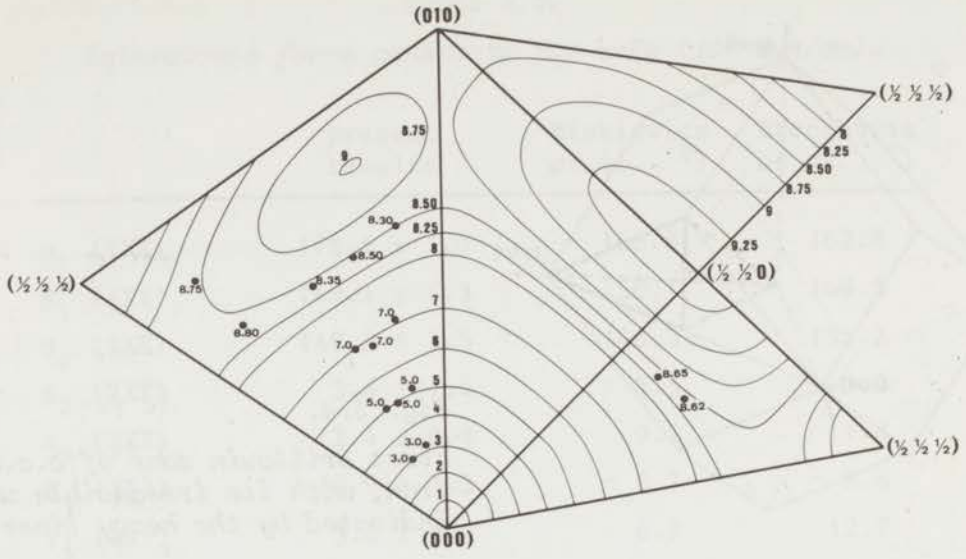

Fig. 5.5a.

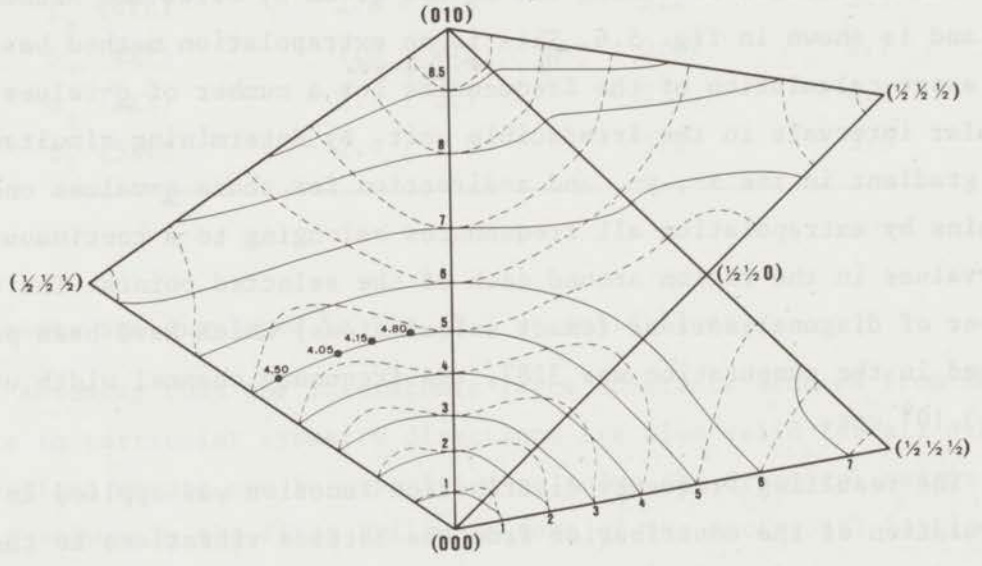

Fig. 5.5b

Lines of constant frequency in the boundary planes of the irreducible unit of the first Brillouin zone, unfolded in the plane $q_z = 0$ (see fig. 5.4). a: highest frequency branch; b: lower lying branches. For symmetry directions compare with fig. 5.2. The dots are observed frequencies. The experimental points of fig. b belong to the frequency series indicated by dashed lines.

section 5.4.

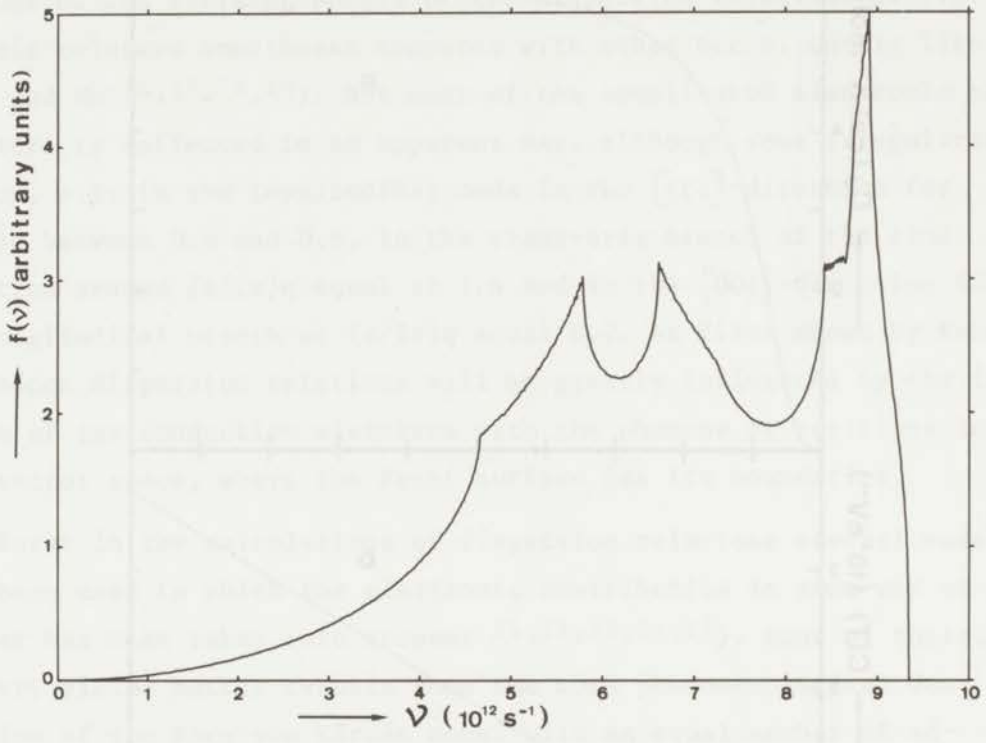

Fig. 5.6.

Phonon frequency distribution function of α-Fe, obtained from a 5-th neighbour Born-von Kármán model.

in expressions (2.35) and (2.38), it is possible to determine the Debye temperature $\Theta_D = h\nu_{max}/k$, as a function of the temperature. The Debye temperature is determined by the condition that both frequency distribution functions $f(\nu)$ and $f_D(\nu)$ should yield equal values for C_V and $C(T)$. Because of the fact that $f(\nu)$ is differently weighted in (2.35) and (2.38), it is not surprising that different results are obtained for the "specific heat"- and the "Debye-Waller factor"- Debye temperature. The results of such calculations are displayed in fig. 5.7c.

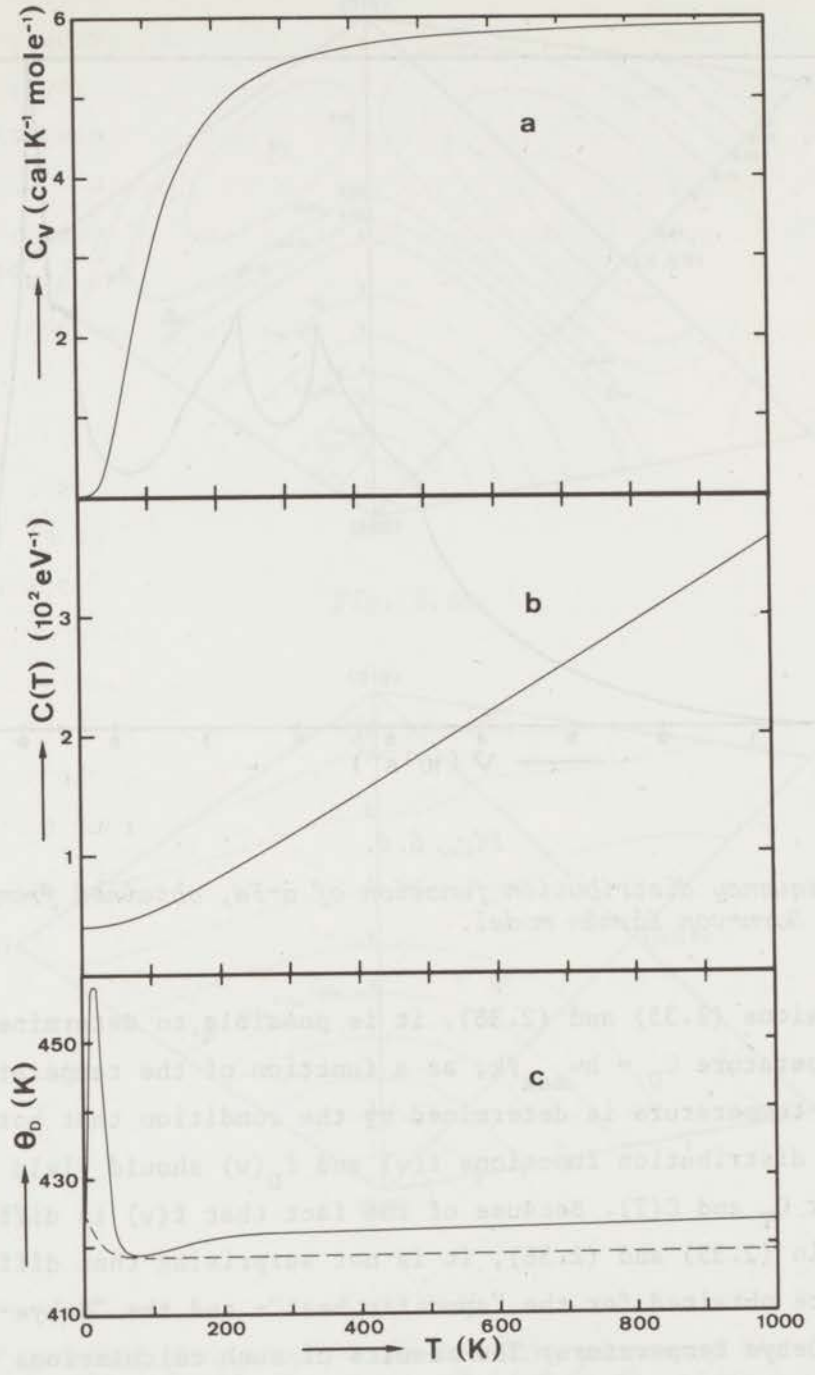

Fig. 5.7.

a: The lattice heat capacity calculated from the frequency distribution function of fig. 5.6.

b: The temperature dependent part C(T) of the Debye-Waller factor calculated from the frequency distribution function of fig. 5.6.

c: Calculated Debye temperatures. The solid line corresponds to the specific heat data, the dashed line to the Debye-Waller factor data.

section 5.5.

5.5. Discussion

One of the striking points of the dispersion relations of fig. 5.2 is their relative smoothness compared with other b.c.c. metals like Mo, W, Ta and Nb [16,17,18,19]. Not much of the complicated electronic band structure is reflected in an apparent way, although some irregularities show up, *e.g.* in the longitudinal mode in the $[\zeta\zeta\zeta]$-direction for $(a/2\pi)q$ between 0.5 and 0.6, in the transverse branch of the same direction around $(a/2\pi)q$ equal to 1.4 and in the $[00\zeta]$-direction for the longitudinal branch at $(a/2\pi)q$ equal 0.7. As first shown by Kohn [20] the phonon dispersion relations will be greatly influenced by the interaction of the conduction electrons with the phonons at positions in wave vector space, where the Fermi surface has its boundaries.

Sofar in the calculations of dispersion relations several models have been used in which the electronic contribution in some way or another has been taken into account [21,22,23,24,25]. None of these, however, yields better results than the more phenomenological description of the Born-von Kármán model with an equal number of adjustable parameters. On the other hand, Schneider and Stoll [26] obtained a rather good fit to the observed dispersion relations of Na, Al and Mg with a four parameter pseudo-potential model, while in a Born-von Kármán analysis one needed at least as many parameters as used for α-Fe. It may thus be concluded that the electronic structure of α-Fe plays an important but as yet not well understood role in its lattice dynamical behaviour.

In fig. 5.2 the dashed curves have been obtained from calculations with a model after Krebs [22], which may be considered as a representative example of models accounting for the electrons. This model is based on the screened Coulomb interaction between ions, the influence of the electrons is considered through the screening parameter of the Coulomb interaction. The interaction between closed ion shells is accounted for by central interaction between first and second neighbours. The short range forces are deduced from the elastic constants, the screening parameter is determined by the number of free electrons n_e.

In our calculation variation of n_e was found to be of very little

influence on the discrepancy between calculated and observed data. Since then Krebs and Hölzl further refined this model [24]), but the fit [25]) obtained by them to our experimental data with a model having 6 adjustable parameters, is no better than a Born-von Kármán fit including third neighbours, which uses 7 parameters. Hence we may conclude that, as yet, the Born-von Kármán model provides the best available interpolation scheme, and in view of the experimental data shown in fig. 5.5 we may safely assume that the derived frequency distribution function is rather accurate.

Comparing the force constants of table 5.5 we observe a rather good agreement between the three sets. A small difference between the three sets occurs in α_1, mainly reflecting a small overall frequency shift with respect to each other, the largest α_1 giving the largest frequencies. An interesting feature is the fact that α_1 is larger than β_1, which is characteristic for all b.c.c. transition metals that have been studied to date-tungsten, tantalum, niobium and molybdenum. This means that forces between first neighbours are attractive, if considered as arising from a potential. This could indicate that in the b.c.c. transition elements the d-electrons are involved in some sort of quasi-covalent bonding, as pointed out by Brockhouse *et al.* [7]).

In the discussion of the specific heat data it is rather hard to compare the calculated and experimental contribution from the lattice vibrations to the specific heat. To do so the experimental data would have to be corrected for the contribution from the electrons [27]), thermal expansion and anharmonic effects [28]), and for the magnetic contribution due to spin waves. Especially the latter becomes important when approaching the Curie temperature (1043 K). The anharmonic contribution is estimated by Foreman [28]) to be of the order of 5-10 percent of C_V, but could also be considerable less. The magnetic contribution represents the greatest uncertainty at higher temperatures. Stringfellow [29]) reports the strong temperature dependence of the spin waves of long wavelengths, which implies a strongly temperature dependent spin wave frequency distribution function. Moreover, spin waves of the shorter wavelengths have not been observed as yet, and therefore frequency distribution functions can only be obtained by extrapolation.

section 5.5.

It is more meaningful to compare the results for the Debye-Waller factor with experimental data obtained from X-ray experiments [30,31]. Houska and Averbach [31] made a study at room temperature and deduced a Debye temperature of 420 K, well in agreement with the value calculated from the present experiment. Haworth [30] studied a higher temperature range, and deduced Debye temperatures, appreciable lower than those from our calculations. However, the scatter in his experimental data is rather large, hence they must be considered as less reliable. Furthermore, we may expect discrepancies between observed data at high temperatures and the calculated data because of neglect of lattice expansion and anharmonicity in the calculation.

References

1. A. Sjölander, Inelastic Scattering of Neutrons by Condensed Systems, Proc. Symp. Brookhaven, 1965, BNL940, (1966), 29.
2. H. Curien, Bull. Soc. Franç. Minér., 75 (1952), 197.
3. P.K. Iyengar, N.S. Satyamurthy and B.A. Dassannacharya, Inelastic Scattering of Neutrons in Solids and Liquids, Proc. Symp. Vienna, 1960, Vienna, IAEA (1961), 555.
4. G.G.E. Low, Proc. Phys. Soc., 79 (1962), 479.
5. M. Hansen and K. Anderko, Constitution of Binary Alloys, second edition, Mc-Graw Hill, New York, 1958.
6. J. Bergsma, C. van Dijk and D. Tocchetti, Phys. Letters, 24A (1967), 270.
7. B.N. Brockhouse, H. Abou-Helal and E.D. Hallman, Solid State Commun., 5 (1967), 211.
8. V.J. Minkiewicz, G. Shirane and R. Nathans, Phys. Rev., 162 (1967), 528.
9. W. van Dingenen and S. Hautecler, Physica 37 (1967), 603.
10. P. Schweiss, A. Furrer and W. Bührer, Helv. Phys. Acta, 40 (1967), 378.
11. See *e.g.* A.D.B. Woods, Inelastic Scattering of Neutrons in Solids and Liquids, Proc. Symp. Chalk River, 1962, Vol. II, Vienna, IAEA (1963), 3.
12. G.L. Squires, Inelastic Scattering of Neutrons in Solids and Liquids, Proc. Symp. Chalk River, 1962, Vol. II, Vienna, IAEA (1963), 71.
13. A.J.E. Foreman and W.M. Lomer, Proc. Phys. Soc., B70 (1957), 1143.
14. J.A. Rayne and B.S. Chandrasekhar, Phys. Rev., 122 (1961), 1714.
15. G. Gilat and L.J. Raubenheimer, Phys. Rev., 144 (1966), 390.
16. A.D.B. Woods and S.H. Chen, Solid State Commun., 2 (1964), 233.
17. S.H. Chen and B.N. Brockhouse, Solid State Commun., 2 (1964), 73.
18. A.D.B. Woods, Phys. Rev., 136 (1964a), A 781.
19. Y. Nakagawa and A.D.B. Woods, Phys. Rev. Letters, 11 (1963), 271
    Y. Nakagawa and A.D.B. Woods, in Lattice Dynamics, edited by R.F. Wallis, Pergamon Press, London, 1965, 39.
20. W. Kohn, Phys. Rev. Letters, 2 (1959), 393. See also:
    E.J. Woll, Jr, and W. Kohn, Phys. Rev., 126 (1962), 1693.

21. R.P. Gupta and P.K. Sharma, phys. stat. sol., 12 (1965), 305.
22. K. Krebs, Phys. Rev., 138 (1965), A 143.
23. P.K. Sharma, Satya Pal and R.P. Gupta, Rev. Roum. Phys., 14 (1969), 247.
24. K. Krebs and K. Hölzl, Solid State Commun., 5 (1967), 159.
25. K. Krebs and K. Hölzl, EUR 3621 e (1969).
26. T. Schneider and E. Stoll, Neutron Inelastic Scattering, Proc. Symp. Copenhagen, 1968, Vol. I, Vienna, IAEA (1968), 101.
27. S.S. Shinozaki and A. Arrott, Phys. Rev., 152 (1966), 611.
28. A.J.E. Foreman, Proc. Phys. Soc., 79 (1962), 1124.
29. M.W. Stringfellow, J. Phys. C, ser. 2, 1 (1968), 950.
30. C.W. Haworth, Phil. Mag., 5 (1960), 1229.
31. C.R. Houska and B.L. Averbach, J. Phys. Chem. Solids, 23 (1962) 1763.

Chapter VI

INVESTIGATION OF THE LATTICE DYNAMICS OF Fe_3Al

6.1. Introduction

The investigation of the lattice dynamics of Fe_3Al in the ordered phase by inelastic neutron scattering is of interest for a number of reasons.

From the experimental point of view very few detailed studies have been made as yet of the dispersion relations of substances which have as many as four atoms per primitive unit cell and hence, in general, twelve phonon branches for each direction. For the observation and identification of the phonon branches it is therefore of paramount importance to make use of the symmetry properties of the system by group-theoretical methods. The application of these methods to lattice vibrations have been reviewed by Maradudin and Vosko [1]) and by Warren [2]). They have been used a.o. by Chen in the analysis of the lattice vibrations of β-tin [3]) and by Waeber for the lattice vibrations of gallium [4]).

Knowledge of the lattice dynamics of Fe_3Al in its ordered phase can be of importance to understand the order-disorder transformation, which Fe_3Al undergoes at about 550 °C, and which has been the subject of a great number of studies [5-14]). Because the structure of Fe_3Al closely resembles that of α-Fe, comparison of the lattice dynamics of α-Fe, Fe_3Al and disordered Fe_3Al could provide information about the character of the acting forces.

Also the magnetic behaviour of ordered Fe_3Al has been and still is the subject of several investigations [15,16,17]). Other reasons for an accurate determination of the lattice dynamics of Fe_3Al are found in a recent theoretical treatment of its dynamical magnetic properties [17]). The results will also be of help for the interpretation of Mössbauer measurements [18]).

A preliminary theoretical analysis of the lattice vibrations of Fe_3Al in the ordered phase has been given by Borgonovi *et al.* [19]). They presented a symmetry classification of the normal modes and calculated some longitudinal phonon branches using a simple Born-von Kármán model

with interactions extending out to second neighbours. The necessary interatomic force constants were estimated from the dynamic properties of α-iron.

The present work describes an experimental inelastic neutron scattering investigation of the phonon dispersion relations. A group-theoretical analysis of the data is carried out following Maradudin and Vosko [1]). Applying a third neighbour Born-von Kármán model interatomic force constants were deduced, which were used for the calculation of the phonon frequency distribution function and some related thermodynamic quantities.

6.2. Crystal structure and some other physical properties of Fe_3Al.

According to Bradley and Jay [5]) Fe_3Al has the structure as illustrated in fig. 6.1. It is the same as that of a large class of Heussler alloys of composition ABC_2. As the figure shows there are two types of iron atoms. The Fe(1) atoms have as nearest neighbours eight Fe(2) atoms, while the Fe(2) atoms are surrounded by four Fe(1) and four Al atoms. This DO_3 type structure can be described as four interpenetrating f.c.c. lattices, one of Al, one of Fe(1) and two of Fe(2). The lattice constant $a = 5.792$ Å is approximately twice that of α-iron ($a = 2.860$ Å). The positions of the four atoms within the primitive unit cell, which has base vectors $\underline{a}_1 = \frac{a}{2}(011)$, $\underline{a}_2 = \frac{a}{2}(101)$ and $\underline{a}_3 = \frac{a}{2}(110)$, are the following:

position	1	Al	a(000)
"	2	Fe(2)	$a(\frac{1}{4}\frac{1}{4}\frac{1}{4})$
"	3	Fe(1)	$a(\frac{1}{2}\frac{1}{2}\frac{1}{2})$
"	4	Fe(2)	$a(\frac{3}{4}\frac{3}{4}\frac{3}{4})$

The primitive unit cell is indicated in fig. 6.1 by dashed lines.

Although the order-disorder transformation in Fe_3Al and its phase diagram are still being investigated, mainly by X-ray and Mössbauer studies, there remains a number of discrepancies in the results. However, we may say that the iron-aluminium alloy which contains 25

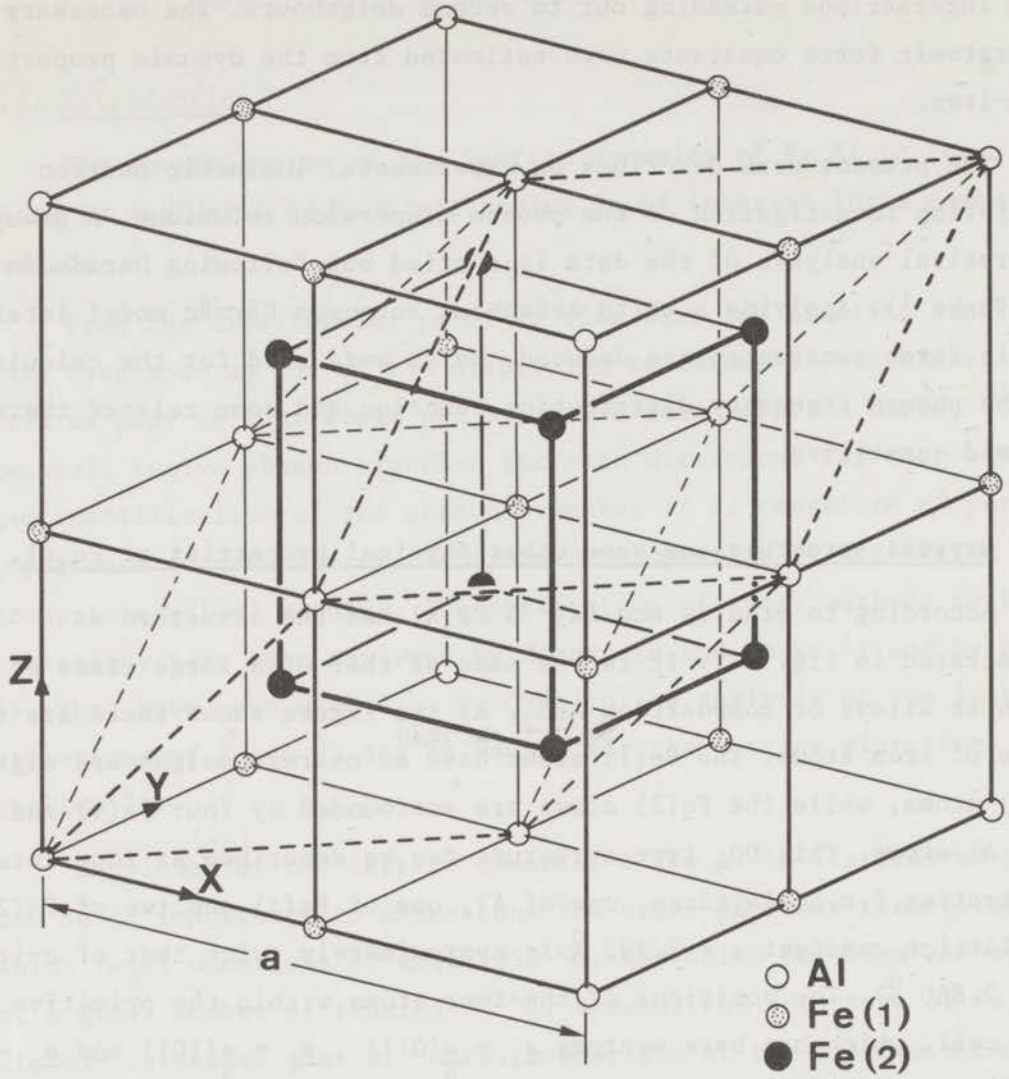

Fig. 6.1.

The crystal structure of ordered Fe_3Al. The dashed lines indicate the primitive unit cell.

atomic percent aluminium, has the DO_3 superlattice structure below about 550 °C, above about 750 °C a fully disordered structure, while in between a CsCl-type structure is found. The CsCl-type structure, in which the Al atoms are distributed randomly over atom sites 1 and 3, may be quenched down.

It is clear that the DO_3-structure of Fe_3Al can be thought of as the b.c.c. iron structure, of which the cell has been doubled in all

directions, and where in the primitive unit cell, chosen as in fig. 6.1, the atom in the origin has been replaced by aluminium. This relationship in structure will certainly extend to the dynamics of both substances.

6.3. Lattice dynamics of Fe_3Al in the Born-von Kármán model

The formal theory has been treated in chapter II. We want now to write down explicit expressions for the coefficients of the dynamical matrix (2.15) for ordered Fe_3Al, including general interactions for first and second neighbours, and central forces for third neighbours. As in α-iron the force constant matrices involved are easily found from simple symmetry considerations. They are for first neighbour interactions:

$$\text{Al - Fe(2)} : \begin{bmatrix} \alpha_1(12) & \beta_1(12) & \beta_1(12) \\ & \alpha_1(12) & \beta_1(12) \\ & & \alpha_1(12) \end{bmatrix}$$

$$\text{Fe(2) - Fe(1)} : \begin{bmatrix} \alpha_1(23) & \beta_1(23) & \beta_1(23) \\ & \alpha_1(23) & \beta_1(23) \\ & & \alpha_1(23) \end{bmatrix} ,$$

for second neighbour interactions:

$$\text{Al - Fe(1)} : \begin{bmatrix} \alpha_2(13) & 0 & 0 \\ & \beta_2(13) & 0 \\ & & \beta_2(13) \end{bmatrix}$$

$$\text{Fe(2) - Fe(2)} : \begin{bmatrix} \alpha_2(24) & 0 & 0 \\ & \beta_2(24) & 0 \\ & & \beta_2(24) \end{bmatrix} ,$$

and for third neighbour interactions:

$$\text{Al - Al :} \quad \begin{bmatrix} \alpha_3(11) & \alpha_3(11) & 0 \\ & \alpha_3(11) & 0 \\ & & 0 \end{bmatrix},$$

$$\text{Fe(2) - Fe(2) :} \quad \begin{bmatrix} \alpha_3(22) & \alpha_3(22) & 0 \\ & \alpha_3(22) & 0 \\ & & 0 \end{bmatrix},$$

$$\text{Fe(1) - Fe(1) :} \quad \begin{bmatrix} \alpha_3(33) & \alpha_3(33) & 0 \\ & \alpha_3(33) & 0 \\ & & 0 \end{bmatrix}.$$

The convention for α_s, β_s, *etc.* is the same as used in chapter V. The indices in parenthesis indicate to which type of atoms the interaction refers. In appendix VIA the coefficients are listed of the dynamical matrix including third neighbours as obtained from (2.15). The elaboration of the coefficients is facilitated by using some of the results of the group-theoretical treatment of the next section.

As shown in section 2.4. the elastic constants can be expressed in terms of the force constants using the method of long waves, *i.e.* expanding the coefficients of the dynamical matrix up to the second order in the components of the wave vector $\underline{q}$.

The results obtained in this way for Fe_3Al are:

$$\frac{ac}{2}_{11} = \alpha_1(12)+\alpha_1(23)+\alpha_2(13)+\alpha_2(24) + 2\alpha_3(11)+4\alpha_3(22)+2\alpha_3(33), \qquad (6.1)$$

$$\frac{ac}{2}_{44} = \alpha_1(12)+\alpha_1(23)+\beta_2(13)+\beta_2(24)+\alpha_3(11)+2\alpha_3(22)+\alpha_3(33)-g, \qquad (6.2)$$

$$\frac{ac}{2}_{12} = 2\beta_1(12)+2\beta_1(23)-\alpha_1(12)-\alpha_1(23)-\beta_2(13)-\beta_2(24)+\alpha_3(11)+2\alpha_3(22)+$$
$$+ \alpha_3(33), \qquad (6.3)$$

section 6.4.

where

$$g = \frac{\{\beta_1(12) - \beta_1(23)\}^2}{\alpha_1(12) + \alpha_1(23) + \alpha_2(24) + 2\beta_2(24)} \quad . \tag{6.4}$$

In the force constant matrices there are eleven independent parameters. The above relations may be used as constraints to reduce this number.

6.4. Group-theoretical treatment of the lattice dynamics of Fe_3Al

6.4.1. Theory

By group-theoretical methods it is possible to simplify the dynamical matrix considerably for values of $\underline{q}$ lying at points of symmetry inside or on the boundary of the Brillouin zone. This is of great help for the determination of the form of the eigenvectors.

The method used in this work is based on the so-called multiplier or weighted representations of the point group of the wave vector $\underline{q}$, *i.e.* of that crystallographic point group whose operations applied to $\underline{q}$ leave it invariant (modulo 2π times a reciprocal lattice vector). This method has been worked out in great detail by Maradudin and Vosko [1], hereafter referred to as MV. No extensive description will therefore be presented here, but only the main features will be given together with those results which are of importance for the description of the lattice dynamics of Fe_3Al. The notation used is the same as that of MV, except for the wave vector $\underline{q}$ and the reciprocal lattice vector $\underline{\tau}$, which by MV are called $\underline{k}$ and $\underline{b}$, respectively.

Let us consider the space group G of the crystal. The symmetry operations can be written $\{S|\underline{v}(S) + \underline{r}(m)\}$. These are thus the operations which take the crystal into itself. Here S is a 3×3 real orthogonal matrix representation of the proper or inproper rotations of the point group of the crystal. $\underline{v}(S)$ is a vector which is smaller than any primitive translation vector of the crystal, and $\underline{r}(m)$ is a translation vector of the crystal. Space groups for which $\underline{v}(S)$ is identically zero are called symmorphic and contain no screw axes and glide planes. The space group of the wave vector $\underline{q}$, $G_{\underline{q}}$, is a subgroup of G. The symmetry

operations of $G_{\underline{q}}$, which is a special class of operations of G, are here denoted by $\{R|\underline{v}(R) + \underline{r}(m)\}$. The rotational elements R of $G_{\underline{q}}$ have the property

$$R\underline{q} = \underline{q} - 2\pi\underline{\tau}(\underline{q},R) \ . \tag{6.5}$$

The translation vector $\underline{\tau}(\underline{q},R)$ of the reciprocal lattice can be nonzero only if $\underline{q}$ lies on the boundary of the Brillouin zone. The purely rotational elements $\{R\}$ of the space group $G_{\underline{q}}$ taken by themselves comprise a point group $G_o(\underline{q})$ called the point group of the wave vector $\underline{q}$. With each element R of the point group $G_o(\underline{q})$ a matrix $T(\underline{q};R)$ is associated. This matrix is defined as follows:

$$T_{\alpha\beta}(\lambda\lambda'|\underline{q};R) = R_{\alpha\beta}\delta\big(\lambda,F_o(\lambda';R)\big) \times \exp\{i\underline{q}\cdot\big[\underline{r}(\lambda)-R\underline{r}(\lambda')\big]\}, \tag{6.6}$$

where $F_o(\lambda';R)$ is the label of that atom into which the atom labeled λ' is transformed by the operation $\{R|\underline{v}(R)+\underline{r}(m)\}$. Thus $T_{\alpha\beta}(\lambda\lambda'|\underline{q};R)$ is nonzero only if $F_o(\lambda';R) = \lambda$. MV show that the matrices $\{T(\underline{q};R)\}$ provide a 3n-dimensional unitary multiplier representation of the point group $G_o(\underline{q})$ of the wave vector $\underline{q}$, *i.e.* they obey a multiplication rule of the form

$$T(\underline{q};R_i)T(\underline{q};R_j) = \phi(\underline{q};R_i,R_j)T(\underline{q};R_iR_j) \tag{6.7}$$

with $$\phi(\underline{q};R_i,R_j) = \exp\big[2\pi i\underline{\tau}(\underline{q},R_i^{-1})\cdot\underline{v}(R_j)\big] \ .$$

For symmorphic space groups $\phi(\underline{q};R_i,R_j)$ equals unity and the set of matrices $\{T(\underline{q};R)\}$ form an ordinary representation of the point group $G_o(\underline{q})$.

The T-matrices have furthermore the property of commuting with the dynamical matrix $D(\underline{q})$ defined in section 2.2. Hence

$$D(\underline{q}) = T^{-1}(\underline{q};R)D(\underline{q})T(\underline{q};R) \ . \tag{6.8}$$

section 6.4.

Equation (6.8) yields relations between elements of $D(\underline{q})$, reducing the number of them which are nonzero and independent, as imposed by spatial symmetry. Sometimes there are additional conditions imposed by time-reversal symmetry, this is the case as the point group of the crystal contains a rotational element S_-, such that $S_- \underline{q} = -\underline{q}$ (hence $-\underline{q}$ is in the "star" of $\underline{q}$). The element S_- forms with the operators of $G_o(\underline{q})$ the coset $S_-G_o(\underline{q})$ with elements S_-R. The point group $G_o(\underline{q})$ together with $S_-G_o(\underline{q})$ form the point group $G_o(\underline{q};-\underline{q})$ in which $G_o(\underline{q})$ is an invariant subgroup. By associating to each element S_-R matrices as defined in (6.6) and multiplying these matrices by the anti-unitary operator K_o MV define the anti-unitary matrix operator $T(\underline{q};S_-R)$. The anti-unitary operator K_o is defined by its effect on an arbitrary vector $\underline{\Psi}$ in the 3n-dimensional space:

$$K_o \underline{\Psi} = \underline{\Psi}^* \quad . \tag{6.9}$$

The extra conditions imposed by time-reversal symmetry are now that also the $T(\underline{q};S_-R)$ commute with the dynamical matrix $D(\underline{q})$. In case $S_- = i$, the inversion, then what has been said before is valid for general $\underline{q}$. In that case one has, for any two atoms λ and λ', related by i, the simple relations

$$D^*_{\alpha\beta}(\lambda'\lambda';\underline{q}) = D_{\alpha\beta}(\lambda\lambda;\underline{q}) \tag{6.10a}$$

and

$$D^*_{\alpha\beta}(\lambda'\lambda;\underline{q}) = D_{\alpha\beta}(\lambda\lambda';\underline{q}) = D^*_{\beta\alpha}(\lambda'\lambda;\underline{q}) \quad . \tag{6.10b}$$

The spatial symmetry also imposes restrictions on the form of the eigenvectors of the eigenvalue equation (2.18). From (6.8) it follows that

$$D(\underline{q})\{T(\underline{q};R)\underline{e}_j(\underline{q})\} = \omega_j^2(\underline{q})\{T(\underline{q};R)\underline{e}_j(\underline{q})\} \quad , \tag{6.11}$$

which tells us that if $\underline{e}_j(\underline{q})$ is an eigenvector of $D(\underline{q})$ with an eigenvalue $\omega_j^2(\underline{q})$, then so is $T(\underline{q};R)\underline{e}_j(\underline{q})$ for every operation R of the point group $G_o(\underline{q})$. Consequently $T(\underline{q};R)\underline{e}_j(\underline{q})$ is in general a linear combination of the eigenvectors of $D(\underline{q})$ corresponding to the eigenvalue $\omega_j^2(\underline{q})$,

which is expressed by

$$T(\underline{q};R)\underline{e}_{\sigma\mu}(\underline{q}) = \sum_{\mu'=1}^{f_\sigma} \tau^{(\sigma)}_{\mu'\mu}(\underline{q};R)\underline{e}_{\sigma\mu'}(\underline{q}) \ . \qquad (6.12)$$

The suffix j in $\underline{e}_j$ has been replaced by the double index $\sigma\mu$, where σ labels the distinct values of $\omega_j^2(\underline{q})$ for given $\underline{q}$ and μ the linearly independent eigenvectors associated with the eigenvalue $\omega_\sigma^2(\underline{q})$. MV show that the f_σ-dimensional matrices $\{\tau^{(\sigma)}(\underline{q};R)\}$ provide a multiplier representation of $G_o(\underline{q})$. In view of the general result of group theory, that the eigenfunctions corresponding to each eigenvalue of an operator transform irreducibly under the symmetry transformations which leave the operator invariant, if no accidental degeneracy is present, the set of matrices $\{\tau^{(\sigma)}(\underline{q};R)\}$ constitute an f_σ-dimensional irreducible multiplier representation of the point group $G_o(\underline{q})$. In order to account for the fact that different eigenvectors may transform according to the same irreducible representation, in (6.12) σ is replaced by s and a label t is introduced, which numbers the eigenvectors, transforming according to the sth irreducible representation. Equation (6.12) then takes the form

$$T(\underline{q};R)\underline{e}_{st\mu}(\underline{q}) = \sum_{\mu'=1}^{f_s} \tau^{(s)}_{\mu'\mu}(\underline{q};R)\underline{e}_{st\mu'}(\underline{q}) \ . \qquad (6.13)$$

The irreducible representation matrices $\{\tau^{(s)}(\underline{q};R)\}$ have been tabulated for all 230 space groups by Kovalev [20].

The number of times the sth irreducible representation is contained in the representation $\{T(\underline{q};R)\}$ is given by the familiar decomposition formula

$$c_s = h^{-1} \sum_R \chi(\underline{q};R)\chi^{(s)}(\underline{q};R)^* \ , \qquad (6.14)$$

where h is the order of the group, $\chi(\underline{q};R) = \mathrm{Tr}T(\underline{q};R)$ and

$$\chi^{(s)}(\underline{q};R) = \mathrm{Tr}\tau^{(s)}(\underline{q};R).$$

The general form of the eigenvector is obtained by applying

section 6.4.

projection operators, the 3n×3n matrices $P^{(s)}_{\mu\mu'}(\underline{q})$ defined by

$$P^{(s)}_{\mu\mu'}(\underline{q}) = (f_s/h) \sum_R \tau^{(s)}_{\mu\mu'}(\underline{q};R)^* \, T(\underline{q};R) \ . \tag{6.15}$$

Application to an arbitrary 3n-dimensional vector $\underline{\Psi}$ results in the so-called symmetry adapted eigenvector $\underline{E}(\underline{q};s\mu)$,

$$\underline{E}(\underline{q};s\mu) = P^{(s)}_{\mu\mu'}(\underline{q})\underline{\Psi} \ , \tag{6.16}$$

which transforms in the same way under the application of $T(\underline{q};R)$ as does the eigenvector $\underline{e}_{st\mu}(\underline{q})$ for any t. In general, $\underline{E}(\underline{q};s\mu)$ is a linear combination of the c_s eigenvectors $\{\underline{e}_{st\mu}(\underline{q})\}$ ($t = 1,2, \ldots c_s$) corresponding to the distinct eigenfrequencies $\{\omega^2_{st}(\underline{q})\}$. Hence

$$D(\underline{q})\underline{E}(\underline{q};s\mu) = \omega^2_s(\underline{q})\underline{E}(\underline{q};s\mu) \tag{6.17}$$

yields the c_s independent complex homogeneous equations in the c_s unknown complex components of the vector $\underline{E}(\underline{q};s\mu)$, from which the c_s eigenvectors $\{\underline{e}_{st\mu}(\underline{q})\}$ and the c_s associated eigenfrequencies $\{\omega^2_{st}(\underline{q})\}$ are found. Hence the problem of solving a 3n×3n eigenvalue equation has been simplified to the problem of the solution of a number of generally smaller $c_s \times c_s$ eigenvalue equations. The total number of these smaller blocks is determined by the condition that

$$\sum_s f_s c_s = 3n \ , \tag{6.18}$$

where f_s, the dimensionality of the sth irreducible representation, usually denotes the degeneracy of the $\{\omega^2_s(\underline{q})\}$.

If for a particular wave vector or crystal point group the symmetry group of the dynamical matrix can be enlarged to include anti-unitary operations, this may impose extra conditions on the form of the eigenvectors and of the irreducible multiplier representations. Under the assumption that the eigenvectors $\underline{e}_{st\mu}(\underline{q})$ of $T(\underline{q};R)$ can be chosen to be eigenvectors of the anti-unitary operators $T(\underline{q};S\_R)$ one obtains

$$e^{*}_{\alpha s t \mu}(\lambda';\underline{q}) = -\exp\left\{-i\underline{q}\cdot\left[\underline{r}(\lambda')-S_{-}\underline{r}(\lambda)\right]\right\}\left\{\sum_{\beta}(S_{-})_{\alpha\beta}e_{\beta s t \mu}(\lambda;\underline{q})\right\} , \qquad (6.19)$$

where λ is sent into λ' by the operation $\{S_{-}|\underline{v}(S_{-})\}$. The symmetry adapted eigenvectors $\underline{E}(\underline{q};s\mu)$ found from (6.16) are not necessarily compatible with (6.19). The criterion for compatability given by MV is that the irreducible representations $\tau^{(s)}(\underline{q};R)$ corresponding to those $T(\underline{q};R)$'s which commute with $T(\underline{q};S_{-}R)$ must be real and that as many as possible of these $\tau^{(s)}(\underline{q};R)$ should be in diagonal form.

Time-reversal symmetry may give rise to extra degeneracies. From the fact that the anti-unitary matrix operator $T(\underline{q};S_{-}R)$ commutes with $D(\underline{q})$ it follows that, if $\underline{e}_{st\mu}(\underline{q})$ is an eigenvector of $D(\underline{q})$ with eigenvalue $\omega^2_{st}(\underline{q})$, then so is $T(\underline{q};S_{-}R)\underline{e}_{st\mu}(\underline{q})$. This means that $T(\underline{q};S_{-}R)\underline{e}_{st\mu}(\underline{q})$ is a linear combination of the eigenvectors of $D(\underline{q})$ whose eigenvalues are equal to $\omega^2_{st}(\underline{q})$. However, if the two sets of eigenvectors are required to be linearly independent by time-reversal symmetry, there must be an additional degeneracy. The transformational behaviour of $\overline{\underline{e}}_{st\mu}(\underline{q}) \equiv T(\underline{q};S_{-}R)\underline{e}_{st\mu}(\underline{q})$ and $\underline{e}_{st\mu}(\underline{q})$ under the operations $T(\underline{q};R)$ provides the criterion for additional degeneracy. This has been formulated according to the behaviour of their irreducible representations, in which three cases have been distinguished, corresponding to:

1) linear dependence of $\overline{\underline{e}}$ and $\underline{e}$, referred to as type one representations,
2) no linear dependence of $\overline{\underline{e}}$ and $\underline{e}$ but with equivalent irreducible representations, called type two representations, and
3) no linear dependence of $\overline{\underline{e}}$ and $\underline{e}$ and corresponding inequivalent representations, referred to as type three.

The criterion is:

$$\sum_{R}\phi(\underline{q};S_{-}R,S_{-}R)\chi^{(s)}(\underline{q};S_{-}R\ S_{-}R) = \begin{cases} h & \text{first type} \\ -h & \text{second type} \\ o & \text{third type} \end{cases} , \qquad (6.20)$$

where

$$\phi(\underline{q};S_{-}R,S_{-}R) = \exp\left\{-i\left[\underline{q}+(S_{-}R)^{-1}\underline{q}\right]\cdot\underline{v}(S_{-}R)\right\}$$

is the multiplier in the so-called multiplier corepresentations of

section 6.4.

$G_o(\underline{q};-\underline{q})$ formed by the matrices $T(\underline{q};S\_R)$ and

$$\chi^{(s)}(\underline{q};S\_R\ S\_R) = \mathrm{Tr}\tau^{(s)}(\underline{q};S\_R\ S\_R).$$

For symmorphic space groups and $S\_ = i$, the inversion operator, (6.20) gets the simple form

$$\sum_R \chi^{(s)}(\underline{q};R^2) = \begin{cases} h & \text{first type} \\ -h & \text{second type} \\ o & \text{third type} \end{cases}, \qquad (6.21)$$

The type one representations does not give additional degeneracy, while the second and third type double the degeneracy.

The above presented compilation of the most relevant results of the multiplier representation theory provides the tools for the block-diagonalisation of the dynamical matrix of Fe_3Al and for the determination of the general form of its eigenvectors and the number of degeneracies present in the different eigenfrequencies.

6.4.2. Application

In the application of the group theory to a specific problem the question arises of which notation to use, extensively discussed by Warren [2]. Here we follow closely the treatment of MV, which more or less implies the use of the tables of irreducible representations given by Kovalev [20]. Therefore it is tried to keep to their notations as far as this does not lead to confusion with symbols used in other parts of this work. Contrary to these two references we use $\underline{q}$ instead of $\underline{k}$ for the wave vector, but retain their numbering (hence $\underline{k}_i = \underline{q}_i$) and choose the notation R for the rotational elements in accordance with MV, while Kovalev has the notation h, again retaining the numbering. Because it is becoming common to label branches of phonon dispersion relations according to the BSW-system [21], we will do the same but present also the corresponding τ-representations from Kovalev. For the point groups the Schoenflies notation [22] is used.

The space group of ordered Fe_3Al is O_h^5, which is symmorphic. In fig. 6.2 the first Brillouin zone of Fe_3Al is displayed with the different points of symmetry indicated in the BSW-notation. We consider first the Σ-direction.

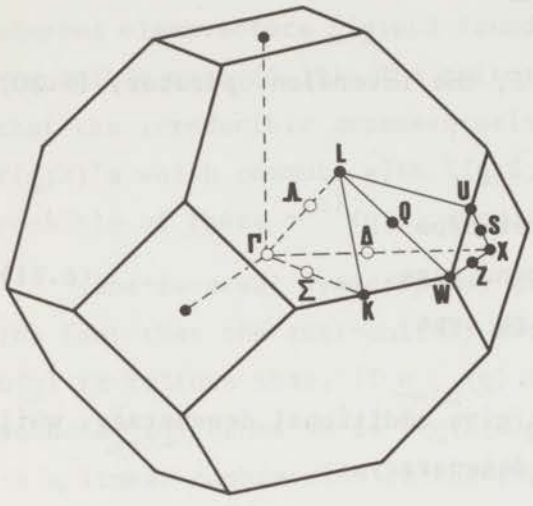

Fig. 6.2.

The first Brillouin zone for a f.c.c. lattice, in which special directions of higher symmetry are indicated by the B.S.W.-notation [21].

Symmetry direction Σ

$$\Sigma = \underline{q}_4 = \frac{2\pi\mu}{a}\,(1,1,0) \quad , \quad 0 < \mu < \tfrac{3}{4} \; .$$

The point group of the wave vector $\underline{q}_4$, $G_o(\underline{q}_4)$ is C_{2v}. It has four rotational elements, R_1, R_{16}, R_{28}, and R_{37}, which are given in matrix form in Appendix VI.B. The irreducible representations are given in table 6.1.

Table 6.1.

Irreducible representations of the group $G_o(\underline{q}_4) = C_{2v}$.

Ref.20	R_1	R_{37}	R_{28}	R_{16}	Ref.21
$\tau^{(1)}$	1	1	1	1	Σ_1
$\tau^{(2)}$	1	-1	-1	1	Σ_2
$\tau^{(3)}$	1	-1	1	-1	Σ_4
$\tau^{(4)}$	1	1	-1	-1	Σ_3

section 6.4.

The 12×12 $T(\underline{q}_4,R)$ matrices are obtained from (6.6) using the atomic positions given in section 6.2. We present them here in a compact way of 4×4 matrices, of which each position is a 3×3 matrix.

$$T(\underline{q}_4;R_1) = \begin{bmatrix} R_1 & & & \\ & R_1 & & \\ & & R_1 & \\ & & & R_1 \end{bmatrix}, \quad T(\underline{q}_4;R_{37}) = \begin{bmatrix} R_{37} & & & \\ & R_{37} & & \\ & & R_{37} & \\ & & & R_{37} \end{bmatrix},$$

$$T(\underline{q}_4;R_{16}) = \begin{bmatrix} R_{16} & 0 & 0 & 0 \\ 0 & 0 & 0 & \rho_4^* R_{16} \\ 0 & 0 & R_{16} & 0 \\ 0 & \rho_4 R_{16} & 0 & 0 \end{bmatrix}, \quad T(\underline{q}_4;R_{28}) = \begin{bmatrix} R_{28} & 0 & 0 & 0 \\ 0 & 0 & 0 & \rho_4^* R_{28} \\ 0 & 0 & R_{28} & 0 \\ 0 & \rho_4 R_{28} & 0 & 0 \end{bmatrix},$$

where $\rho_4 = \exp(i2\pi\mu)$.
The traces for the different T-matrices are:

$$\chi(\underline{q}_4;R_1) = 12, \quad \chi(\underline{q}_4;R_{37}) = 4, \quad \chi(\underline{q}_4;R_{16}) = -2, \quad \chi(\underline{q}_4;R_{28}) = 2.$$

The number of times a certain irreducible representation is contained in the T-representation is obtained using (6.14) and table 6.1. One finds $c_1 = 4$, $c_2 = 1$, $c_3 = 3$ and $c_4 = 4$. Hence,

$$\{T(\underline{q}_4,R)\} = \{T(\Sigma,R)\} = 4\Sigma_1 \oplus \Sigma_2 \oplus 3\Sigma_4 \oplus 4\Sigma_3 . \qquad (6.22)$$

Since all irreducible representations are one-dimensional, spatial symmetry does not cause degeneracy of the normal modes. Because the space group of Fe_3Al is symmorphic and contains the inversion operator i, time-reversal symmetry may be invoked using (6.21). Since $R^2 = R_1$ for all four operators, all representations are of the first kind and therefore time-reversal symmetry does not produce any additional degeneracy.

The symmetry adapted eigenvectors $\underline{E}(\underline{q};s\mu)$ are obtained using

(6.15) and (6.16). The different steps leading to the results presented below are given in Appendix VI.C.

$$\underline{E}(\underline{q}_4;11)=\begin{bmatrix} a_1 \\ a_1 \\ o \\ b_1 \\ b_1 \\ c_1 \\ d_1 \\ d_1 \\ o \\ \rho_4 b_1 \\ \rho_4 b_1 \\ -\rho_4 c_1 \end{bmatrix}, \quad \underline{E}(\underline{q}_4;21)=\begin{bmatrix} o \\ o \\ o \\ a_2 \\ -a_2 \\ o \\ o \\ o \\ o \\ -\rho_4 a_2 \\ \rho_4 a_2 \\ o \end{bmatrix}, \quad \underline{E}(\underline{q}_4;31)=\begin{bmatrix} a_3 \\ -a_3 \\ o \\ b_3 \\ -b_3 \\ o \\ c_3 \\ -c_3 \\ o \\ \rho_4 b_3 \\ -\rho_4 b_3 \\ o \end{bmatrix}, \quad \underline{E}(\underline{q}_4;41)=\begin{bmatrix} o \\ o \\ a_4 \\ b_4 \\ b_4 \\ c_4 \\ o \\ o \\ d_4 \\ -\rho_4 b_4 \\ -\rho_4 b_4 \\ \rho_4 c_4 \end{bmatrix}.$$

Application of (6.17) using the dynamical matrix presented in Appendix VI.A and the derived $\underline{E}$ vectors, provides the different blocks of the dynamical matrix, which transform according to the different irreducible representations. This is presented in Appendix VI.D. As can also be seen from (6.22) the 12×12 matrix $D(\underline{q})$ blocks down to a 4×4, a single valued, a 3×3 and a 4×4 matrix.

Symmetry direction Δ

$$\Delta = \underline{q}_6 = \frac{2\pi\mu}{a}(0,0,1), \qquad 0 < \mu < 1.$$

The point group of $\underline{q}_6$ is C_{4v}. It has eight rotational elements as shown in the irreducible representation table 6.2. The elements R are given in Appendix VI.B.

section 6.4.

Table 6.2.

Irreducible representations of the group $G_o(\underline{q}_6) = C_{4v}$.

Ref.20	R_1	R_4	R_{14}	R_{15}	R_{26}	R_{27}	R_{37}	R_{40}	Ref.21
$\tau^{(1)}$	1	1	1	1	1	1	1	1	Δ_1
$\tau^{(2)}$	1	1	1	1	-1	-1	-1	-1	Δ_1'
$\tau^{(3)}$	1	1	-1	-1	1	1	-1	-1	Δ_2
$\tau^{(4)}$	1	1	-1	-1	-1	-1	1	1	Δ_2'
$\tau^{(5)}$	$\begin{pmatrix} 1 & 0 \\ 0 & 1 \end{pmatrix}$	$\begin{pmatrix} \bar{1} & 0 \\ 0 & \bar{1} \end{pmatrix}$	$\begin{pmatrix} i & 0 \\ 0 & \bar{i} \end{pmatrix}$	$\begin{pmatrix} \bar{i} & 0 \\ 0 & i \end{pmatrix}$	$\begin{pmatrix} 0 & 1 \\ 1 & 0 \end{pmatrix}$	$\begin{pmatrix} 0 & \bar{1} \\ \bar{1} & 0 \end{pmatrix}$	$\begin{pmatrix} 0 & \bar{i} \\ i & 0 \end{pmatrix}$	$\begin{pmatrix} 0 & i \\ \bar{i} & 0 \end{pmatrix}$	Δ_5
$\tau'^{(5)}$	$\begin{pmatrix} 1 & 0 \\ 0 & 1 \end{pmatrix}$	$\begin{pmatrix} \bar{1} & 0 \\ 0 & \bar{1} \end{pmatrix}$	$\begin{pmatrix} 0 & \bar{1} \\ 1 & 0 \end{pmatrix}$	$\begin{pmatrix} 0 & 1 \\ \bar{1} & 0 \end{pmatrix}$	$\begin{pmatrix} 0 & 1 \\ 1 & 0 \end{pmatrix}$	$\begin{pmatrix} 0 & \bar{1} \\ \bar{1} & 0 \end{pmatrix}$	$\begin{pmatrix} 1 & 0 \\ 0 & \bar{1} \end{pmatrix}$	$\begin{pmatrix} \bar{1} & 0 \\ 0 & 1 \end{pmatrix}$	Δ_5

Equation (6.6) provides the T-matrices:

$$T(\underline{q}_6;R_1) = \begin{bmatrix} R_1 & & & \\ & R_1 & & \\ & & R_1 & \\ & & & R_1 \end{bmatrix}, \quad T(\underline{q}_6;R_4) = \begin{bmatrix} R_4 & & & \\ & R_4 & & \\ & & R_4 & \\ & & & R_4 \end{bmatrix},$$

$$T(\underline{q}_6;R_{14}) = \begin{bmatrix} R_{14} & 0 & 0 & 0 \\ 0 & 0 & 0 & \rho_6^* R_{14} \\ 0 & 0 & R_{14} & 0 \\ 0 & \rho_6 R_{14} & 0 & 0 \end{bmatrix}, \quad T(\underline{q}_6;R_{15}) = \begin{bmatrix} R_{15} & 0 & 0 & 0 \\ 0 & 0 & 0 & \rho_6^* R_{15} \\ 0 & 0 & R_{15} & 0 \\ 0 & \rho_6 R_{15} & 0 & 0 \end{bmatrix},$$

$$T(\underline{q}_6;R_{26}) = \begin{bmatrix} R_{26} & 0 & 0 & 0 \\ 0 & 0 & 0 & \rho_6^* R_{26} \\ 0 & 0 & R_{26} & 0 \\ 0 & \rho_6 R_{26} & 0 & 0 \end{bmatrix}, \quad T(\underline{q}_6;R_{27}) = \begin{bmatrix} R_{27} & 0 & 0 & 0 \\ 0 & 0 & 0 & \rho_6^* R_{27} \\ 0 & 0 & R_{27} & 0 \\ 0 & \rho_6 R_{27} & 0 & 0 \end{bmatrix},$$

$$T(\underline{q}_6;R_{37}) = \begin{bmatrix} R_{37} & & & \\ & R_{37} & & \\ & & R_{37} & \\ & & & R_{37} \end{bmatrix}, \quad T(\underline{q}_6;R_{40}) = \begin{bmatrix} R_{40} & & & \\ & R_{40} & & \\ & & R_{40} & \\ & & & R_{40} \end{bmatrix},$$

where $\rho_6 = \exp(i\pi\mu)$.
We find for the characters $\chi(\underline{q}_6;R)$:

$$\begin{aligned} \chi(\underline{q}_6;R_1) &= 12 & \qquad \chi(\underline{q}_6;R_4) &= -4 \\ \chi(\underline{q}_6;R_{14}) &= 2 & \qquad \chi(\underline{q}_6;R_{15}) &= 2 \\ \chi(\underline{q}_6;R_{26}) &= 2 & \qquad \chi(\underline{q}_6;R_{27}) &= 2 \\ \chi(\underline{q}_6;R_{37}) &= 4 & \qquad \chi(\underline{q}_6;R_{40}) &= 4 \end{aligned}$$

Decomposition gives:

$c_1 = 3, \quad c_2 = 0, \quad c_3 = 0, \quad c_4 = 1, \quad c_5 = 4.$

and hence

$$\{T(\underline{q}_6;R)\} = \{T(\Delta,R)\} = 3\Delta_1 + \Delta_2' + 4\Delta_5. \tag{6.23}$$

Since Δ_5 is two-dimensional the four branches belonging to this irreducible representation are twofold degenerate by spatial symmetry. Applying (6.21) shows that all representations are of the first kind ($R_{14}^2 = R_{15}^2 = R_4$ and $R^2 = R_1$) and, consequently, time-reversal symmetry gives no additional degeneracy.

For the derivation of the symmetry adapted eigenvectors $\underline{E}(\underline{q}_6;s\mu)$ one has now to remember what has been said in subsection 6.4.1 about the compatibility of these vectors from (6.16) with (6.19). We may include here the anti-unitary symmetry operations $T(\underline{q}_6;S_-)$, where $S_- = R_{25} = i$, the inversion operator, which according to its definition given in subsection 6.4.1 is

section 6.4.

$$T(\underline{q}_6;S_-) = K_o \begin{bmatrix} R_{25} & 0 & 0 & 0 \\ 0 & 0 & 0 & \rho_6^2 R_{25} \\ 0 & 0 & R_{25} & 0 \\ 0 & \rho_6^2 R_{25} & 0 & 0 \end{bmatrix} .$$

Here K_o is defined by (6.9). One can easily verify that $T(\underline{q}_6;S_-)$ commutes with $T(\underline{q}_6;R)$ for all R. Consequently, on the corresponding irreducible representations the restrictions are imposed that they are real and that as many of them as possible are diagonal. For this reason in table 6.2 also the representation $\tau'^{(5)}$ has been included. This irreducible representation is obtained from the one listed by Kovalev, $\tau^{(5)}$, by a similarity transformation with a unitary matrix [1]).

The symmetry adapted eigenvectors are again obtained by applying (6.15) and (6.16) using the real representations of table 6.2. The result is

$$\underline{E}(\underline{q}_6;11)= \begin{bmatrix} 0 \\ 0 \\ a_1 \\ 0 \\ 0 \\ b_1 \\ 0 \\ 0 \\ c_1 \\ 0 \\ 0 \\ \rho_6 b_1 \end{bmatrix} , \quad E(\underline{q}_6;41)= \begin{bmatrix} 0 \\ 0 \\ 0 \\ 0 \\ 0 \\ a_4 \\ 0 \\ 0 \\ 0 \\ 0 \\ 0 \\ -\rho_6 a_4 \end{bmatrix} , \quad E'(\underline{q}_6;51)= \begin{bmatrix} a_5 \\ a_5 \\ 0 \\ b_5 \\ b_5 \\ 0 \\ c_5 \\ c_5 \\ 0 \\ d_5 \\ d_5 \\ 0 \end{bmatrix} , \quad E'(\underline{q}_6;52)= \begin{bmatrix} -a_5 \\ a_5 \\ 0 \\ -\rho_6^* d_5 \\ \rho_6^* d_5 \\ 0 \\ -c_5 \\ c_5 \\ 0 \\ -\rho_6 b_5 \\ \rho_6 b_5 \\ 0 \end{bmatrix} .$$

Since the anti-unitary operators could be included in the group we may impose (6.19) on the symmetry adapted eigenvectors. This gives the additional information: b_1 = real, a_4 = imaginary and $d_5 = \rho_6 b_5^*$. Furthermore from the normalisation condition it follows that $a_4 = i\sqrt{2}/2$.

The different blocks of the block-diagonalised dynamical matrix for this direction obtained by applying (6.17) are presented in

Appendix VI.D. $E'(\underline{q}_6;51)$ and $E'(\underline{q}_6;52)$ represent the two sets of eigenvectors corresponding to the twofold degenerate 4×4 matrix.

Symmetry direction Λ

$$\Lambda = \underline{q}_5 = \frac{2\pi\mu}{a}(1,1,1), \quad 0 < \mu < 0.5.$$

The point group of $\underline{q}_5$ is C_{3v}. It has 6 rotational elements, shown together with the irreducible representations in table 6.3. Explicit expressions for the R operators can be found in Appendix VI.B.

Table 6.3.

Irreducible representations of the group $G_o(\underline{q}_5) = C_{3v}$.

Ref.20	R_1	R_5	R_9	R_{37}	R_{41}	R_{45}	Ref.21
$\tau^{(1)}$	1	1	1	1	1	1	Δ_1
$\tau^{(2)}$	1	1	1	-1	-1	-1	Δ_2
$\tau^{(3)}$	$\begin{pmatrix}1&0\\0&1\end{pmatrix}$	$\begin{pmatrix}\varepsilon&0\\0&\varepsilon^2\end{pmatrix}$	$\begin{pmatrix}\varepsilon^2&0\\0&\varepsilon\end{pmatrix}$	$\begin{pmatrix}0&1\\1&0\end{pmatrix}$	$\begin{pmatrix}0&\varepsilon\\\varepsilon^2&0\end{pmatrix}$	$\begin{pmatrix}0&\varepsilon^2\\\varepsilon&0\end{pmatrix}$	Δ_3
$\tau'^{(3)}$	$\begin{pmatrix}1&0\\0&1\end{pmatrix}$	$\begin{pmatrix}-\frac{1}{2}&\frac{\sqrt{3}}{2}\\-\frac{\sqrt{3}}{2}&-\frac{1}{2}\end{pmatrix}$	$\begin{pmatrix}-\frac{1}{2}&-\frac{\sqrt{3}}{2}\\\frac{\sqrt{3}}{2}&-\frac{1}{2}\end{pmatrix}$	$\begin{pmatrix}1&0\\0&-1\end{pmatrix}$	$\begin{pmatrix}-\frac{1}{2}&\frac{\sqrt{3}}{2}\\\frac{\sqrt{3}}{2}&\frac{1}{2}\end{pmatrix}$	$\begin{pmatrix}-\frac{1}{2}&-\frac{\sqrt{3}}{2}\\-\frac{\sqrt{3}}{2}&\frac{1}{2}\end{pmatrix}$	Δ_3

$\varepsilon = \exp(i2\pi/3)$.

The T matrices obtained with (6.6) are

$$T(\underline{q}_5;R_1) = \begin{bmatrix} R_1 & & \\ & R_1 & \\ & & R_1 \end{bmatrix}, \quad T(\underline{q}_5;R_5) = \begin{bmatrix} R_5 & & \\ & R_5 & \\ & & R_5 \end{bmatrix},$$

section 6.4.

$$T(\underline{q}_5;R_9) = \begin{bmatrix} R_9 & & & \\ & R_9 & & \\ & & R_9 & \\ & & & R_9 \end{bmatrix}, \quad T(\underline{q}_5;R_{37}) = \begin{bmatrix} R_{37} & & & \\ & R_{37} & & \\ & & R_{37} & \\ & & & R_{37} \end{bmatrix},$$

$$T(\underline{q}_5;R_{41}) = \begin{bmatrix} R_{41} & & & \\ & R_{41} & & \\ & & R_{41} & \\ & & & R_{41} \end{bmatrix}, \quad T(\underline{q}_5;R_{45}) = \begin{bmatrix} R_{45} & & & \\ & R_{45} & & \\ & & R_{45} & \\ & & & R_{45} \end{bmatrix}.$$

The characters $\chi(\underline{q}_5;R)$ are:

$$\begin{aligned} \chi(\underline{q}_5;R_1) &= 12, & \chi(\underline{q}_5;R_{37}) &= 4, \\ \chi(\underline{q}_5;R_5) &= 0, & \chi(\underline{q}_5;R_{41}) &= 4, \\ \chi(\underline{q}_5;R_9) &= 0, & \chi(\underline{q}_5;R_{45}) &= 4. \end{aligned}$$

Decomposition gives:

$c_1 = 4, \quad c_2 = 0, \quad c_3 = 4.$

Hence

$$\{T(\underline{q}_5;R)\} = \{T(\Lambda;R)\} = 4\Lambda_1 \oplus 4\Lambda_3 . \qquad (6.24)$$

Since Λ_3 is two-dimensional the four branches belonging to this irreducible representation are two-fold degenerate by spatial symmetry. Similar arguments as for the Σ- and Δ-directions can be used to show that time-reversal gives no additional degeneracy.

For the same reasons as for the Δ-direction the real irreducible representation $\tau'^{(3)}$ has been included in table 6.3.
The symmetry adapted eigenvectors are:

$$\underline{E}(\underline{q}_5;11) = \begin{bmatrix} a_1 \\ a_1 \\ a_1 \\ b_1 \\ b_1 \\ b_1 \\ c_1 \\ c_1 \\ c_1 \\ d_1 \\ d_1 \\ d_1 \end{bmatrix}, \quad \underline{E}'(\underline{q}_5;31) = \begin{bmatrix} a_3 \\ a_3 \\ -2a_3 \\ b_3 \\ b_3 \\ -2b_3 \\ c_3 \\ c_3 \\ -2c_3 \\ d_3 \\ d_3 \\ -2d_3 \end{bmatrix}, \quad \underline{E}'(\underline{q}_5;32) = \begin{bmatrix} a'_3 \\ -a'_3 \\ 0 \\ b'_3 \\ -b'_3 \\ 0 \\ c'_3 \\ -c'_3 \\ 0 \\ d'_3 \\ -d'_3 \\ 0 \end{bmatrix}.$$

The irreducible blocks of the dynamical matrix obtained with these vectors are presented in Appendix VI.D. $\underline{E}'(\underline{q}_5;31)$ and $\underline{E}'(\underline{q}_5;32)$ represent the two sets of eigenvectors for the two-fold degenerate Λ_3 representation.

The ultimate goal of the group-theoretical analysis of the lattice vibrations set in this work is the acquisition of the framework in which the solution of the dynamical matrix in the main symmetry directions can be found in the most simple way. Since solutions for special points of higher symmetry like the origin and points at the zone boundaries can be obtained by continuity from those of the symmetry lines, a group-theoretical analysis of these symmetry points does not simplify the problem of solving the dynamical matrix. For this reason no explicit block-diagonalisation by group theory has been made for these points. For completeness, we will present the result for the decomposition of the representations in their irreducible representations, again in Kovalev and BSW notation, and their compatibility relations with the representations of the lines of symmetry.

Because the point groups of the wave vectors along the symmetry lines Δ, Σ and Λ are subgroups of the point group of the wave vector at a terminal symmetry point, the irreducible representation for such a point must provide a reducible representation of its subgroups (see

section 6.4.

e.g. Warren [2]). The irreducible representation of the subgroup is said to be compatible with the irreducible representation of the group at the symmetry point, when the former is contained in the decomposition of the latter. This can easily be checked with (6.14). These compatibility relations may also be found in tables given by Koster *et al.* [23]).

Symmetry point Γ

$\Gamma = \underline{q}_{11} = (0,0,0)$. The point group is O_h, which has 48 rotational elements [20,22]). Following the now familiar procedure one finds by decomposition:

$$\{T(\underline{q}_{11};R)\} = \{T(\Gamma;R)\} = \tau^{(4)} \oplus 3\tau^{(10)} = \Gamma'_{25} \oplus 3\Gamma_{15} \,. \qquad (6.25)$$

Both representations are three-dimensional. They have the following compatibility with the irreducible representations in Δ-, Σ- and Λ-direction:

$$\left.\begin{aligned}
\Gamma'_{25} &: \tau^{(4)} + \tau^{(5)} = \Delta'_2 + \Delta_5 \,, \\
\Gamma_{15} &: \tau^{(1)} + \tau^{(5)} = \Delta_1 + \Delta_5 \,, \\
\Gamma'_{25} &: \tau^{(1)} + \tau^{(2)} + \tau^{(4)} = \Sigma_1 + \Sigma_2 + \Sigma_3 \,, \\
\Gamma_{15} &: \tau^{(1)} + \tau^{(3)} + \tau^{(4)} = \Sigma_1 + \Sigma_4 + \Sigma_3 \,, \\
\Gamma'_{25} &: \tau^{(1)} + \tau^{(3)} = \Lambda_1 + \Lambda_3 \,, \\
\Gamma_{15} &: \tau^{(1)} + \tau^{(3)} = \Lambda_1 + \Lambda_3 \,.
\end{aligned}\right\} \qquad (6.26)$$

Symmetry point L

$L = \underline{q}_9 = \frac{\pi}{a}(1,1,1)$. The point group is D_{3d}, which has 12 rotational elements [20,22]). Decomposition in its irreducible representations gives

$$\begin{aligned}
\{T(\underline{q}_9;R)\} = \{T(L;R)\} &= 2\tau^{(1)} \oplus 2\tau^{(4)} \oplus 2\tau^{(5)} \oplus 2\tau^{(6)} \,, \\
&= 2L_1 \oplus 2L'_1 \oplus 2L_3 \oplus 2L'_3 \,.
\end{aligned} \qquad (6.27)$$

L_1 and L_1' are one-dimensional, L_3 and L_3' are two-dimensional. The compatibility with the irreducible representations in the Λ-direction is as follows:

$$\Lambda_1 : L_1 + L_1' \quad ; \qquad \Lambda_3 : L_3 + L_3' \quad . \tag{6.28}$$

Symmetry point X

$X = \underline{q}_{10} = \frac{2\pi}{a}(0,0,1)$. The point group is D_{4h}, which has 16 rotational elements [20,22]. Decomposition gives:

$$\begin{aligned} \{T(\underline{q}_{10};R)\} = \{T(X;R)\} &= \tau^{(1)} \oplus 2\tau^{(4)} \oplus \tau^{(6)} \oplus \tau^{(9)} \oplus 3\tau^{(10)} \\ &= M_1 \oplus 2M_2' \oplus M_3' \oplus M_5 \oplus 3M_5' \quad . \end{aligned} \tag{6.29}$$

M_1, M_2' and M_3' are one-dimensional, M_5 and M_5' two-dimensional. The compatibility with the irreducible representations of Δ- and Σ-directions is:

$$\begin{aligned} &M_1 : \Delta_1, \Sigma_1 \quad ; \qquad M_3' : \Delta_2', \Sigma_3 \quad ; \\ &M_2' : \Delta_1, \Sigma_3 \quad ; \qquad M_5' : \Delta_5, \Sigma_1, \Sigma_4 \; ; \\ &M_5 : \Delta_5, \Sigma_2, \Sigma_3 \; . \end{aligned} \tag{6.30}$$

6.5. Inelastic structure factors of Fe_3Al

As already mentioned in section 3.6, knowledge of the inelastic structure factor, defined by (3.39), is of great importance for the proper performance of neutron scattering experiments, in which the phonon dispersion relations are measured. In the calculation of these structure factors the eigenvectors of the dynamical matrix are needed. As shown in section 6.4 some of these eigenvectors are completely determined by symmetry, while others are found to have a relatively simple general form. The consequence of this is that the inelastic structure factors are not very sensitive to the parameters used in the model for which the dynamical matrix is solved, but depend mainly on

section 6.5.

the lattice structure. This insensitivity to the model parameters is demonstrated by the success in estimating the inelastic structure factor by comparing Fe_3Al with α-Fe.

It is possible to describe the dynamics of α-Fe with respect to the same lattice as that of Fe_3Al. For this purpose one must double the iron cell axis. In fig. 6.3a,b the effect of doubling the iron cell on the $(1\bar{1}0)$-plane and the (001)-plane of the reciprocal lattice is shown. The dashed lines indicate the zones of the original reciprocal

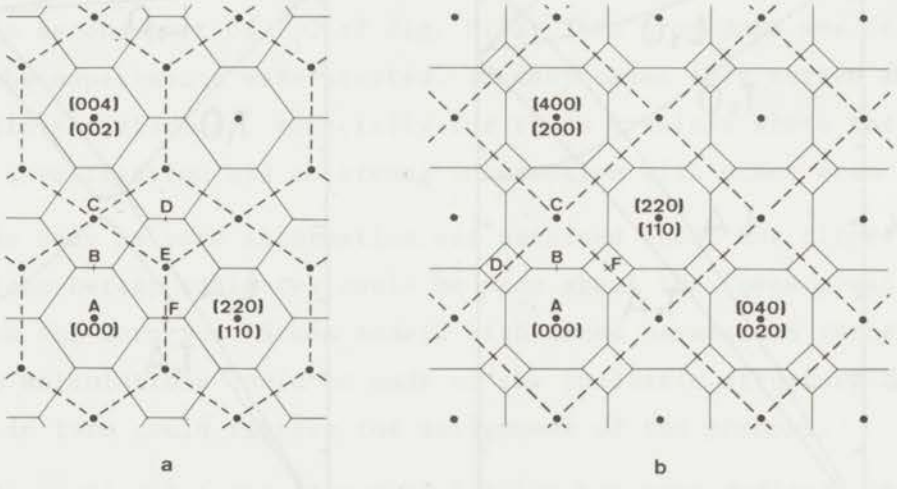

Fig. 6.3.

The $(1\bar{1}0)$-plane (a) and the (001)-plane (b) of the reciprocal lattice of Fe_3Al (zones indicated by solid lines) and α-Fe (zones indicated by dashed lines).

cell (corresponding to the b.c.c. lattice), while the solid lines mark the zones of the reciprocal lattice corresponding to the new f.c.c. lattice. For the description of the dispersion relations with respect to this lattice there are groups of equivalent line segments which were inequivalent in the original α-iron lattice. Such line segments are for instance in the [001]-direction: A-B; C-B and E-D, and in the [110]-direction A-F, E-B and C-D. Thus in the new description the parts of the dispersion relations originally corresponding to such a group of segments are now compressed in each single segment of the group, the consequence being an increase in the number of different phonon branches. In fig. 6.4a phonon dispersion relations of α-iron in the [001]-direction

in the new description are displayed. The curves are based on a second neighbour Born-von Kármán model. In fig. 6.4b an analogous calculation

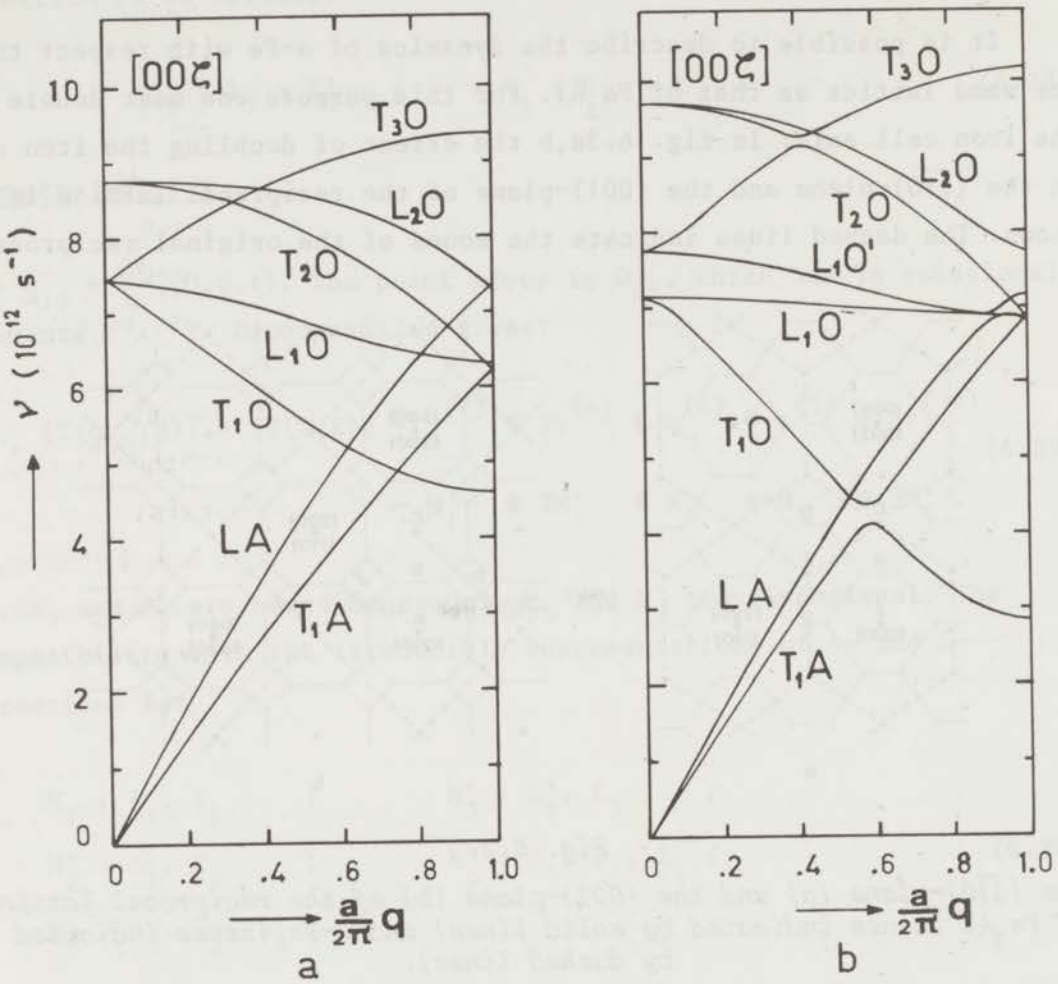

Fig. 6.4.

Calculated phonon dispersion relations in α-Fe (a) and Fe_3Al (b) by means of a second-neighbour Born-von Kármán model. The dispersion relations of both systems are described with respect to the reciprocal lattice of Fe_3Al.

with preliminary parameters for Fe_3Al is presented. The branches of fig. 6.4a can be obtained from a combination of the branches in the $[00\zeta]$-direction and along $[\frac{1}{2}\frac{1}{2}\zeta]$ in the normal description (compare fig. 5.2). For instance T_1A and T_2O are equivalent to the part of the T branch in the $[00\zeta]$-direction between 0 - 0.5 and 0.5 - 1, respectively, and T_1O is equivalent to Π between 0 - 0.5 along $[\frac{1}{2}\frac{1}{2}\zeta]$. The close relationship between the two structures is borne out in

section 6.5.

fig. 6.4a,b by the qualitative behaviour of the dispersion relations of both substances. Because of lower symmetry in Fe_3Al some of the branches which cross for α-Fe deflect away from each other in Fe_3Al since they belong to the same irreducible representation [2]), while the L_1O branch of α-iron splits up into two branches.

It seems reasonable to expect that related branches have to be observed at related positions in reciprocal space. For instance, for the observation of the T_1A branch of fig. 6.4b, one would choose the same configuration in reciprocal space as for the first part of T_1A and the second part of T_1O of fig. 6.4a. This procedure was followed when the experiments were started. In many cases this turned out to be quite satisfactory, especially for those q-values where the branch under investigation had no strong interaction with other branches.

As soon as more information was obtained about the dispersion relations better estimates could be made about the force constants used in the Born-von Kármán model. With these parameters rather accurate calculations could be made of the inelastic structure factor, which in turn could improve the assignment of the phonons.

In section 3.6 the structure lattice has been defined, which is meaningful when the conditions are satisfied for (3.42), *i.e.* $\underline{e}_j(\lambda;\underline{q}) = c(\lambda;\underline{q})\underline{e}_j$ with $c(\lambda;\underline{q})$ a complex number. It is obvious that for Fe_3Al the structure lattice is just the α-Fe lattice. From the symmetry adapted eigenvectors found by the group-theoretical analysis of the previous section it can be seen that the reduced structure factor has the form (3.42) for all branches of the Λ- and Δ-directions, and for the Σ_2 and the three Σ_4 branches of the Σ-direction.
The reduced inelastic structure factors for these branches, calculated with a third-neighbour Born-von Kármán model with central interactions between third neighbours, are presented in fig. 6.5. The labelling is consistent with the group-theoretical treatment of section 6.4.
The parameters used are those of table 6.5, first column, which will be discussed below.

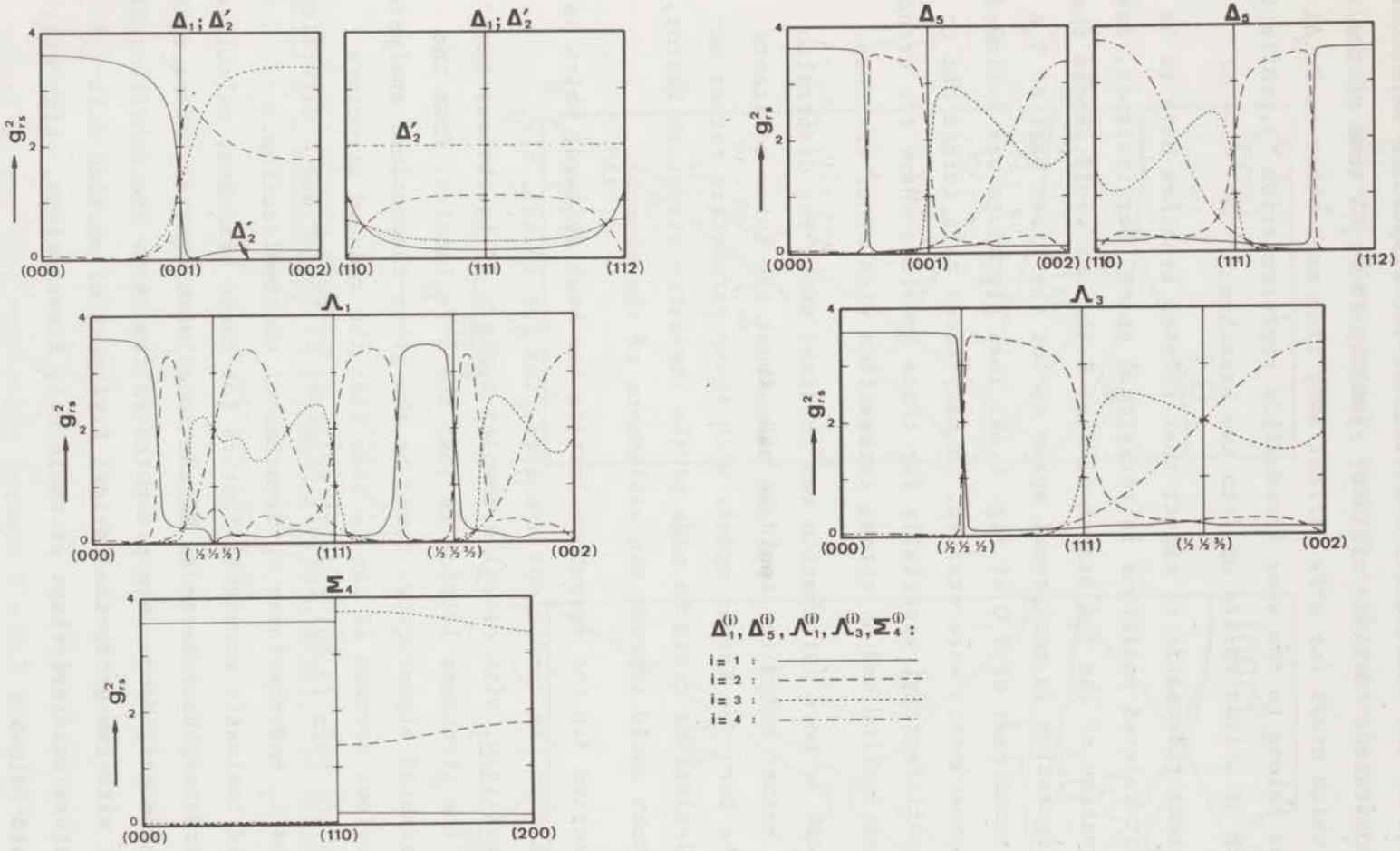

Fig. 6.5. Reduced inelastic structure factors for Fe_3Al.

section 6.6.

Table 6.4.

*Phonon frequencies in Fe_3Al at room temperature (in units of $10^{12}s^{-1}$). The estimated accuracy is better than 0.10, except for the values marked by *, which have an accuracy between 0.10 and 0.15.*

$\frac{a}{2\pi}\cdot q$	ν	ν	ν	ν	ν	ν	ν	ν
	$\Delta_1^{(1)}$	$\Delta_1^{(2)}$	$\Delta_1^{(3)}$	$\Delta_2^{(1)}$	$\Delta_5^{(1)}$	$\Delta_5^{(2)}$	$\Delta_5^{(3)}$	$\Delta_5^{(4)}$
0		7.10	10.45*	6.40				
0.05						6.40		
0.10		6.95		6.40		6.15	7.20	
0.15						6.00		
0.20	1.90*	6.95	10.50*	6.40		5.95	7.45	
0.25	2.40*				2.00	5.65		
0.30	2.90*	6.80		6.40	2.35	5.50	7.70	
0.35					2.65	5.25		
0.40	3.80*	6.90	10.25*	6.45	3.05	5.05	7.75	
0.45					3.40	4.80		
0.50	4.70*	6.80			3.80	4.55	7.70	
0.525					3.95			
0.55					4.15	4.40	7.75	
0.58					4.20	4.35		
0.60	5.20*	6.75	10.20*	6.50	4.10	4.50	7.60	10.60*
0.65					3.90	4.80		
0.70	5.70*	6.75		6.60	3.75	5.05	7.45	10.60*
0.75					3.55	5.35		
0.80	6.15*	6.75	9.80*	6.65	3.35	5.55	7.25	10.60*
0.85					3.20	5.90		
0.90	6.50*			6.60	3.10	6.10	6.85	10.80*
0.95					3.05	6.35		
1.00	6.50*		9.70*		3.00	6.60		10.90*

$\frac{a}{2\pi}\cdot q$	ν	ν	ν	ν	ν	ν	ν	ν	ν
	$\Sigma_1^{(1)}$	$\Sigma_1^{(2)}$	$\Sigma_1^{(3)}$	$\Sigma_1^{(4)}$	$\Sigma_4^{(1)}$	$\Sigma_4^{(3)}$	$\Sigma_3^{(1)}$	$\Sigma_3^{(2)}$	$\Sigma_3^{(3)}$
0		6.30		10.50*		10.50*			7.10
0.10		6.20							7.30
0.20		5.80		10.50*		10.50*			7.45
0.30	3.30	5.45			1.00		2.25		7.60
0.40	4.35	5.10		10.40*	1.30	10.55*	2.95		7.60
0.50	4.80	5.35	7.60				3.65		
0.60	4.35	6.00	7.15	10.20*	1.85	10.55*	4.25		
0.70	4.20	6.60	6.80					4.75	
0.80	4.40	6.20	7.30	10.20*	2.30	10.70*		5.30	
0.90	4.65		7.50					5.75	
1.00	(4.95)	4.95	7.70	10.45*	2.70	10.80*		6.15	
1.10	4.20	5.30	7.70					6.55	
1.20	3.70	5.75	7.40	10.80*	3.05	10.90*		6.70	
1.30	3.20	6.10						6.80	
1.40						10.90*			
1.414	3.05	6.50		10.90*	3.10			6.70	

$\frac{a}{2\pi}\cdot q$	ν	ν	ν	ν	ν	ν	ν	ν
	$\Lambda_1^{(1)}$	$\Lambda_1^{(2)}$	$\Lambda_1^{(3)}$	$\Lambda_1^{(4)}$	$\Lambda_3^{(1)}$	$\Lambda_3^{(2)}$	$\Lambda_3^{(3)}$	$\Lambda_3^{(4)}$
0			7.10	10.50*		6.40	7.10	
0.05								
0.10		6.05	7.20			6.10	7.20	
0.15								
0.20	2.40	5.70	7.60	10.30*		5.80	7.25	10.45*
0.25	2.95							
0.30	3.60	5.25	7.75			5.65	7.40	
0.33					1.50			
0.35	4.10							
0.40	4.55	4.95	7.80	10.25*		5.50	7.55	10.55*
0.44					2.00			
0.45		5.10						
0.50	4.70	5.45	7.50			5.25	7.65	
0.55		5.90			2.50			
0.60	4.70	6.30	7.10	10.05*		5.10	7.75	10.60*
0.65	4.90	6.65			3.00			
0.70	5.05	6.60	6.75			4.60	7.75	
0.75	5.25		7.00					
0.765					3.50			
0.80	5.45	6.10	7.20	9.90*		4.15	7.75	10.55*
0.852								
0.866	5.80	5.80	7.35		4.00	4.00	7.80	

6.6. Experiment and results

By means of the previously described triple-axis crystal spectrometer a great number of phonons has been observed in a single crystal of ordered Fe_3Al.* The crystal was 2.2 cm in diameter and 5 cm long. It was obtained from Metaalinstituut T.N.O., Delft.

Although strong super-reflections were found, it was not possible to determine quantitatively the degree of ordering by neutron scattering, due to strong extinction in a crystal of such large size.

From the literature [8]) it may, however, safely be concluded that for an alloy of the stoichiometric composition the ordering is very close to 100%. The full widths at half height of rocking curves for the (220), (400), (222) and (333) reflections were around 20'.

The experimental technique was mainly the same as described in chapter V for the measurements of α-Fe, except that improved monochromator and analyser crystals were utilized. In the present experiment zinc crystals were applied, which gave a higher intensity than

* A short report about these measurements appeared in Physics Letters [41]).

the previously used copper crystals. For the observation of the optical branches of high energy the alternative analysing technique was used of the inverse beryllium method, described in chapter IV.
The great advantage of this technique over the conventional diffraction technique, its much higher intensity in the final beam, made it indispensable for the observation of the high energetic phonons. A disadvantage is that the scattering data have to be interpreted with considerable care. Since not only neutrons scattered by a single spot in q-space can reach the detector, but also those scattered by a whole line in q-space [24], there is a chance of getting contributions from phonons belonging to different branches because of abrupt variation of the inelastic structure factor in the region of observation.

The observed phonon frequencies for the different branches are presented in table 6.4 and also displayed in figs. 6.6 and 6.7.

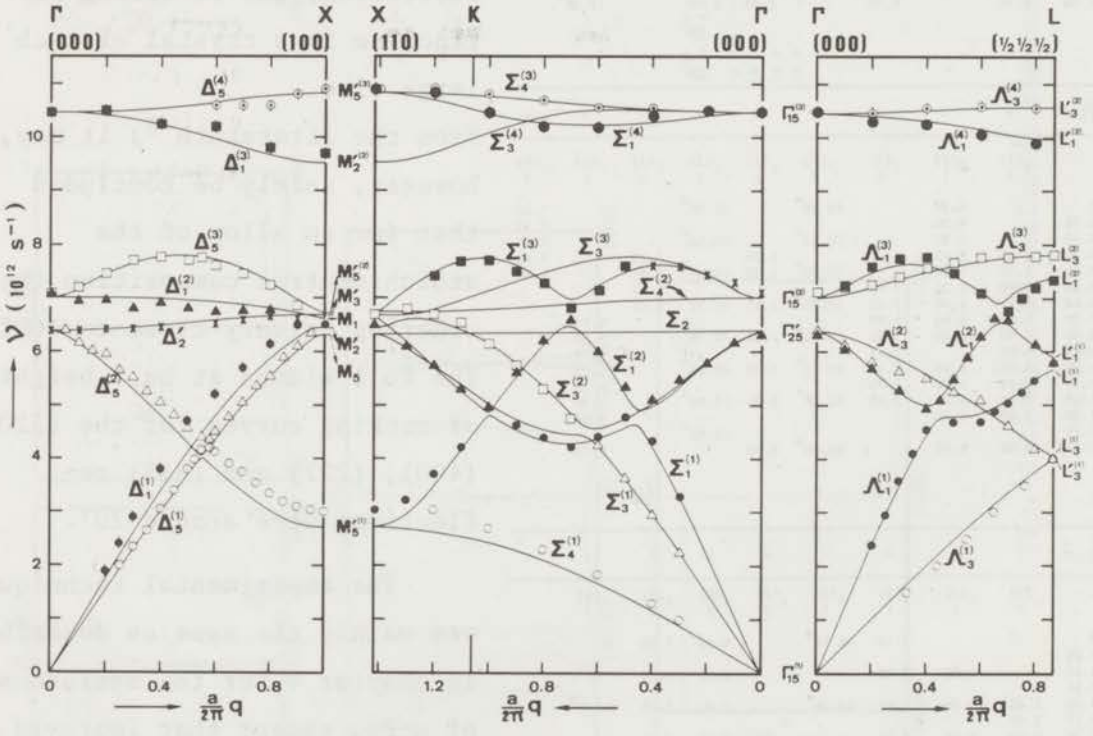

Fig. 6.6.

Phonon dispersion relations of Fe_3Al. The dots are experimental points. The solid lines represent a least squares fit to the experimental points with a third-neighbour Born-von Kármán model with central interactions between third neighbours. The elastic constants were imposed as constraints on the force constants.

section 6.6.

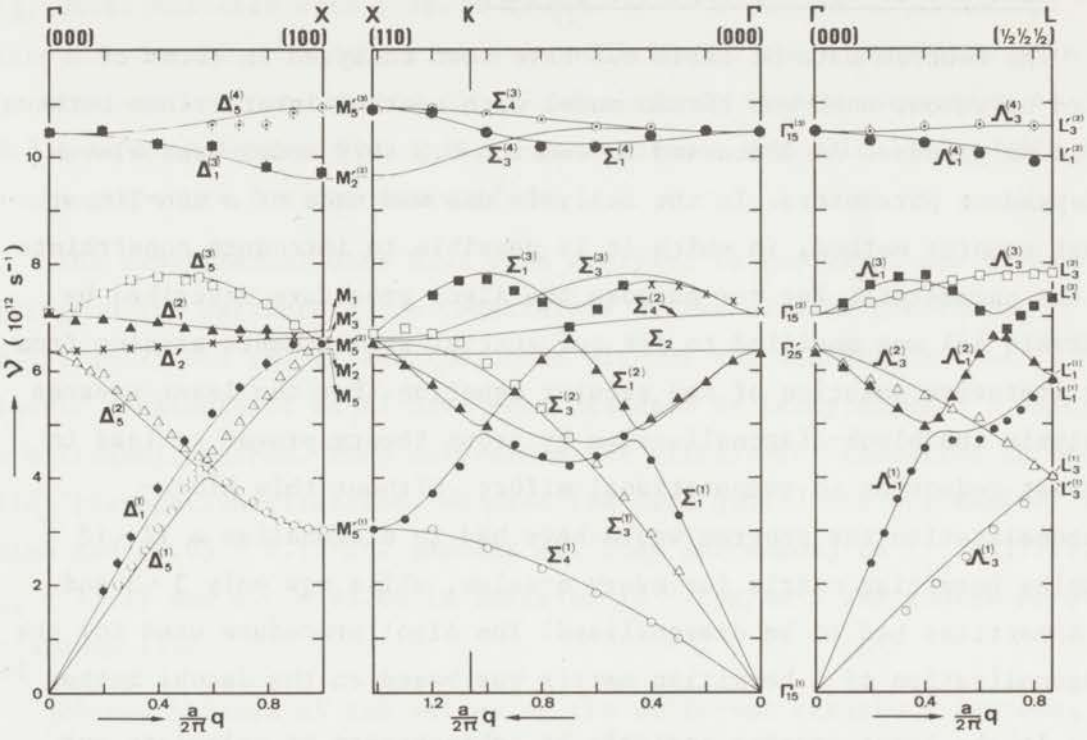

Fig. 6.7.

Phonon dispersion relations of Fe_3Al. The dots are experimental points. The solid lines represent a least squares fit to the experimental points with a third-neighbour Born-von Kármán model with central interactions between third neighbours.

The labelling is in accordance with the treatment of section 6.4. All data were collected at room temperature. For the Λ- and Δ-direction the experimental set is complete, but in the Σ-direction some branches have been measured incompletely, or not at all because of experimental difficulties, *e.g.* lack of scattering intensity or mixing with other branches. As the Σ_2 branch has zero structure factor both for measurements in the (110)- and the (001)-plane it could only have been measured in a non-symmetry plane, which is very complicated.

Not only scattering by more phonons at the same time, but also the occurrence of a great number of parasitic Bragg reflections caused by the larger cell of Fe_3Al, made it much more difficult to perform the experiments than in the case of α-Fe. Bragg scattering from the sample in the direction of the analysing system always gives rise to spurious peaks in the observed intensity. The observation of the $\Delta_1^{(1)}$-branch and $\Lambda_3^{(1)}$-branch especially suffered from this parasitic scattering.

6.7. Analysis of the experimental results

The neutron data of table 6.4 have been analysed in terms of a third neighbour Born-von Kármán model with central interactions between third neighbours. As discussed in section 6.3 this model uses eleven independent parameters. In the analysis use was made of a non-linear least squares method, in which it is possible to introduce constraints on the parameters. For our purpose the Algol procedure described by Rietveld [25]) was modified to fit our special requirements arising from the iterative solution of the secular equation. For the least squares analysis the block-diagonalisation by group theory proved to lead to a great reduction in computational effort. Without this block-diagonalisation the program would have had to diagonalise a 12×12 complex hermitian matrix for every q-value, while now only 3×3 and 4×4 matrices had to be diagonalised. The Algol procedure used for the diagonalisation of a hermitian matrix was based on the Jacobi method [26]).

In the least squares analysis it is necessary to calculate not only the quantities which have to fit the experimental data, *i.e.* the frequencies ν_i, but also their derivatives with respect to the model parameters p_k. These derivatives were obtained by a perturbation-like method in the following way:

$$\frac{2\nu_i \, \partial \nu_i}{\partial p_k} = \sum_{\ell,m} B^{\dagger}_{i\ell} \, dD^k_{\ell m} \, B_{mi} = \sum_{\ell,m} B_{\ell i} \, dD^k_{\ell m} \, B_{mi} \equiv d\Lambda^i_k$$

or

$$\frac{\partial \nu_i}{\partial p_k} = \frac{1}{2\nu_i} d\Lambda^i_k \quad , \tag{6.31}$$

where B is the unitary matrix of the eigenvectors obtained from the solution of the secular equation for the frequencies

$$\left| D(\underline{q}) - 4\pi^2 \nu^2 E \right| = 0$$

and dD^k is a matrix, whose elements are those of the dynamical matrix

section 6.7.

$D(\underline{q})$ differentiated with respect to p_k.
Since the Jacobi procedure yields in addition to the eigenvalues also the eigenvectors, the method of calculating the $\partial\nu_i/\partial p_k$ according to (6.31) is much faster than that of performing a new calculation with the Jacobi procedure for the derivatives.

The experimental data have been analysed in two ways, one by imposing on the parameters the constraints of the elastic constants, (6.1), (6.2) and (6.3), and the other without any constraint. The elastic constants of Fe_3Al have been measured by Leamy *et al.*[27]) using an ultrasonic method. They determined the ultrasonic velocities in the [110] propagation direction. We used the data quoted for the sample which had 25.05 ± 0.15 at. percent Al. They correspond to c_{11} = 17.10, c_{44} = 13.17 and c_{12} = 13.06 in units of 10^{11} dyn/cm^2. The quoted error is around 1.5%.

Since, because of the values of the different structure factors, some of the Σ-branches could not be observed individually, an analysis was made first for the different irreducible representations of the Δ- and Λ-directions. In this analysis the elastic constants were imposed as constraints on the parameters, the force constants. Fig. 6.6 shows the least squares fit to the experimental data of such an analysis. In order to avoid that too much weight was given to those branches which had very many experimental points, an equal mesh in q-space for the experimental points was used, thus omitting some of the data in the analysis. In a second analysis no constraints were put on the parameters, but now also the data of the Σ_4-branches were included. The fit to the experimental data is shown in fig. 6.7. In figs. 6.6 and 6.7 the group-theoretical labelling according to section 6.4 is used. The label assignment in the symmetry points Γ and X is uniquely obtained from (6.26) and (6.30). For the assignment in the point L, in addition to (6.28) the form of the polarisation vectors had to be considered.

The fit of fig. 6.7, based on the analysis without constraints, is better than the one of 6.6, showing a discrepancy between the ultrasonic and neutron data. This will be discussed in section 6.8. The two sets of force constants deduced in the two different analyses are given

in table 6.5. Here also the elastic constants deduced from the interatomic force constants by means of (6.1) - (6.4) are presented.

Table 6.5

Interatomic force constants of Fe_3Al

(units 10^2 dyn/cm)

	1)	2)
$\alpha_1(12)$	177.8 ± 2.3	177.1 ± 1.4
$\alpha_1(23)$	146.9 ± 3.8	147.8 ± 2.5
$\beta_1(12)$	191.4 ± 3.9	193.8 ± 2.6
$\beta_1(23)$	144.7 ± 4.0	143.8 ± 2.8
$\alpha_2(13)$	58.7 ±10.3	111.3 ± 6.9
$\alpha_2(24)$	21.0 ± 9.0	30.5 ± 5.1
$\beta_2(13)$	1.9 ± 5.8	-24.2 ± 4.2
$\beta_2(24)$	13.9 ± 4.4	7.8 ± 2.6
$\alpha_3(11)$	3.1 ± 2.5	2.6 ± 1.6
$\alpha_3(22)$	14.2 ± 1.9	15.1 ± 1.3
$\alpha_3(33)$	14.6 ± 3.1	19.6 ± 2.1

1) With the elastic constants c_{11} = 17.10, c_{44} = 13.17, and c_{12} = 13.06 in units of 10^{11} dyn/cm^2 imposed as constraints.

2) Analysis without constraints; the resulting values for the elastic constants are c_{11} = 19.9, c_{44} = 12.2, and $c_{12} = 14.6\times10^{11}$ dyn/cm^2.

The second set has been used for the calculation of the frequency distribution function. The program used for this is the same as that for iron, except that the diagonalisation of the dynamical matrix for the points in the irreducible unit of the first Brillouin zone of Fe_3Al now had to be done with the Jacobi procedure for complex matrices. Since this procedure is rather time consuming for a 12×12 matrix, the total number of diagonalisations has been limited to 217. A frequency channel width was used of 0.006×10^{12}cps. The resulting frequency distribution function is displayed in fig. 6.8. We also calculated

section 6.7.

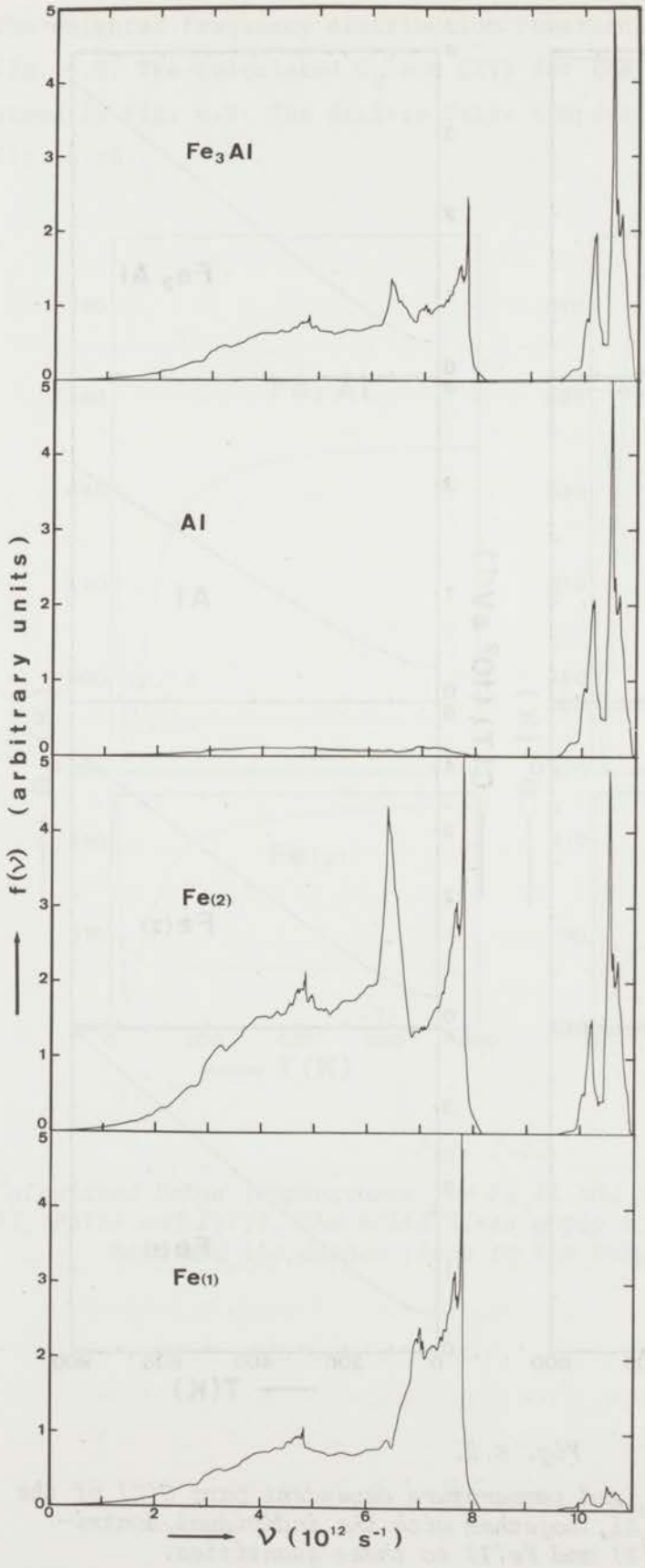

three functions which we will call weighted frequency distribution functions. In this calculation the weight of the frequencies is taken as the square of the absolute value of the polarisation vector of the different atoms for every $\underline{q}$ in reciprocal space. It can be shown that, if the weighted frequency distribution functions are used for the calculation of the specific heat (2.35) and the mean square displacements of the atoms (2.38), the contributions of the particular atoms are obtained. For the definition of the Debye-Waller factor of different atoms in the primitive unit cell ref. [28]) may be consulted.

Fig. 6.8.

Phonon frequency distribution function of Fe_3Al together with the weighted frequency distribution functions of Al, Fe(2) and Fe(1). In the interest of clarity these curves have not been normalised.

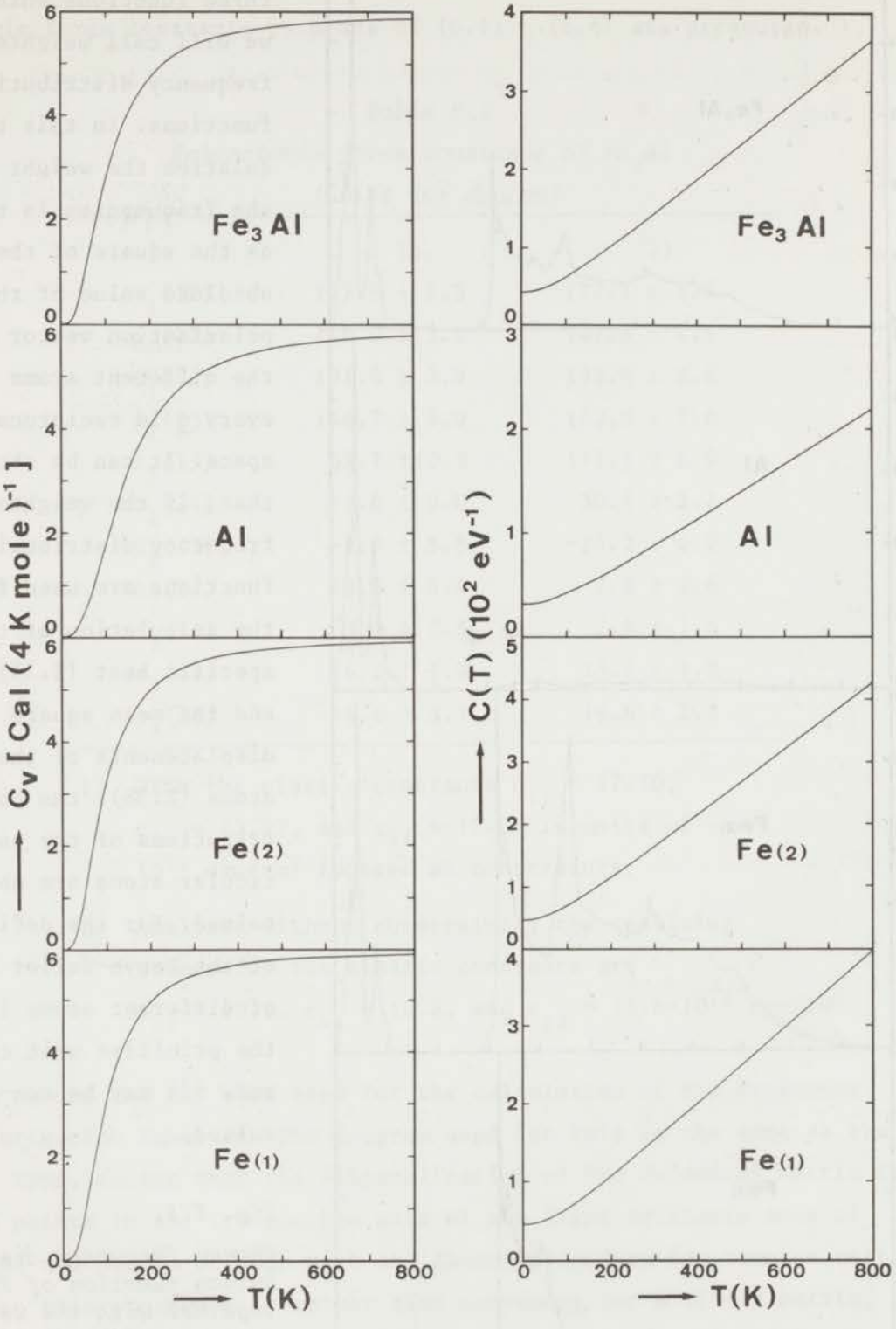

Fig. 6.9.

Calculated heat capacity C_v and temperature dependent part C(T) of the Debye-Waller factor for Fe_3Al, together with the individual contributions of Al, Fe(2) and Fe(1) to these quantities.

section 6.7.

The weighted frequency distribution functions are also displayed in fig. 6.8. The calculated C_V and C(T) for the different functions are shown in fig. 6.9. The derived Debye temperatures are displayed in fig. 6.10.

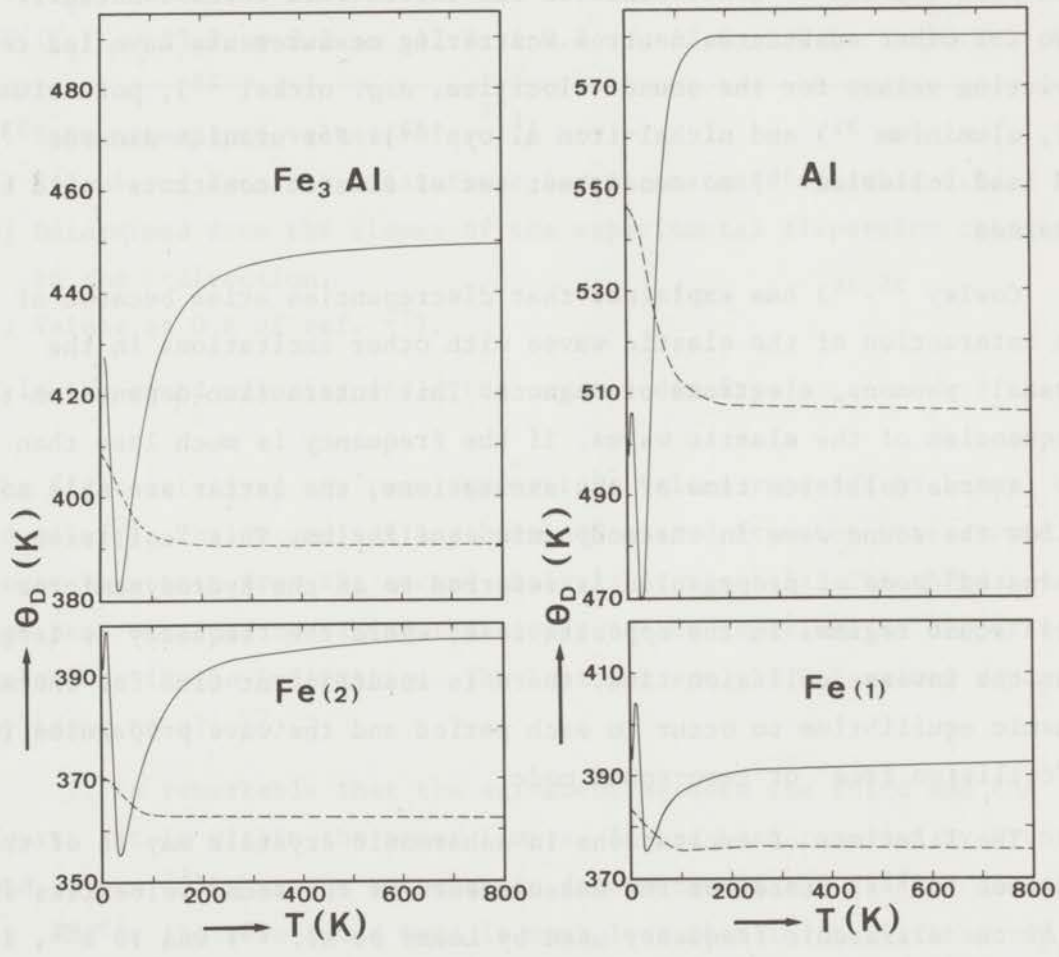

Fig. 6.10.

Calculated Debye temperatures for Fe_3Al and for the individual atoms Al, Fe(2) and Fe(1). The solid lines apply to the calculated specific heat and the dashed lines to the Debye-Waller factor.

6.8. Discussion

As already mentioned in the previous section the fit to the experimental data shown in fig. 6.7 is better than that shown in fig. 6.6, in which the elastic constants as measured by an ultrasonic technique have been imposed as constraints on the interatomic force constants. Also for other substances neutron scattering measurements have led to deviating values for the sound velocities, *e.g.* nickel [29]), potassium [30]), aluminium [31]) and nickel-iron alloys [32]). For uranium dioxyde [33]) and lead telluride [34]) no consistent set of elastic constants could be obtained.

Cowley [35,36]) has explained that discrepancies arise because of the interaction of the elastic waves with other excitations in the crystal: phonons, electrons or magnons. This interaction depends on the frequencies of the elastic waves. If the frequency is much less than the inverse collision time of the excitations, the latter are able to follow the sound wave in thermodynamic equilibrium. This "collision dominated" mode of propagation is referred to as the hydrodynamic or first sound regime. In the opposite case, where the frequency is larger than the inverse collision time, there is insufficient time for thermodynamic equilibrium to occur in each period and the wave propagates in a "collision free" or zero-sound mode.

The lifetimes of excitations in anharmonic crystals may be of the order of 10^{-11}s. Since for the measurements of the sound velocities in Fe_3Al the ultrasonic frequency used by Leamy *et al.* [27]) was $10^7 s^{-1}$, it is obvious that these measurements belong to the first sound region. The phonon frequencies detected in the present experiment were of the order of $10^{12} s^{-1}$ and may therefore be dominated by the zero-sound regime.

It has been shown by Cowley [35,36]) that the corrections to the elastic constants from anharmonic effects are different for the two regimes. Moreover, the corrections for the high-frequency region have only the point group symmetry of the crystal, whereas the low-frequency elastic constants have higher symmetry.

In table 6.6 four sets of elastic constants for the three acoustic waves in the Σ-direction are presented.

section 6.8.

Table 6.6.

Elastic constants for Fe_3Al in units of 10^{11} dyn/cm²

	1)	2)	3)	4)
$\rho V^2(\Sigma_1)$	28.2 ± 0.4	29.4 ± 0.3	28.6 ± 1.2	29.3 ± 0.6
$\rho V^2(\Sigma_4)$	2.02 ± 0.03	2.65 ± 0.03	2.60 ± 0.25	2.38 ± 0.05
$\rho V^2(\Sigma_3)$	13.2 ± 0.3	12.2 ± 0.2	13.0 ± 0.6	13.8 ± 0.3

1) Room temperature values ref. [27].

2) Calculated from the interatomic force constants of table 6.5.

3) Determined from the slopes of the experimental dispersion relations in the Σ-direction.

4) Values at 0 K of ref. [27].

V is the sound velocity and ρ the crystal density.

The first set gives the room temperature values reported by Leamy *et al.* [27]. The second set has been calculated from the interatomic force constants from the second analysis (table 6.5). The third set has been obtained by taking the slopes to the experimental dispersion relations in the Σ-direction. The last set are the 0 K values reported by Leamy *et al.* [27].

It is remarkable that the agreement between the third and the fourth set is within the error limits. It has been reported by Svensson and Buyers [37] that the temperature dependence of the elastic constants in KBr in the zero sound mode is much less than in the first sound mode. Since at 0 K both modes should yield equal results, the fair agreement between the last two sets of table 6.6 indeed suggests that zero sound modes have been observed in Fe_3Al.

The calculated dispersion curves of figs. 6.6 and 6.7 have a feature that could not always be observed experimentally, namely that branches belonging to the same irreducible representation never cross. Crossing of such branches can only occur in very special cases, as has been discussed by Warren [2]. Since in none of our calculations crossing of branches belonging to the same representation was found it is believed that accidental degeneracies of such branches in Fe_3Al are not possible.

However, the phonon branches $\Delta_5^{(1)}$ and $\Delta_5^{(2)}$ have been measured very carefully near the point of "accidental degeneracy", and within the experimental resolution no discontinuity was observed when we passed over from $\Delta_5^{(1)}$ to $\Delta_5^{(2)}$. Even no change in linewidth was detected, indicating that there is very little interaction between the two branches in this point.

The two sets of interatomic force constants give some indication about the changes in the interactions due to the presence of Al atoms as compared to α-Fe. First of all it seems remarkable that in Fe_3Al $\alpha_1(12) - \beta_1(12) < 0$. This indicates that the interaction between first-neighbour Al and Fe atoms is repulsive, contrary to the first-neighbour interactions in α-Fe. This was considered as an indication of some quasi covalency in α-Fe. The repulsive force seems in contradiction with the prevailing conception that in Fe_3Al some quasi-covalent bonding exists between first neighbours, caused by hybridization of s, p and d electrons [38]).

Pauling [39]) explained on the basis of the resonating-valence-bond theory [40]) the observed lattice parameter and the difference in magnetic moments between the Fe(1) and Fe(2) atoms as found by neutron diffraction [15]). Al is a so-called hypoelectronic atom, which has an excess of orbitals over electrons in the valence shell. Such an atom can increase its valence by accepting an electron from a hyperelectronic atom, which has an excess of electrons over orbitals in the valence shell, or a buffer atom. The latter can donate or accept electrons without change in valence. Fe is such a buffer atom. By removing half an electron from the Fe(2) to the Al atoms the metallic radius of Al is decreased so much that it would fit in the iron lattice without causing too much strain. Pauling [39]) estimates the metallic radius of Al originally 13% larger than that of the Fe atoms, and after electron transfer only 3.7%. This electron transfer to Al from the Fe(2) atoms implies that the magnetic moment of the Fe(2) atoms decreases from 2.22 Bohr magnetons to 1.64, while that of the Fe(1) atoms remains almost the same, 2.14. The observed values are 1.50 and 2.18, respectively [15]), in good agreement with this. In line with the reasoning given above the repulsive force between Al and Fe(2) may be explained by assuming that,

section 6.8.

although quasi-covalent bonding occurs, the attractive interaction not completely compensates the repulsive force because the metallic radius of the Al atom is still somewhat too large.

Since $\alpha_1(23) \simeq \beta_1(23)$ it may be concluded that the first-neighbour interaction between Fe(1) and Fe(2) has become neutral, but has not changed considerably otherwise. However, the second-neighbour interaction between Fe(2) atoms has decreased drastically. If this interaction in iron was determined by overlap of d orbitals, then this is much less the case in Fe_3Al. The fact that the force constants for the second neighbour interaction between Fe(1) and Al are larger, but still much smaller than the corresponding parameters in α-iron could indicate a preference for overlap with the p orbitals of Al.

That the interaction is predominantly determined by first neighbours is also reflected in the weighted frequency distribution functions. Fig. 6.8 shows that the contribution from the Al atom to the total frequency distribution stems mainly from the high energy region of the optic phonons, while the Fe(1) contribution mainly stems from the acoustic region. Comparison with the frequency distribution of α-Fe of fig. 5.6 shows that the Fe(1) atoms behave much the same as the Fe atoms in α-iron, while the Fe(2) atoms represent more the average behaviour of the Fe_3Al lattice. This is also demonstrated by the Debye temperatures derived for the individual atoms.

In the relatively small interaction between second neighbours may also be a clue for understanding the phase transition at about 820 K, above which temperature the Al and Fe(1) atoms redistribute themselves randomly over the lattice sites 1 and 3.

Since the description of the lattice dynamics in a Born-von Kármán model is phenomenological rather than physically realistic, one must be careful in attributing too much physical meaning to the individual force constants of this description. Moreover, including more parameters, which would lead to a better fit, could change the value of some of the force constants. Other force constants would also be obtained if one allows a certain amount of disorder, the possibility of which is not excluded by experimental investigations. However, a calculation per-

formed under the assumption that only 94% of the Al atoms were in position 1 and 6% randomly distributed over the other lattice sites showed that the force constants maintained their general character as discussed above.

It may here also be concluded that for the description of the lattice dynamics of Fe_3Al, just as for α-Fe, the Born-von Kármán model provides a good interpolation scheme, and it is believed that the calculated frequency distribution function represents the real lattice dynamical behaviour of Fe_3Al at room temperature. The extrapolation of the derived thermodynamic quantities to other temperatures is much less reliable, since for instance no anharmonic effects have been incorporated.

Appendix VI.A

Coefficients of the dynamical matrix $D(\underline{q})$ for ordered Fe_3Al, derived from expression (2.15).

$$D_{ii}(11;\underline{q}) = \frac{1}{m}\Big[8\alpha_1(12)+2\alpha_2(13)+4\beta_2(13)+8\alpha_3(11)-4\alpha_3(11)C_{2,i}\{C_{2,i+1}+C_{2,i+2}\}\Big] ,$$

$$D_{i,i+1}(11;\underline{q}) = \frac{1}{m}\Big[4\alpha_3(11)\ S_{2,i}S_{2,i+1}\Big] ,$$

$$D_{ii}(12;\underline{q}) = \frac{1}{(mM)^{\frac{1}{2}}}\Big[4\alpha_1(12)\{C_iC_{i+1}C_{i+2} - i\ S_iS_{i+1}S_{i+2}\}\Big]\cdot p_1 ,$$

$$D_{i,i+1}(12;\underline{q}) = \frac{1}{(mM)^{\frac{1}{2}}}\Big[4\beta_1(12)\{S_iS_{i+1}C_{i+2} - i\ C_iC_{i+1}S_{i+2}\}\Big]\cdot p_1 ,$$

$$D_{ii}(13;\underline{q}) = -\frac{1}{(mM)^{\frac{1}{2}}}\Big[2\alpha_2(13)C_{2,i} + 2\beta_2(13)C_{2,i+1} + 2\beta_2(13)C_{2,i+2}\Big]\cdot p_2 ,$$

$$D_{i,i+1}(13;\underline{q}) = 0,$$

$$D_{ii}(14;\underline{q}) = -\frac{1}{(mM)^{\frac{1}{2}}}\Big[4\alpha_1(12)\{C_iC_{i+1}C_{i+2} + i\ S_iS_{i+1}S_{i+2}\}\Big]\cdot p_3 ,$$

$$D_{i,i+1}(14;\underline{q}) = \frac{1}{(mM)^{\frac{1}{2}}}\Big[4\beta_1(12)\{S_iS_{i+1}C_{i+2} + i\ C_iC_{i+1}S_{i+2}\}\Big]\cdot p_3,$$

$$D_{ii}(22;\underline{q}) = \frac{1}{M}\Big[4\alpha_1(12)+4\alpha_1(23)+2\alpha_2(24)+4\beta_2(24)+8\alpha_3(22)+$$
$$-4\alpha_3(22)\ C_{2,i}\{C_{2,i+1}+C_{2,i+2}\}\Big] ,$$

$$D_{i,i+1}(22;\underline{q}) = \frac{1}{M}\Big[4\alpha_3(22)\ S_{2,i}S_{2,i+1}\Big] ,$$

$$D_{ii}(23;\underline{q}) = -\frac{1}{M}\Big[4\alpha_1(23)\{C_iC_{i+1}C_{i+2} - i\ S_iS_{i+1}S_{i+2}\}\Big]\cdot p_1 ,$$

$$D_{i,i+1}(23);\underline{q}) = \frac{1}{M}\left[4\beta_1(23)\{S_iS_{i+1}C_{i+2} - i\,C_iC_{i+1}S_{i+2}\}\right]\cdot p_1\ ,$$

$$D_{ii}(24;\underline{q}) = -\frac{1}{M}\left[2\alpha_2(24)\,C_{2,i} + 2\beta_2(24)\,C_{2,i+1} + 2\beta_2(24)\,C_{2,i+2}\right]\cdot p_2\ ,$$

$$D_{i,i+1}(24,\underline{q}) = 0,$$

$$D_{ii}(33;\underline{q}) = \frac{1}{M}\left[8\alpha_1(23)+2\alpha_2(13)+4\beta_2(13)+8\alpha_3(33)-4\alpha_3(33)C_{2,i}(C_{2,i+1}+C_{2,i+2})\right],$$

$$D_{i,i+1}(33;\underline{q}) = \frac{1}{M}\left[4\alpha_3(33)\,S_{2,i}S_{2,i+1}\right]\ ,$$

$$D_{ij}(34;\underline{q}) = D_{ij}(23;\underline{q})\ ,$$

$$D_{ij}(44;\underline{q}) = D_{ij}(22;\underline{q})\ ,$$

$$D_{ij}(\lambda\lambda';\underline{q}) = D_{ji}(\lambda\lambda';\underline{q}) = D_{ji}^{*}(\lambda'\lambda;\underline{q})\ .$$

The meaning of the symbols is as follows:

$C_i = \cos\frac{a}{4}q_i$, $S_i = \sin\frac{a}{4}q_i$, $C_{2,i} = \cos\frac{a}{2}q_i$ and $S_{2,i} = \sin\frac{a}{2}q_i$

with i = 1,2,3 corresponding to x,y,z.
Further:

$$p_1 = (C_1C_2C_3 - S_1S_2C_3 - S_1C_2S_3 - C_1S_2S_3) + i(S_1S_2S_3 - C_1C_2S_3 - C_1S_2C_3 - S_1C_2C_3),$$

$p_2 = (p_1)^2$ and $p_3 = (p_1)^3$. m and M are the masses of Al and Fe, respectively. The value of i,i+1, i+2 has to be taken modulo 3.

Appendix VI.B

Matrix representation of the rotational elements used in the T-representations of the Σ-, Δ-, and Λ-directions of Fe_3Al. The elements are presented in two groups: under the first group of rotational elements the four sublattices of Fe_3Al go into themselves, while under the second group the sublattices 2 and 4 interchange.

1.

$$R_1 = \begin{pmatrix} 1 & 0 & 0 \\ 0 & 1 & 0 \\ 0 & 0 & 1 \end{pmatrix} \quad \text{ident.} \quad , \quad R_4 = \begin{pmatrix} \bar{1} & 0 & 0 \\ 0 & \bar{1} & 0 \\ 0 & 0 & 1 \end{pmatrix} \quad 180^\circ \text{ rot.}[001] \, ,$$

$$R_5 = \begin{pmatrix} 0 & 1 & 0 \\ 0 & 0 & 1 \\ 1 & 0 & 0 \end{pmatrix} \quad 240^\circ \text{ rot.}[111] \, , \quad R_9 = \begin{pmatrix} 0 & 0 & 1 \\ 1 & 0 & 0 \\ 0 & 1 & 0 \end{pmatrix} \quad 120^\circ \text{ rot.}[111] \, ,$$

$$R_{40} = \begin{pmatrix} 0 & \bar{1} & 0 \\ \bar{1} & 0 & 0 \\ 0 & 0 & 1 \end{pmatrix} \quad \text{refl.}(110) \quad , \quad R_{37} = \begin{pmatrix} 0 & 1 & 0 \\ 1 & 0 & 0 \\ 0 & 0 & 1 \end{pmatrix} \quad \text{refl.}(\bar{1}10) \, ,$$

$$R_{45} = \begin{pmatrix} 0 & 0 & 1 \\ 0 & 1 & 0 \\ 1 & 0 & 0 \end{pmatrix} \quad \text{refl.}(\bar{1}01) \quad , \quad R_{41} = \begin{pmatrix} 1 & 0 & 0 \\ 0 & 0 & 1 \\ 0 & 1 & 0 \end{pmatrix} \quad \text{refl.}(0\bar{1}1) \, ,$$

2.

$$R_{14} = \begin{pmatrix} 0 & \bar{1} & 0 \\ 1 & 0 & 0 \\ 0 & 0 & 1 \end{pmatrix} \quad 90^\circ \text{ rot.}[001] \, , \quad R_{15} = \begin{pmatrix} 0 & 1 & 0 \\ \bar{1} & 0 & 0 \\ 0 & 0 & 1 \end{pmatrix} \quad 270^\circ \text{ rot.}[001] \, ,$$

$$R_{16} = \begin{pmatrix} 0 & 1 & 0 \\ 1 & 0 & 0 \\ 0 & 0 & \bar{1} \end{pmatrix} \quad 180^\circ \text{ rot.}[110] \, , \quad R_{25} = \begin{pmatrix} \bar{1} & 0 & 0 \\ 0 & \bar{1} & 0 \\ 0 & 0 & \bar{1} \end{pmatrix} \quad \text{inversion} \, ,$$

$$R_{26} = \begin{pmatrix} \bar{1} & 0 & 0 \\ 0 & 1 & 0 \\ 0 & 0 & 1 \end{pmatrix} \quad \text{refl.}(100) \quad , \quad R_{27} = \begin{pmatrix} 1 & 0 & 0 \\ 0 & \bar{1} & 0 \\ 0 & 0 & 1 \end{pmatrix} \quad \text{refl.}(010) \, ,$$

$$R_{28} = \begin{pmatrix} 1 & 0 & 0 \\ 0 & 1 & 0 \\ 0 & 0 & \bar{1} \end{pmatrix} \quad \text{refl.}(001) \, .$$

Appendix VI.C

We present here the steps leading to the symmetry adapted eigenvectors $\underline{E}$ for the Σ-direction of Fe_3Al.

We first apply the operation $T(\underline{q};R)$ on an arbitrary vector Ψ, where

$$\Psi = \begin{bmatrix} \psi_x(1) \\ \psi_y(1) \\ \psi_z(1) \\ \psi_x(2) \\ \psi_y(2) \\ \psi_z(2) \\ \psi_x(3) \\ \psi_y(3) \\ \psi_z(3) \\ \psi_x(4) \\ \psi_y(4) \\ \psi_z(4) \end{bmatrix}$$

The result is:

$$T(\underline{q}_4,R_1)\Psi = \begin{bmatrix} \psi_x(1) \\ \psi_y(1) \\ \psi_z(1) \\ \psi_x(2) \\ \psi_y(2) \\ \psi_z(2) \\ \psi_x(3) \\ \psi_y(3) \\ \psi_z(3) \\ \psi_x(4) \\ \psi_y(4) \\ \psi_z(4) \end{bmatrix} \quad ; \qquad T(\underline{q}_4;R_{16})\Psi = \begin{bmatrix} \psi_y(1) \\ \psi_x(1) \\ -\psi_z(1) \\ \rho_4^*\psi_y(4) \\ \rho_4^*\psi_x(4) \\ -\rho_4^*\psi_z(4) \\ \psi_y(3) \\ \psi_x(3) \\ -\psi_z(3) \\ \rho_4\psi_y(2) \\ \rho_4\psi_x(2) \\ -\rho_4\psi_z(2) \end{bmatrix}$$

$$T(\underline{q}_4;R_{28})\Psi = \begin{bmatrix} \psi_x(1) \\ \psi_y(1) \\ -\psi_z(1) \\ \rho_4^*\psi_x(4) \\ \rho_4^*\psi_y(4) \\ -\rho_4^*\psi_z(4) \\ \psi_x(3) \\ \psi_y(3) \\ -\psi_z(3) \\ \rho_4\psi_x(2) \\ \rho_4\psi_y(2) \\ -\rho_4\psi_z(2) \end{bmatrix} ; \qquad T(\underline{q}_4;R_{37})\Psi = \begin{bmatrix} \psi_y(1) \\ \psi_x(1) \\ \psi_z(1) \\ \psi_y(2) \\ \psi_x(2) \\ \psi_z(2) \\ \psi_y(3) \\ \psi_x(3) \\ \psi_z(3) \\ \psi_y(4) \\ \psi_x(4) \\ \psi_z(4) \end{bmatrix}$$

Using (6.15) and the data of table 6.1 we get:

$$P^{(1)}(\underline{q}_4) = \tfrac{1}{4}\{T(\underline{q}_4;R_1) + T(\underline{q}_4;R_{16}) + T(\underline{q}_4;R_{28}) + T(\underline{q}_4;R_{37})\}$$

$$P^{(2)}(\underline{q}_4) = \tfrac{1}{4}\{T(\underline{q}_4;R_1) + T(\underline{q}_4;R_{16}) - T(\underline{q}_4;R_{28}) - T(\underline{q}_4;R_{37})\}$$

$$P^{(3)}(\underline{q}_4) = \tfrac{1}{4}\{T(\underline{q}_4;R_1) - T(q_4;R_{16}) + T(\underline{q}_4;R_{28}) - T(\underline{q}_4;R_{37})\}$$

$$P^{(4)}(\underline{q}_4) = \tfrac{1}{4}\{T(q_4;R_1) - T(\underline{q}_4;R_{16}) - T(\underline{q}_4;R_{28}) + T(\underline{q}_4;R_{37})\}$$

Applying (6.16) we obtain:

$$\underline{E}(\underline{q}_4;11) = \tfrac{1}{4}\cdot \begin{bmatrix} 2\psi_x(1) + 2\psi_y(1) \\ 2\psi_x(1) + 2\psi_y(1) \\ 0 \\ \psi_x(2) + \psi_y(2) + \rho_4^*\{\psi_x(4) + \psi_y(4)\} \\ \psi_x(2) + \psi_y(2) + \rho_4^*\{\psi_x(4) + \psi_y(4)\} \\ 2\psi_z(2) - 2\rho_4^*\psi_z(4) \\ 2\psi_x(3) + 2\psi_y(3) \\ 2\psi_x(3) + 2\psi_y(3) \\ 0 \\ \psi_x(4) + \psi_y(4) + \rho_4\{\psi_y(2) + \psi_x(2)\} \\ \psi_x(4) + \psi_y(4) + \rho_4\{\psi_y(2) + \psi_x(2)\} \\ 2\psi_z(4) - 2\rho_4\psi_z(2) \end{bmatrix}$$

$$\underline{E}(\underline{q}_4;21) = \tfrac{1}{4}\cdot\begin{bmatrix} 0 \\ 0 \\ 0 \\ \psi_x(2) - \psi_y(2) + \rho_4^*\{\psi_y(4) - \psi_x(4)\} \\ -[\psi_x(2) - \psi_y(2) + \rho_4^*\{\psi_y(4) - \psi_x(4)\}] \\ 0 \\ 0 \\ 0 \\ 0 \\ \psi_x(4) - \psi_y(4) + \rho_4\{\psi_y(2) - \psi_x(2)\} \\ -[\psi_x(4) - \psi_y(4) + \rho_4\{\psi_y(2) - \psi_x(2)\}] \\ 0 \end{bmatrix}$$

$$\underline{E}(\underline{q}_4,31) = \tfrac{1}{4}\cdot\begin{bmatrix} 2\psi_x(1) - 2\psi_y(1) \\ -\{2\psi_x(1) - 2\psi_y(1)\} \\ 0 \\ \psi_x(2) - \psi_y(2) + \rho_4^*\{\psi_x(4) - \psi_y(4)\} \\ -[\psi_x(2) - \psi_y(2) + \rho_4^*\{\psi_x(4) - \psi_y(4)\}] \\ 0 \\ 2\psi_x(3) - 2\psi_y(3) \\ -\{2\psi_x(3) - 2\psi_y(3)\} \\ 0 \\ \psi_x(4) - \psi_y(4) + \rho_4\{\psi_x(2) - \psi_y(2)\} \\ -[\psi_x(4) - \psi_y(4) + \rho_4\{\psi_x(2) - \psi_y(2)\}] \\ 0 \end{bmatrix}$$

$$\underline{E}(\underline{q}_4;41) = \tfrac{1}{4}\cdot\begin{bmatrix} 0 \\ 0 \\ 4\psi_z(1) \\ \psi_x(2) + \psi_y(2) - \rho_4^*\{\psi_x(4) + \psi_y(4)\} \\ \psi_x(2) + \psi_y(2) - \rho_4^*\{\psi_x(4) + \psi_y(4)\} \\ 2\psi_z(2) + 2\rho_4^*\,\psi_z(4) \\ 0 \\ 0 \\ 4\psi_z(3) \\ \psi_x(4) + \psi_y(4) - \rho_4\{\psi_x(2) + \psi_y(2)\} \\ \psi_x(4) + \psi_y(4) - \rho_4\{\psi_x(2) + \psi_y(2)\} \\ 2\psi_z(4) + 2\rho_4\,\psi_z(2) \end{bmatrix}$$

The general form of these vectors is equivalent to that given in subsection 6.4.2.

Appendix VI.D

As an example how the different blocks of the block-diagonalised dynamical matrix are obtained by applying (6.17), we choose here the block of the symmetry adapted eigenvector $E(\underline{q}_4;31)$ of the Σ direction. (6.17) then results in two equivalent sets of four homogeneous equations:

$$\{D_{11}(11;\underline{q}_4) - D_{12}(11;\underline{q}_4)\}a_3 + \{D_{11}(12;\underline{q}_4) - D_{12}(12;\underline{q}_4)\}p_1 b_3 +$$
$$+ D_{11}(13;\underline{q}_4)p_2 c_3 + \{D_{11}(12;\underline{q}_4) - D_{12}(12;\underline{q}_4)\}p_3\rho_4 b_3 = \omega_3^2 a_3$$

$$\{D_{11}(12;\underline{q}_4) - D_{12}(12;\underline{q}_4)\}p_1^* a_3 + \{D_{11}(22;\underline{q}_4) - D_{12}(22;\underline{q}_4)\}b_3 +$$
$$+ \{D_{11}(23;\underline{q}_4) - D_{12}(23;\underline{q}_4)\}p_1 c_3 + D_{11}(24;\underline{q}_4)p_2\rho_4 b_3 = \omega_3^2 b_3$$

$$D_{11}(13;\underline{q}_4)p_2^* a_3 + \{D_{11}(23;\underline{q}_4) - D_{12}(23;\underline{q}_4)\}p_1^* b_3 +$$
$$+ \{D_{11}(33;\underline{q}_4) - D_{12}(33;\underline{q}_4)\}c_3 + \{D_{11}(23;\underline{q}_4) - D_{12}(23;\underline{q}_4)\}p_1\rho_4 b_3 = \omega_3^2 c_3$$

$$\{D_{11}(12;\underline{q}_4) - D_{12}(12;\underline{q}_4)\}p_3^* a_3 + D_{11}(24;\underline{q}_4)p_2^* b_3 +$$
$$+ \{D_{11}(23;\underline{q}_4) - D_{12}(23;\underline{q}_4)\}p_1^* c_3 + \{D_{11}(22;\underline{q}_4) - D_{12}(22;\underline{q}_4)\}\rho_4 b_3 = \rho_4\omega_3^2 b_3$$

p_1, p_2, p_3 are the symbols defined in Appendix 6.A.
Since for the Σ-direction the phase factor $\rho_4 = p_2^*$, the second and fourth equation are equivalent, so that the set may be reduced to three homogeneous equations:

$$[D_{11}(11)-D_{12}(11)]a_3 + \sqrt{2}[D_{11}(12)-D_{12}(12)]p_1\sqrt{2}\, b_3 + D_{11}(13)p_2 c_3 = \omega_3^2 a_3$$

$$\sqrt{2}\left[D_{11}(12)-D_{12}(12)\right]p_1^* a_3 + \left[D_{11}(22)+D_{11}(24)-D_{12}(22)\right]\sqrt{2}\, b_3 +$$

$$+ \sqrt{2}\left[D_{11}(23)-D_{12}(23)\right]p_1 c_3 = \omega_3^2\, \sqrt{2}\, b_3$$

$$D_{11}(13)p_2^* a_3 + \sqrt{2}\left[D_{11}(23)-D_{12}(23)\right]\sqrt{2}\, b_3 + \left[D_{11}(33)-D_{12}(33)\right]c_3 = \omega_3^2\, c_3$$

Here we have left out $\underline{q}_4$ in the notation. The reason for $\sqrt{2}\, b_3$ everywhere, is that it allows the corresponding simplification of the normalisation condition for $\underline{E}(\underline{q}_4;31)$, in which b_3^2 occurs twice as often as a_3^2 and c_3^2. In this way all blocks may be obtained for the different $\underline{E}$. The result is:

Σ-direction

Σ_1:

$D_{11}(11)+D_{12}(11)$	$\sqrt{2}\left[D_{11}(12)+D_{12}(12)\right]p_1$	$2D_{13}(12)p_1$	$D_{11}(13)p_2$
$\sqrt{2}\left[D_{11}(12)+D_{12}(12)\right]p_1^*$	$\left[D_{11}(22)+D_{11}(24)+D_{12}(22)\right]$	0	$\sqrt{2}\left[D_{11}(23)+D_{12}(23)\right]p_1$
$-2D_{13}(12)p_1^*$	0	$D_{33}(22)-D_{33}(24)$	$2D_{13}(23)p_1$
$D_{11}(13)p_2^*$	$\sqrt{2}\left[D_{11}(23)+D_{12}(23)\right]p_1^*$	$-2D_{13}(23)p_1^*$	$D_{11}(33)+D_{12}(33)$

Σ_2:

$D_{11}(22)-D_{11}(24)-D_{12}(22)$

Σ_3:

$D_{11}(11)-D_{12}(11)$	$\sqrt{2}\left[D_{11}(12)-D_{12}(12)\right]p_1$	$D_{11}(13)p_2$
$\sqrt{2}\left[D_{11}(12)-D_{12}(12)\right]p_1^*$	$\left[D_{11}(22)+D_{11}(24)-D_{12}(22)\right]$	$\sqrt{2}\left[D_{11}(23)-D_{12}(23)\right]p_1$
$D_{11}(13)p_2^*$	$\sqrt{2}\left[D_{11}(23)-D_{12}(23)\right]p_1^*$	$D_{11}(33)-D_{12}(33)$

Σ_4:

$D_{33}(11)$	$2D_{13}(12)p_1$	$\sqrt{2}\ D_{11}(12)$	$D_{33}(13)p_2$
$-2D_{13}(12)p_1^*$	$\left[D_{11}(22)-D_{11}(24)+D_{12}(22)\right]$	0	$2\,D_{13}(23)p_1$
$\sqrt{2}\ D_{11}(12)p_1^*$	0	$\left[D_{33}(22)+D_{33}(24)\right]$	$\sqrt{2}\ D_{11}(23)p_1$
$D_{33}(13)p_2^*$	$-2D_{13}(23)p_1^*$	$\sqrt{2}\ D_{11}(23)p_1^*$	$D_{33}(33)$

Δ-direction

Δ_1:

$D_{33}(11)$	$\sqrt{2}\ D_{11}(12)p_1$	$D_{33}(13)p_2$
$\sqrt{2}\ D_{11}(12)p_1^*$	$\left[D_{33}(22)+D_{33}(24)\right]$	$\sqrt{2}\ D_{11}(23)p_1$
$D_{33}(13)p_2^*$	$\sqrt{2}\ D_{11}(23)p_1^*$	$D_{33}(33)$

Δ_2':

$D_{33}(22)-D_{33}(24)$

Δ_5:

$D_{11}(11)$	$[D_{11}(12)+D_{12}(12)]p_1$	$D_{11}(13)p_2$	$[D_{11}(12)-D_{12}(12)]p_1$
$[D_{11}(12)-D_{11}(12)]p_1^*$	$D_{11}(22)$	$[D_{11}(23)+D_{12}(23)]p_1$	$D_{11}(24)$
$D_{11}(13)p_2^*$	$[D_{11}(23)-D_{12}(23)]p_1^*$	$D_{11}(33)$	$[D_{11}(23)+D_{12}(23)]p_1^*$
$[D_{11}(12)+D_{12}(12)]p_1^*$	$D_{11}(24)$	$[D_{11}(23)-D_{12}(23)]p_1$	$D_{11}(22)$

Λ-direction

Λ_1:

$[D_{11}(11)+2D_{12}(11)]$	$[D_{11}(12)+2D_{12}(12)]p_1$	$D_{11}(13)p_2$	$[D_{11}^*(12)+2D_{12}^*(12)]p_3$
$[D_{11}^*(12)+2D_{12}^*(12)]p_1^*$	$[D_{11}(22)+2D_{12}(22)]$	$[D_{11}(23)+2D_{12}(23)]p_1$	$D_{11}(24)p_2$
$D_{11}(13)p_2^*$	$[D_{11}^*(23)+2D_{12}^*(23)]p_1^*$	$[D_{11}(33)+2D_{12}(33)]$	$[D_{11}(23)+2D_{12}(23)]p_1$
$[D_{11}(12)+2D_{12}(12)]p_3^*$	$D_{11}(24)p_2^*$	$[D_{11}^*(23)+2D_{12}^*(23)]p_1^*$	$[D_{11}(22)+2D_{12}(22)]$

Λ_3:

$[D_{11}(11)-D_{12}(11)]$	$[D_{11}(12)-D_{12}(12)]p_1$	$D_{11}(13)p_2$	$[D_{11}^*(12)-D_{12}^*(12)]p_3$
$[D_{11}^*(12)-D_{12}^*(12)]p_1^*$	$[D_{11}(22)-D_{12}(22)]$	$[D_{11}(23)-D_{12}(23)]p_1$	$D_{11}(24)p_2$
$D_{11}(13)p_2^*$	$[D_{11}^*(23)-D_{12}^*(23)]p_1^*$	$[D_{11}(33)-D_{12}(33)]$	$[D_{11}(23)-D_{12}(23)]p_1$
$[D_{11}(12)-D_{12}(12)]p_3^*$	$D_{11}(24)p_2^*$	$[D_{11}^*(23)-D_{12}^*(23)]p_1^*$	$[D_{11}(22)-D_{12}(22)]$

References

1. A.A. Maradudin and S.H. Vosko, Revs. Modern Phys., 40 (1968), 1.
2. J.L. Warren, Revs. Modern Phys., 40 (1968), 38.
3. S.H. Chen, Phys. Rev., 163 (1967), 3.
4. W.B. Waeber, J. Phys. C, 2 (1969), 882, 903.
5. A.J. Bradley and A.H. Jay, Proc. R. Soc., A136 (1932), 210.
6. A. Taylor and R.M. Jones, J. Phys. Chem. Solids, 6 (1958), 16.
7. YA.P. Selisskiy, Fiz. metal. metalloved., 21 (1966), 894-UDC.548.53.
8. Tetsuo Eguchi, Hidehiko Matsuda, Kensuki Oki, Shin-ichiro Kiyoto, and Kikue Yasutake, Trans. Jap. Inst. Metals, 8 (1967), 174.
9. L. Cser, J. Ostanevich and L. Pál, phys. stat. sol., 20 (1967), 581, 591.
10. F.W. Schapink, Scripta Met., 2 (1968), 635.
11. V.V. Nemoshkalenko, O.N. Rasumov, and V.V. Gorskii, phys. stat. sol., 29 (1968), 45.
12. L. Guttman, H.C. Schnyders, and G.J. Aray, Phys. Rev. Letters, 22 (1969), 517.
13. L. Guttman and H.C. Schnyders, Phys. Rev. Letters, 22 (1969), 520.
14. M.R. Lesoille and P.M. Gielen, phys. stat. sol., 37 (1970), 127.
15. S.J. Pickart and R. Nathans, Phys. Rev., 123 (1961), 1163.
16. M.B. Stearns, Phys. Rev., 168 (1968), 588.
17. F. Leoni and C. Natoli, Physica, 40 (1969), 553.
18. W. Gläser, Neutron Inelastic Scattering, Vol. I, Proc. Symp. Copenhagen, 1968, Vienna, IAEA (1968), 242.
19. G. Borgonovi, G. Logiudice, and D. Tocchetti, J. Phys. Chem. Solids, 28 (1967), 467.
20. O.V. Kovalev, Irreducible Representations of the Space Groups, Academy of Sciences of the Ukrainian SSR, Kiev, 1961 (English transl.: Gordon and Breach Science Publishers, New York, 1964).
21. L.P. Bouckaert, R. Smoluchowski, and E. Wigner, Phys. Rev., 50 (1936), 58.
22. G.F. Koster, Space Groups and their Representations, in "Solid State Physics", Vol. V, edited by F. Seitz and D. Turnbell, Academic Press, New York, 1957.

23. G.F. Koster, J.O. Dimmock, R.G. Wheeler, and H. Statz, Properties of the Thirty-two Point Groups, M.I.T. Press, Cambridge, Massachusetts, 1963.
24. J. Bergsma, thesis Leiden, (1970); also RCN-121, (1970).
25. H.M. Rietveld, RCN-67, (1967).
26. J.H. Wilkinson, The Algebraic Eigenvalue Problem, Clarendon Press, Oxford, 1965.
27. H.J. Leamy, E.D. Gibson, and F.X. Kayser, Acta Met., 15 (1967), 1827.
28. I.I. Gurevich and L.V. Tarasov, Low-energy Neutron Physics, Physics Institute of the Academy of Sciences of the USSR, Moscow (English transl.: edited by R.I. Sharp and S. Chomet, North-Holland Publishing Company, Amsterdam, 1968).
29. R.J. Birgeneau, J. Cordes, G. Dolling, and A.D.B. Woods, Phys. Rev., 136 (1964), A1359.
30. R.A. Cowley, A.D.B. Woods, and G. Dolling, Phys.Rev., 150 (1966), 487.
31. R. Stedman and G. Nilsson, Phys. Rev., 145 (1966), 492.
32. E.D. Hallman and B.N. Brockhouse, Can. J. Phys., 47 (1969), 1117.
33. G. Dolling, R.A. Cowley, and A.D.B. Woods, Can. J. Phys., 43 (1965), 1397.
34. W. Cochran, R.A. Cowley, G. Dolling, and M.M. Elcombe, Proc. Roy. Soc., 293 (1966), 433.
35. R.A. Cowley, Proc. Phys. Soc., 90 (1967), 1127.
36. R.A. Cowley, W.J.L. Buyers, E.C. Svensson, and G.L. Paul, Neutron Inelastic Scattering, Vol. I, Proc. Symp. Copenhagen, 1968, Vienna, IAEA (1968), 281.
37. E.C. Svensson and W.J.L. Buyers, Phys. Rev., 165 (1968), 1063.
38. L. Brewer, Electronic Structure and Alloy Chemistry of the Transition Elements, edited by P.A. Beck, John Wiley and Sons, New York, 1963, 221.
39. L. Pauling, Quantum Theory of Atoms, Molecules, and the Solid State, edited by P.-O. Löwdin, Academic Press, New York, 1966, 303.
40. L. Pauling, The Nature of the Chemical Bond, third edition, Cornell University Press, New York, 1960.
41. C. van Dijk, Phys. Letters, 32A (1970), 255.

Chapter VII

CONCLUDING REMARKS

The present study shows that coherent inelastic neutron scattering not only may provide a complete picture of the lattice vibrations of structurally simple systems such as α-Fe, but also for more complicated substances such as Fe_3Al, which has 4 atoms per primitive unit cell. For these more complicated systems in particular it is of great importance to perform a group-theoretical analysis of the lattice vibrations. Such an analysis enables one to recognise those features which are conditioned by the symmetry of the crystal.

By means of the Born-von Kármán model the dynamics of both α-Fe and Fe_3Al could phenomenologically very well be described. This opens the possibility of separating the contribution of the lattice vibrations to the thermodynamic quantities from those due to other excitations in the crystal. For example, the magnetic contribution to the specific heat for α-Fe might be calculated as a function of temperature by subtracting from the experimentally determined specific heat the contribution of the lattice vibrations (fig. 5.7) and that of the electrons, which is known from other experiments.

The force constants obtained in the Born-von Kármán description give some insight in the character of the acting forces and the differences in the interatomic potentials of α-Fe and Fe_3Al. However, due to the lack of an adequate theory, not much information is obtained about the role that the electronic structure plays in the lattice dynamics of these two specimens. Moreover, the observed dispersion relations do not exhibit clear effects, which can directly be related to the shape of the Fermi surface, and thus no direct experimental evidence is obtained about the electron-phonon interactions of the systems studied. One might, however, expect more information on this from a study of the phonons at liquid nitrogen or lower temperatures. Changes of phonon line widths would occur if strong electron-phonon interactions take place. In the case of Fe_3Al such a study might also aid in clarifying the discrepancies between the velocities of sound measured by ultrasonic and neutron scattering techniques.

It is well known that in many of the phase transitions occurring in crystalline solids the lattice vibrations have a decisive influence. One may wonder what kind of information the present study of the lattice dynamics of Fe_3Al bears on this problem, or which additional studies should be made to better understand this phenomenon in Fe_3Al. It is clear that a description of the lattice dynamics within the framework of a harmonic theory, which has temperature independent parameters, never will predict a phase transition. This is not even the case when anharmonic terms are introduced by means of a perturbation method. More succesful in this respect would be methods using self-consistent potentials [1]).

An additional difficulty resides in the fact that the situation for Fe_3Al is somewhat unclear. From the literature it can not be uniquely decided what exactly happens at around 550°C. It is very well possible that two phases, DO_3- and B2-structure (CsCl), are in equilibrium above this temperature [2]). Furthermore a double Curie-point has been observed in this neighbourhood, depending upon the thermal history [3]). For this reason the vibrational spectrum is certainly not the only factor which plays a role in the phase transformations, but knowledge about changes in the vibrational behaviour will still provide more insight in the system. A neutron study of the 50% disordered alloy probably can be made at room temperature, since by quenching from above 550°C the B2-structure is obtained [3]). A fair guess of its vibrational behaviour can already be made on the basis of what is now known about ordered Fe_3Al, allowing for the change in symmetry. In the B2-phase the positions 1 and 3 (see fig. 6.1) are randomly occupied by Al and Fe(1) atoms. Hence there are only two inequivalent positions, say 1 and 2. A set of force constants may be obtained from table 6.4, second column, by taking for the first neighbour interaction the average interactions of (1-2) and (1-3), for the second-neighbour (1-1)-interactions the (1-3)-interactions and for (2-2) the (2-4)-interaction. For the third-neighbour interactions between (1-1)-atoms, the average of (1-1)- and (2-2)-interactions is taken and for the (2-2)-interactions the (2-4)-interactions. With these force constants the dispersion relations in the symmetry directions of B2-type Fe_3Al have been calculated. They are displayed in fig. 7.1, together with, for comparison, the calculated dispersion relations of ordered Fe_3Al and α-Fe.

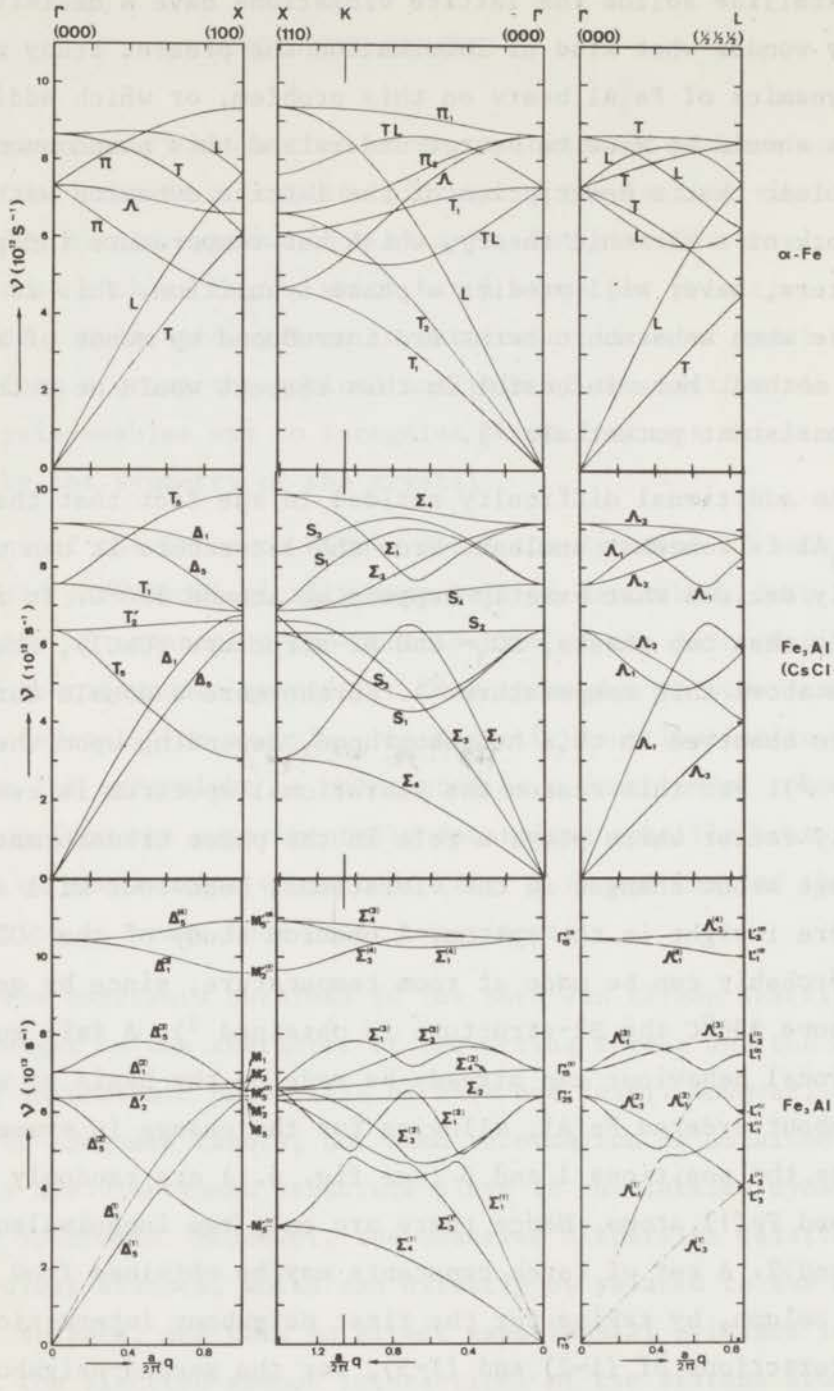

Fig. 7.1. Calculated phonon dispersion relations for α-Fe, CsCl-type Fe_3Al and ordered Fe_3Al, displayed with respect to the DO_3-lattice. The labelling for α-Fe is according to Fig. 5.2 and that for CsCl-type Fe_3Al to the group-theoretical description with respect to the CsCl-lattice.

The relation between the B2- and DO_3-structures in reciprocal space is shown in fig. 7.2 (that between the DO_3- and the α-Fe structures was shown in fig. 6.3), for the $(1\bar{1}0)$-and (001)-planes of the reciprocal lattice.

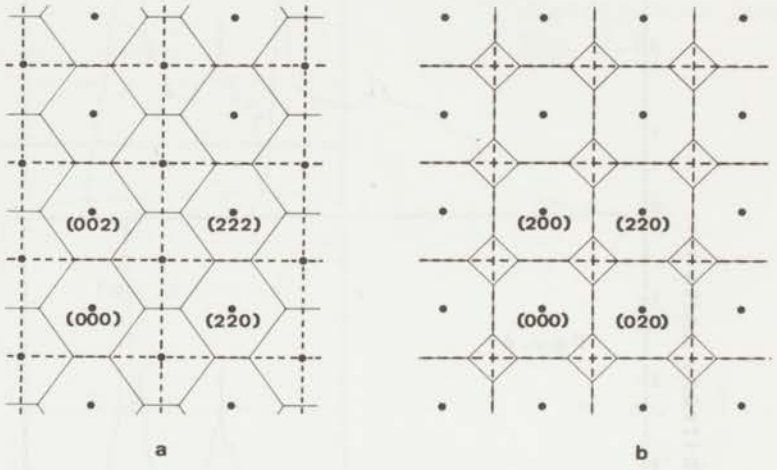

Fig. 7.2. The $(1\bar{1}0)$- and (001)-planes of the reciprocal lattice of ordered Fe_3Al (solid lines) and CsCl-type Fe_3Al (dashed lines).

The frequency distribution functions for the disordered crystal have also been calculated and are shown in fig. 7.3. Comparison with fig. 6.8 reveals as most remarkable difference the disappearance of the frequency gap in the spectrum. The Debye temperature, shown in fig. 7.4, deduced from the Debye-Waller factor calculation is about the same as that for ordered Fe_3Al and is in rather good agreement with X-ray measurements of Nemnonov et al. [4]), which reported 380°C and 390°C, respectively, for the DO_3- and B2-type alloy. The specific heat Debye temperature differs by about 20°, which indicates that as a consequence of the different vibrational spectrum the thermodynamic functions may be different.

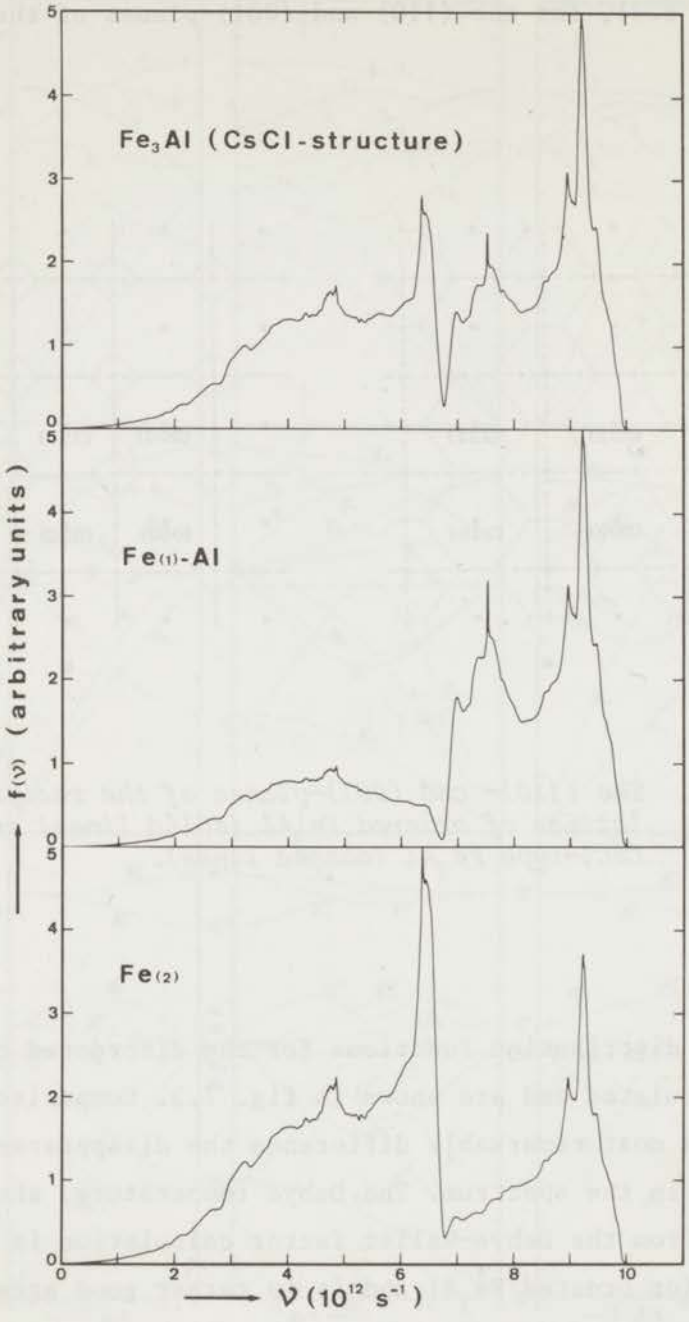

Fig. 7.3. The frequency distribution function for CsCl-type Fe Al together with the weighted frequency distribution functions (cf. fig. 6.8) for the (Fe(1)-Al)- and Fe(2)-atoms.

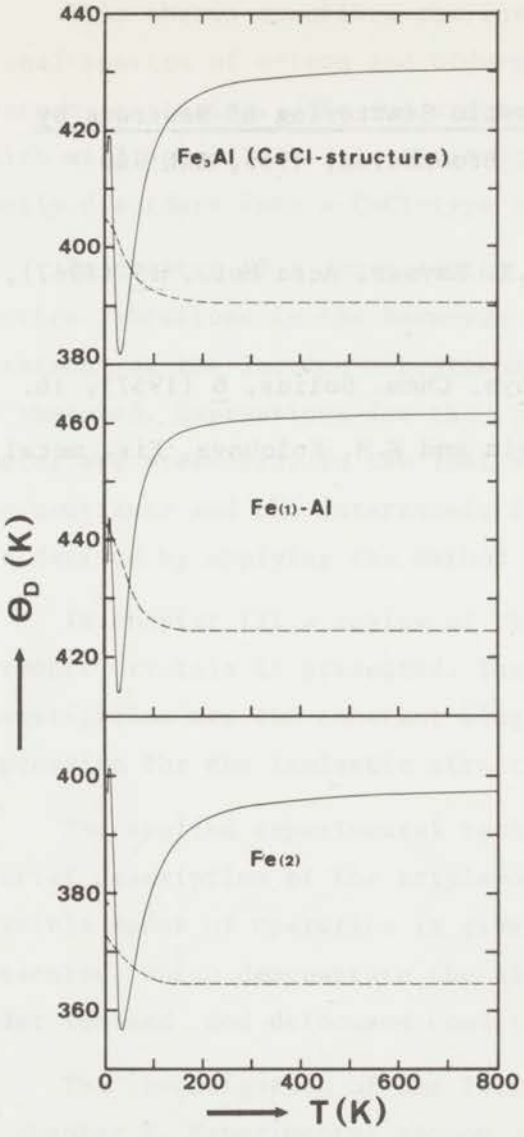

Fig. 7.4.

Debye temperatures calculated from the specific heat (solid curve) and the Debye-Waller factor (dashed curve) using the frequency distribution functions of Fig. 7.3.

Other useful information could be obtained by the investigation of the behaviour of the high optical phonons at the zone boundary of the Λ-direction during heating from below to beyond the transition temperature. Fig. 7.1 shows that on passing the transition temperature the frequency gap, which exists in ordered Fe_3Al, must disappear.

Very often phonons are well defined also in the neighbourhood of the transition temperature and consequently frequency changes as a function of temperature can probably be determined rather accurately by neutron inelastic scattering. This method could thus be superior for the study of the character of the phase transition to that of critical X-ray scattering, where the intensity of a vanishing reflection has to be established.

References

1. N. Boccara, Symposium on Inelastic Scattering of Neutrons by Condensed Systems, Proc. Symp. Brookhaven, 1965, BNL 940 (1966), 44.

2. H.J. Leamy, E.D. Gibson and F.X. Kayser, Acta Met., 15 (1967), 1827.

3. A. Taylor and R.M. Jones, J. Phys. Chem. Solids, 6 (1957), 16.

4. S.A. Nemnonov, L.D. Finkelshtein and K.M. Kolobova, Fiz. metal. metalloved., 9, (1960), 243.

SUMMARY

This thesis describes the investigation of the lattice-vibrational spectra of α-iron and ordered Fe_3Al by means of inelastic neutron scattering. α-Fe and ordered Fe_3Al are structurally related, which will be reflected in their dynamical behaviour. Ordered Fe_3Al partly disorders into a CsCl-type structure beyond about 550°C.

In chapter II a short review is given of the description of the lattice vibrations in the Born-von Kármán theory. After the classical treatment of the lattice vibrations, the quantum mechanical approach is sketched. Expressions for the specific heat and the Debye-Waller factor are presented. In the last section relations between the elastic constants and the interatomic force constants in crystal lattices are derived by applying the method of long waves.

In chapter III a review of the theory of neutron scattering by harmonic crystals is presented. The most important results for this investigation are the coherent single-phonon cross section and the expression for the inelastic structure factor.

The applied experimental technique is described in Chapter IV. A brief description of the triple-axis crystal spectrometer and its possible modes of operation is given. Experimental data on α-Fe are presented, which demonstrate the effect of operating the spectrometer under focused and defocused conditions.

The investigation of the lattice dynamics of α-Fe is reported in chapter V. Experimental phonon dispersion relations for directions of higher symmetry are presented. A least-squares analysis was made with a fifth-neighbour Born-von Kármán model. This analysis yielded interatomic force constants which were used for the calculation of the lattice-vibrational frequency distribution function and some related thermodynamic quantities. The data are compared with those obtained by other neutron studies and X-ray investigations. The experimental dispersion relations are also compared with a calculation according to Krebs' model, which takes into account electronic effects on the lattice vibrations.

In chapter VI the investigation of the lattice dynamics of ordered Fe_3Al is presented. The treatment is also in the phenomenological Born-von Kármán model. The number of parameters is restricted to 11 by considering interactions out to third neighbours, with central interactions between third neighbours. Since the phonon spectrum of Fe_3Al, which has 4 atoms per primitive unit cell, is rather complicated, a group-theoretical classification was made of its normal modes using the method of the multiplier representations. Such a treatment is important to obtain a simplification of the dynamical matrix and information about the polarisation vectors of the different vibrations. The polarisation vectors are needed for the calculation of the inelastic structure factors. Reduced inelastic structure factors are presented for purely longitudinal or transverse phonon branches. Experimental dispersion relations were analysed by means of a least-squares method, which yielded two sets of interatomic force constants. One of the sets was obtained by imposing on it the constraints of the elastic constants as measured by an ultrasonic technique. The difference between the two sets is attributed to the different ways in which sound waves and low frequency phonons are affected by anharmonic effects. The interatomic force constants were also used for the calculation of the frequency distribution function and related thermodynamic quantities.
A striking feature in the force constants is the relative small interaction between second neighbours as compared to that in α-Fe.

Chapter VII contains some general remarks about the two neutron studies. A few speculations are made about the change in the vibrational spectrum of Fe_3Al in the neighbourhood of the phase transition from the ordered structure to the CsCl-type structure.

SAMENVATTING

In dit proefschrift wordt het onderzoek van de roostervibraties in α-ijzer en in geordend Fe_3Al met behulp van inelastische neutronenverstrooiïng beschreven. α-Fe en geordend Fe_3Al vertonen een structurele verwantschap, die ook in het dynamisch gedrag tot uiting zal komen. Geordend Fe_3Al ondergaat een gedeeltelijke ontordening boven ongeveer 550°C, waar een CsCl-type structuur ontstaat.

In hoofdstuk II wordt een kort overzicht gegeven van de beschrijving van roostervibraties in de born-vonkármántheorie. Na de klassieke behandeling van de roostertrillingen, wordt de overgang naar de quantummechanica kort geresumeerd. Uitdrukkingen worden gegeven voor de soortelijke warmte en de debye-wallerfactor. In de laatste paragraaf worden relaties afgeleid tussen de elasticiteitsconstanten en de interatomaire krachtconstanten in kristalroosters door grote golflengten te beschouwen.

Een overzicht van de verstrooiïngstheorie van neutronen in harmonische kristalroosters is te vinden in hoofdstuk III. De belangrijkste resultaten in verband met dit onderzoek zijn de uitdrukkingen voor de coherente werkzame doorsnede voor één-fononverstrooiïng en voor de inelastische structuurfactor.

Hoofdstuk IV geeft een beschrijving van de toegepaste experimentele techniek. In het kort wordt hier de drie-kristalspectrometer beschreven en een aantal mogelijke wijzen van bedrijf behandeld. Experimentele gegevens betreffende α-ijzer worden gerapporteerd als een demonstratie van het effect dat optreedt, wanneer de spectrometer onder al of niet gefocusseerde omstandigheden wordt bedreven.

In hoofdstuk V wordt het onderzoek van de roosterdynamica van α-Fe weergegeven. De experimenteel bepaalde dispersierelaties voor de fononen in de symmetrierichtingen en in bepaalde richtingen langs de grens van de brillouinzone worden hier gepresenteerd. Deze gegevens worden met behulp van een kleinste-kwadratenmethode geanalyseerd in termen van het born-vonkármánmodel, waarbij interacties tot en met de vijfde buren in aanmerking worden genomen.

Het resultaat is een groep van 13 interatomaire krachtconstanten, waarmee de frequentieverdeling van de roostertrillingen werd berekend. Met behulp van deze verdeling werden de soortgelijke warmte en de debye-wallerfactor bepaald en de hiermee corresponderende debyetemperaturen afgeleid. De gegevens worden vergeleken met die verkregen uit andere onderzoekingen met neutronen en met die uit röntgenwerk. De experimentele dispersierelaties worden ook vergeleken met een berekening volgens een model van Krebs, dat bepaalde invloeden van elektronen op het gedrag van de roostervibraties in aanmerking neemt.

In hoofdstuk VI wordt het onderzoek van de roosterdynamica van Fe_3Al in de geordende fase beschreven. De behandeling is eveneens met behulp van het fenomenologische born-vonkármánmodel. Het aantal parameters blijft beperkt tot 11 door slechts wisselwerkingen tot en met de derde buren in aanmerking te nemen, waarbij centrale wisselwerking tussen de derde buren wordt verondersteld. Omdat het fononenspectrum van Fe_3Al, dat 4 atomen per primitieve eenheidscel bezit, nogal gecompliceerd is, werden de normaaltrillingen met behulp van groepentheorie geclassificeerd, waarbij gebruik werd gemaakt van de methode van de multiplicatorvoorstellingen. Een dergelijke behandeling is van belang voor het verkrijgen van een vereenvoudiging van de dynamische matrix en van inzicht in de vorm van de polarisatievectoren van de verschillende roostervibraties. De polarisatievectoren zijn nodig voor de berekening van inelastische structuurfactoren. Voor de zuiver longitudinale of transversale vibraties worden gereduceerde inelastische structuurfactoren gegeven. De experimenteel bepaalde dispersierelaties werden geanalyseerd met behulp van een kleinste-kwadratenmethode, hetgeen resulteerde in twee stellen interatomaire krachtconstanten. Eén stel werd verkregen door te eisen dat ook werd voldaan aan de voorwaarden opgelegd door de elasticiteitsconstanten, gemeten met een ultrasone methode. Het verschil tussen deze twee stellen krachtconstanten wordt toegeschreven aan de verschillende invloeden, die geluidsgolven en fononen van lage frequentie ondervinden van anharmonisch gedrag van het kristalrooster. De interatomaire krachtconstanten werden ook gebruikt voor de berekening van de frequentieverdeling en verwante thermodynamische grootheden.

Hoofdstuk VII bevat enige algemene opmerkingen betreffende de twee gemaakte studies met behulp van neutronen. Enige speculaties worden gemaakt over de verandering in het vibratiespectrum van Fe_3Al in de buurt van de fase-overgang van de geordende naar een CsCl-type structuur.

Teneinde te voldoen aan de wens van de Faculteit der Wiskunde en Natuurwetenschappen volgen hier enkele persoonlijke gegevens.

Na het behalen van het diploma H.B.S.-B in 1952 aan de Christelijke Hogere Burgerschool te Veenendaal, begon ik mijn studie aan de Rijksuniversiteit te Utrecht. Het candidaatsexamen wis- en natuurkunde, letter a, werd in 1956 afgelegd en het doctoraal examen natuurkunde (experimentele richting) met bijvakken wiskunde en mechanica in 1960. In de periode 1958 - 1960 maakte ik als wetenschappelijk medewerker met studietoelage deel uit van de F.O.M.-werkgroep voor thermonucleaire reacties TN II-Plasmafysica-Utrecht, gedurende welke periode het experimentele hoofdonderzoek voor het doctoraal examen werd verricht.

In juni 1960 trad ik in dienst van de Stichting Reactor Centrum Nederland, welke mij gedurende 3 jaren detacheerde bij het Institutt for Atomenergi te Kjeller in Noorwegen, waar ik verbonden was aan de Noors-Nederlandse Reactorschool. Sedert 1963 ben ik werkzaam in het onderzoekcentrum te Petten in de groep Neutronenfysica.

Het experimentele deel van het in dit proefschrift beschreven werk werd uitgevoerd bij de Hoge Flux Reactor te Petten in de jaren 1967 - 1970.